UNIVERSITY OF CALIFORNIA SAN DIEGO

Investigations into the regulation of gene expression by translation elongation control in yeast

A dissertation submitted in partial satisfaction of the requirements for the degree Doctor of Philosophy

in

Chemistry

by

Alexander T. Harvey

Committee in charge:

Professor Brian M. Zid, Chair
Professor Eric J. Bennett
Professor Terence T. Hwa
Professor Simpson Joseph

2022

The dissertation of Alexander T. Harvey is approved, and it is acceptable in quality and form for publication on microfilm and electronically.

University of California San Diego

2022

TABLE OF CONTENTS

LIST OF ABBREVIATIONS

AA	Amino acids
AID	Auxin-inducible Degron
ATC	Anhydrotetracycline
AUG	Start codon
bp	Base pair(s)
CDS	Coding sequence
CHX	Cycloheximide
LTM	Lactimidomycin
miRFP	Monomeric infrared fluorescent protein
mRNA	Messenger RNA
NGD	No-Go Decay
nLuc	Nanoluciferase
ORF	Open reading frame
qPCR	Quatitative polymerase chain reaction
RLU	Relative light unit
RNA-seq	RNA sequencing
RO	Ribosome occupancy
RPF	Ribosome protected fragment
RQC	Ribosome quality control
RT	Reverse transcription
TE	Translational efficiency
TET	Tetracycline
UTR	Untranslated Region
WT	Wild-type
YFP	Yellow fluorescent protein

LIST OF FIGURES

LIST OF TABLES

ACKNOWLEDGEMENTS

I am above all extremely grateful to my advisor Dr. Brian Zid, as his guidance, patience and passion for science over the last five years was critical to my success today. I would also like to thank the other members of my committee, Dr. Eric Bennett, Dr. Terence Hwa, and Dr. Simpson Joseph. Their feedback and advice throughout graduate school helped shape my research project and make this dissertation possible. I am thankful to my labmates in the Zid Lab as well, who were always friendly and supportive. Finally, I thank all my friends and family whose love and support made this long journey both possible and bearable.

Chapter 2, in part, consists of material from a manuscript submitted for publication as it may appear in RNA Biology, 2022, entitled "Differential translation elongation directs protein synthesis in response to acute glucose deprivation in yeast," by Anna R. Guzikowski, Alexander T. Harvey, Jingxiao Zhang, Shihui Zhu, Kyle Begovich, Cohn, M.H.; James E. Wilhelm, and Brian M. Zid. The dissertation author is the second author of this work.

Chapter 3, in part, consists of material from a manuscript that will be submitted for publication, 2022, entitled "Quantification of elongation stalls and impact on gene expression in yeast", by Vince Harjono, Wanfu Hou, Alexander T. Harvey, Arvind R. Subramaniam, and Brian M. Zid. The dissertation author is the third author of this work.

VITA

EDUCATION

2022 Ph.D. in Chemistry, University of California San Diego

2015 B.S. in Biochemistry, University of California Santa Barbara

PUBLICATIONS

Guzikowski A.R., **Harvey A.T.**, Zhang, J., Zhu, S., Begovich, K., Cohn, M.H., Wilhelm, J.E., & Zid, B.M. (2022). "Differential translation elongation directs protein synthesis in response to acute glucose deprivation in yeast", *Submitted for publication*

Harjono, V., Hou, W., **Harvey, A.T.**, Subramaniam, A.R., & Zid, B.M. (2022). "Quantification of elongation stalls and impact on gene expression in yeast", *Manuscript prepared for submission*

Chen Y.S., Tracy S., Harjono V., **Harvey A.T.**, Xu, F., Moresco, J.J., Yates III, J.R., & Zid, B.M. (2022). "Rvb1/Rvb2 proteins couple transcription and translation during glucose starvation". *bioRxiv*

ABSTRACT OF THE DISSERTATION

Investigations into the regulation of gene expression by translation elongation control in yeast

by

Alexander T. Harvey

Doctor of Philosophy in Chemistry

University of California San Diego, 2022

Professor Brian M. Zid, Chair

The control of gene expression is a highly complex process that is vital to an organism's adaptation to fluctuating environments. The majority of a cell's energy is directed towards protein synthesis, necessitating a tight regulation of the translation process. Past research has predominantly focused on the translational control of initiation, but there has been a growing appreciation for the complex interplay between both initiation and elongation rates. In this dissertation I use the budding-yeast *Saccharomyces cerevisiae* as a model organism to study the translational regulation of elongation. I attempt to determine the role of elongation during adaptative stress response and seek to quantify elongation rates across distinct conditions. In Chapter 2 we explore the regulation of translation during the stress response to glucose starvation. We use ribosomal profiling and *in vivo* luciferase reporter assays to demonstrate a slowdown of elongation rates during glucose starvation. Chapter 3 includes a discussion of the development of a luciferase reporter for quantification of elongation rates during translation. We quantify the impact of synonymous codon substitutions on the elongation rate of yeast-optimized yellow fluorescent protein (YFP) and provide further insight into the surveillance of translation and the roles of the proposed translation sensors Hel2 and Dhh1 in mediating ribosome pausing events. Chapter 4 investigates the effects of Dhh1 on the translational repression observed during glucose starvation. We identify a correlation between the shift in ribosome polarity we observe during glucose starvation and Dhh1 enrichment during glucose starvation previously published CLIP-seq dataset by (Cary et al., 2015) and detail the results of polysome profiling and luciferase reporter assays performed in a conditional Dhh1 knockdown.

Chapter 1: Introduction

The central dogma of biology encompasses the flow of information encoded in the genome. Information is stored by DNA and transcribed to mRNA. In turn, mRNA is translated by ribosomes to produce protein. Translation is a highly complex process tightly controlled by the cell, but the process can be summarized in three primary phases: initiation, elongation, and termination. In eukaryotes, the initiation stage commences once the preinitiation complex, composed of the 40S ribosomal subunit and several additional initiation factors, recognizes the AUG start codon of the mRNA. The 60S ribosomal subunit and the initiator methionine tRNA assemble with the 40S subunit to form the 80S ribosome (Jackson et al., 2010; Kozak, 1999).

Following initiation, the ribosome translocates along the mRNA sequence and proceeds through a series of conformational changes with the assistance of several elongation factors as it incorporates sequential amino acids onto a nascent polypeptide. Each three-nucleotide mRNA codon is selectively recognized by amino-acyl tRNAs in complex with eukaryotic factor 1A (eEF-1A) that contain a complementary anticodon sequence, allowing initial binding and accommodation to the ribosomal A site upon GFP hydrolysis and eEF-1A release (Dever et al., 2018; Dever and Green, 2012). Peptide bond formation is catalyzed with the peptidyl-tRNA in the P site and the nascent polypeptide is transferred to the A site. Finally, eukaryotic elongation factor 2 (eEF2) catalyzes translocation of the tRNAs to the E and P sites and the deacylated-tRNA is released from the E site as the ribosome continues to the next codon. Termination takes place once the ribosome reaches a stop codon at the end of the mRNA open reading frame. These codons are not coded for by any tRNAs and allow ribosome release factors to bind to the empty A site and facilitate the release of the polypeptide. The ribosome can then be released from the transcript, allowing the ribosomal components to be recycled for the next round of translation (Dever and Green, 2012).

Initiation is the most complex stage and the primary rate limiting step of translation, allowing for a wide variety of regulatory mechanisms to modulate translation rates in a gene-specific manner

during development and in response to environmental conditions (Costello et al., 2017; Janapala et al., 2019; Liu and Qian, 2014; Sheikh and Fornace, 1999; Sonenberg and Hinnebusch, 2009). For example, the phosphorylation of eIF2 (eukaryotic initiation factor 2) is a conserved regulatory response to diverse stressors in both yeast and mammalian cells (Crawford and Pavitt, 2019; Pakos-Zebrucka et al., 2016). eIF2 is an essential factor that delivers Met-tRNA through a GTP-dependent mechanism during the formation of the preinitiation complex prior to protein synthesis. Phosphorylation of eIF2α prevents the GTP-binding required to return eIF2 to its active state.

Less attention has been focused on other steps of translation although it is becoming increasingly appreciated that cells have evolved regulatory steps to control translation apart from initiation. Regulation of elongation rate has been identified in a diverse range of cellular processes, from meiosis and cell-cycle control (Sabi and Tuller, 2019; Sivan et al., 2007)

For example, eEF2 has been shown to be phosphorylated in response to acute hyperosmotic and oxidative stresses in yeasts (Sanchez et al., 2019; Teige et al., 2001; Wu et al., 2019). Phosphorylation reduces eEF2 activity, thereby generally attenuating elongation and global protein production (Kenney et al., 2014; Tavares et al., 2014). Mammalian systems also rely on eEF2 phosphorylation via eEF2 kinase to adapt to nutrient deprivation and ribosomal stress (Gismondi et al., 2014; Kang and Lee, 2001; Leprivier et al., 2013). It has also become increasingly apparent that the redundancy of the genetic code, which utilizes 61 codons to encode for only 20 amino acids, provides an additional layer of information by which cells can modulate the translation rates of otherwise similar polypeptide sequences (D'Onofrio and Abel, 2014). Previous research has attempted to quantify this effect with a metric called codon optimality, a species-specific value for each codon taking into factors implicated in elongation rate, including tRNA availability and demand, frequency of use in the genome, GC content, and interactions with the ribosome exit tunnel (Gardin et al., 2014; Pechmann and Frydman, 2013; Presnyak et al., 2015; Reis et al., 2004).

As the process of translation is highly conserved across eukaryotic organisms, further exploration of how translational elongation is controlled is necessary to the understanding of how life functions. It is critical to understand how the cell regulates protein synthesis and maintains homeostasis during adverse conditions if we are to gain further insight into the conditions that can occur as these processes malfunction during disease and aging (Tahmasebi et al., 2018). The breakdown in the regulatory mechanisms of translation are particularly detrimental in neuronal cells, which rely on a sophisticated balance of localized translation levels to respond appropriately to complex external stimuli (Kapur and Ackerman, 2018; Tahmasebi et al., 2018). Aberrant alterations of translational elongation rates specifically can result in the misfolding of proteins and the loss of translational fidelity (Kapur and Ackerman, 2018).

In this dissertation I use the budding-yeast *Saccharomyces cerevisiae* as a model organism to study the translational regulation of elongation. In Chapter 2 we explore the regulation of translation during the stress response to glucose starvation. We use ribosomal profiling and *in vivo* luciferase reporter assays to demonstrate a slowdown of elongation rates during glucose starvation. Chapter 3 includes a discussion of the development of a luciferase reporter for quantification of elongation rates during translation. We quantify the impact of synonymous codon substitutions on the elongation rate of yeast-optimized yellow fluorescent protein (YFP) and provide further insight into the surveillance of translation and the roles of the proposed translation sensors Hel2 and Dhh1 in mediating ribosome pausing events. Chapter 4 investigates the effects of Dhh1 on the translational repression observed during glucose starvation. We identify a correlation between the shift in ribosome polarity we observe during glucose starvation and Dhh1 enrichment during glucose starvation previously published CLIP-seq dataset by (Cary et al., 2015) and detail the results of polysome profiling and luciferase reporter assays performed in a conditional Dhh1 knockdown.

Chapter 2: Elongation slowdown during glucose starvation and stationary phase

2.1 Abstract

Protein synthesis is energetically expensive and its rate is influenced by factors including cell type and environment. Suppression of translation is a canonical response observed during stressful changes to the cellular environment. In particular, inhibition of the initiation step of translation has been highlighted as the key control step in stress-induced translational suppression as mechanisms that quickly suppress initiation are well-conserved across organisms and stressors. However, cells have also evolved complex regulatory means to control translation beyond initiation. Here, we examine the role of the elongation step of translation in yeast subjected to acute glucose deprivation. Use of ribosome profiling and *in vivo* reporter assays demonstrated elongation rates slow progressively following glucose removal. We observed ribosome distribution broadly shifts towards the 3' end of transcripts after both acute and gradual glucose deprivation but not in response to other stressors. Additionally, on assessed mRNAs, a correlation exists between ribosome density and protein production pre-stress but is lost after. Together, these results indicate that stress-regulated elongation causes ribosomes to slow and build up on a considerable proportion of the transcriptome in response to glucose withdrawal. Finally, we report ribosomes that build up along transcripts are competent to resume elongation and complete protein synthesis upon readdition of glucose to starved cells. This suggests yeast have evolved mechanisms to slow translation elongation in response to glucose starvation which do not preclude continuation of protein production from those ribosomes, thereby averting a need for new initiation events to take place to synthesize new protein.

2.2 Introduction

The ability to adapt to rapidly fluctuating environmental conditions is a vital aspect for an organism's long-term survival. The budding-yeast *Saccharomyces cerevisiae*, a unicellular and rapidly growing eukaryote, is particularly sensitive and responsive to such stressors. Rapid growth requires a massive investment of cellular energy into new protein synthesis (Kafri et al., 2016); however organisms including yeast face a dynamic environment that necessitates rapid adaptation to fluctuations in conditions such as nutrient availability, temperature, osmotic balance, and oxidation state. Such adaptations require alterations of gene expression that take place at both the transcriptional and translational level in a coordinated stress response (Advani and Ivanov, 2019; Crawford and Pavitt, 2019). An important component of response to acute, sudden stress is regulation and reduction of protein synthesis from pre-existing cytoplasmic mRNAs (Liu and Qian, 2014). Logically, reduced translation tends to follow stress induction as the existing transcriptome is no longer programmed for survival under current, newly stressful conditions. In addition, reducing translation from mRNAs encoding proteins that facilitate growth is prudent at the onset of severe stress as it circumvents the time required for nuclear changes in transcription to impact gene expression. Lowering translation also reduces energy consumption and is therefore considered a general hallmark of post-transcriptional gene regulation as rapidly growing cells respond to acute stress.

Decades of research have parsed mechanisms that limit protein synthesis in response to acute stresses (Sheikh and Fornace, 1999). The focus of previous research has largely focused on regulation at the step of initiation, as it is the rate limiting step of translation during growth conditions (Costello et al., 2017; Janapala et al., 2019; Liu and Qian, 2014). For example, the phosphorylation of eIF2 (eukaryotic initiation factor 2) is a conserved regulatory response to diverse stressors in both yeast and mammalian cells (Crawford and Pavitt, 2019; Pakos-Zebrucka et al., 2016). eIF2 is an essential factor that delivers Met-tRNA through a GTP-dependent mechanism during the formation of the preinitiation complex prior

to protein synthesis. Phosphorylation of eIF2α prevents the GTP-binding required to return eIF2 to its active state.

Less attention has been focused on other steps of translation although it is becoming increasingly appreciated that cells have evolved regulatory steps to control translation in response to stress apart from initiation. For example, eEF2 (eukaryotic elongation factor 2), the protein that catalyzes GTP-dependent ribosome translocation during the elongation step of protein synthesis, has been shown to be phosphorylated in response to acute hyperosmotic and oxidative stresses in yeasts (Sanchez et al., 2019; Teige et al., 2001; Wu et al., 2019). Phosphorylation reduces eEF2 activity, thereby generally attenuating elongation and global protein production (Kenney et al., 2014; Tavares et al., 2014). Mammalian systems also rely on eEF2 phosphorylation via eEF2 kinase to adapt to nutrient deprivation and ribosomal stress (Gismondi et al., 2014; Kang and Lee, 2001; Leprivier et al., 2013). In response to heat shock, researchers have shown that mammalian and yeast cells globally accumulate ribosomes close to their start codons, approximately 60-100 nucleotides downstream of the AUG, which indicates those ribosomes successfully initiated and were slowed early in elongation (Mühlhofer et al., 2019; Shalgi et al., 2013).

Abrupt glucose deprivation is a particularly arduous stress for log phase yeast to face because glucose is their preferred carbon source and a key substrate in fermentative growth (Ashe et al., 2000; Kim et al., 2013). Relatedly, understanding how simpler eukaryotic organisms have evolved to confront glucose starvation is relevant to understanding complex human diseases such as diabetes and cancer (Diaz-Ruiz et al., 2011; Jochem et al., 2019; Pineau and Ferreira, 2010). During glucose starvation in yeast, a rapid collapse in global translation is observed within the first minute (Ashe et al., 2000). Rapid inhibition of RNA-binding by initiation factors such as eIF4A results in a global drop in translation initiation as the loss of 40S ribosome scanning factors prevents translation initiation downstream of the formation of the 43S preinitiation complex (Bresson et al., 2020; Castelli et al., 2011). Exact

mechanisms that regulate this rapid shutdown are unknown and do not appear to be the result of previously characterized pathways of translational control (Ashe et al., 2000; Bresson et al., 2020).

While it has been reported that, after 10 minutes of glucose starvation, there is extensive cessation of S^{35} methionine incorporation, researchers have also observed that housekeeping mRNAs remain engaged in polysomes at both a relative and an absolute level (Arribere et al., 2011; Zid and O'Shea, 2014). For example, ribosomes remain bound to the coding sequence (CDS) of the essential glycolytic gene *PGK1* after 10 and 15 minutes of glucose starvation (Brengues et al., 2005; Zid and O'Shea, 2014). As glucose starvation leads to an extensive reduction in initiation (Ashe et al., 2000; Janapala et al., 2019), this result strongly suggests that elongation does not take place at pre-stress rates. If elongation did not slow, we would expect to see ribosomes run off the 1,251bp *PGK1* CDS after approximately three minutes as the basal elongation rate of log phase yeast is reported to range between 3-10 amino acids per second (Karpinets et al., 2006; Riba et al., 2019). This result seems at odds with a common narrative that ribosomes run off mRNAs in response to severe stress. Runoff is highlighted as a crucial early step in a process that sequesters abundant, pro-growth, and pre-existing mRNAs into phase separated granules (Khong and Parker, 2018; Lee and Seydoux, 2019; Moon et al., 2019). Importantly, this narrative is well-founded and ribosome runoff does occur as evidenced by a large collapse in the polysome repeatedly shown to take place on the timescale of minutes in glucose-starved yeast (Arribere et al., 2011; Ashe et al., 2000; Brengues et al., 2005; Holmes et al., 2004). *PGK1*'s high occupancy observed simultaneously with polysome collapse indicate ribosome runoff is heterogeneous. Therefore, a gene expression program dependent on differential translation elongation may play a key role in regulating protein synthesis following glucose starvation and explain, at least in part, why some ribosomes run off transcripts and some remain bound to them.

Intrigued by this observation of heterogeneous ribosome behavior, we sought to better understand how yeast regulate protein synthesis and alter ribosome-mRNA interactions in the initial minutes following glucose starvation. In this study, we focused not only on general levels of

engagement but where along mRNAs ribosomes bind. We found that glucose starvation causes ribosomes to accumulate downstream on the 3' ends of many mRNAs. This coincides with a progressively slower rate of elongation, a result we validated with *in vivo* approaches. We also explored protein synthesis in log phase and glucose starvation conditions to further support our measurements of slowed elongation and observed that the extent of ribosome engagement on a transcript is not sufficient to predict differences in protein synthesis between pre- and post-stress conditions. Additionally, we propose ribosomes that build up on transcripts can resume elongation following glucose readdition. Furthermore, successful protein synthesis can be observed from these ribosomes independent of newly initiated ones.

2.3 Results

Ribosome profiling is a sequencing technique that isolates fragments of mRNAs bound by ribosomes which are turned into sequencing libraries. It is common for researchers to prepare ribosome profiling and traditional RNA-seq libraries from the same sample to calculate ribosome occupancy (RO) on a gene-by-gene basis and compare changes between samples. Such changes are traditionally ascribed as alterations in translational efficiency (TE) for a given gene (Gerashchenko et al., 2012; Ingolia et al., 2009; Li et al., 2017; Pop et al., 2014; Sen et al., 2015; Wang et al., 2019). However, analysis of the distribution and movements of ribosomes along transcripts at nucleotide resolution can provide deeper insight into translational regulation compared to simply considering RO changes. Using ribosome profiling, we first examined the distribution of reads, known as ribosome-protected fragments (RPFs), along mRNAs that have important roles in glycolysis and growth of a similar or longer length to the 1,251bp *PGK1* transcript (Figure 2.1A). Ribosomes remain bound to the entire length of these mRNAs in log phase and after 15 minutes of glucose starvation. This indicates elongation is regulated in a way where ribosome runoff is not ubiquitous. If runoff were ubiquitous because of unaltered transit rates, we would expect preexisting transcripts of this length to be largely or completely devoid of ribosomes given that new initiation and aggregate protein synthesis are markedly reduced genome-wide (Ashe et al., 2000; Janapala et al., 2019).

We were struck by the shift in the pattern of RPF reads along these genes from the upstream 5' end in log phase towards the downstream 3' end during stress. Plotting the distribution of read density along thousands of yeast transcripts revealed a general shift away from the start codon when compared to log phase. This indicates strong repression in translation initiation (Figure 2.1B; top and middle panels). This more general increase in downstream read distribution further supports the notion that ribosome runoff is heterogeneous, given that polysome collapse also occurs in glucose starvation conditions. Importantly, a group of stress-induced genes known to be upregulated transcriptionally and translationally mirror the distribution pattern observed during log phase (Figure 2.1B; bottom panel).

These stress-responsive genes, mostly heat shock proteins, display a decreasing or negative ramp of distribution reported to be characteristic of well-translated genes (Shah et al., 2013). These stress-induced genes evade the general halt in initiation that occurs during glucose starvation and demonstrate cells were undergoing stress response.

We next assessed whether this small group of stress-responsive genes, which are uniquely upregulated in response to stress, have greater RO values after 15 minutes of glucose starvation compared to the rest of the transcriptome. If genes that are well-translated in log phase underwent massive runoff during stress, we would expect lower occupancy on those transcripts and higher occupancy on upregulated genes. Surprisingly, while transcriptional induction of stress-responsive mRNAs is very high compared to the entire genome, the magnitude of their RO at 15 minutes starvation did not vary from other genes, including the 150 genes that were most highly engaged with ribosomes during log phase (Figure 2.1C). We also calculated the proportion of preexisting versus stress-induced mRNAs in our samples (Figure 2.1D). Stress-induced transcripts made up a relatively small proportion of libraries after 15 minutes of starvation. Moreover, the 150 most abundant mRNAs during log phase maintain high RPF and mRNA read counts after 15 minutes of stress compared to both stress-induced genes and the rest of transcriptome, further highlighting their sustained engagement with ribosomes.

Because ribosome profiling and RNA-seq quantify relative changes in RPF and mRNA abundances, we used polysome profiling to assess absolute changes in ribosome engagement to more rigorously test our hypothesis that high ribosome occupancy on pre-stress mRNAs continues during stress. Polysome profiling was performed on log phase and glucose starved samples, followed by RNA quantification of select genes with normalization to an exogenous spike-in RNA using qRT-PCR. Fractions were pooled and five total groups were analyzed: a total RNA pool, a free RNA pool, a monosome pool, and two polysome fractions made of a combined disome plus trisome pool and, finally, a dense polysome pool (Figure 2.2). The polysomes from glucose starved cultures yielded concentrations for several pro-growth, abundant log phase mRNAs that were roughly 2-fold lower than

polysomes from glucose replete, log phase cultures. We also assessed the movement of 18S rRNA, stress-induced heat shock genes, and genes that are extremely long, each greater than 6,000bp, given that the median yeast gene length is 1,280bp. This more targeted approach corroborated our global ribosome profiling data by further showing there is an incomplete ribosome runoff during glucose starvation. Some transcripts do undergo runoff and leave the polysome. In addition, the polysome collapses but neither process is universal nor complete. If ribosome runoff was a straightforward, universal explanation for how translation is regulated in response to glucose starvation, we would expect the magnitude of the shift of abundant growth genes out of heavier polysomes to be much greater. We would also expect the shift of these growth genes to be several fold higher than the shift observed for extremely long genes, which we wouldn't expect to be able to undergo as much runoff during 15 minutes of starvation, given their length and ribosome transit rates. Our data also agrees with previous polysome profiling experiments that showed the continued presence of *PGK1* mRNAs in polysomes during acute glucose starvation (Arribere et al., 2011; Brengues et al., 2005). Together, our ribosome profiling and polysome profiling experiments highlight that ribosomes remain engaged with preexisting mRNAs during glucose starvation.

As ribosomal runoff on many growth-related mRNAs appears incomplete, we next sought to measure protein expression for select mRNAs. As *PGK1* is highly expressed pre-stress and continues to maintain some association with polysomes, we were curious if the efficiency of protein expression would be reduced when compared to an upregulated stress-response gene such as *HSP30*. To test this, we added TAP tags to both and performed immunoprecipitations from log phase and glucose starvation cultures supplemented with S^{35} methionine (Figure 2.3). Quantification of protein production revealed that, during log phase when *HSP30* has very few ribosome counts, we were unable to detect protein production above background while ribosomes bound to *PGK1* showed robust protein production. Therefore, a consistent relationship exists between RPF reads and protein production in the absence of stress. However, during glucose starvation, despite *PGK1* having about 25-fold higher RPF counts along

its transcripts, there was not a significant difference in S^{35} incorporation into Pgk1 and Hsp30 proteins. Together, this indicates that differential elongation during glucose starvation results in divergent levels of protein production in a gene-dependent manner. Importantly, this highlights that careful consideration must be made prior to assuming high levels of ribosome-mRNA interactions on a given transcript necessitate robust translation of that mRNA.

In order to further assess protein production *in vivo*, we adopted a yeast-optimized NanoLuciferase (nLuc) previously described (Masser et al., 2016). With the addition of a C-terminal PEST degradation sequence, the half-life of nLuc can be reduced from ~45 minutes to ~5 minutes or less. This dramatic reduction of background protein levels allows for closer to real-time measurement of active translation. Addition of cycloheximide to samples, a translation elongation inhibitor, can be used as a proxy for determining background luminescence of previously synthesized proteins. By monitoring the luminescence of cycloheximide-inhibited cells unable to synthesize new protein, any increases in luminescence from cell cultures without cycloheximide is indicative of newly synthesized nLuc. This is particularly relevant in glucose starvation conditions due to the low level of translation for most genes. First, it was necessary to recapitulate the S^{35} protein synthesis data. We first assessed two nLucPEST reporters, one expressed downstream of the Pab1 promoter and 5'UTR and one downstream of the Hsp30 promoter and 5'UTR. During log phase growth, the Pab1prUTR reporter was robustly translated while the Hsp30prUTR reporter was not expressed (Figure 2.4A). During 15 minutes of glucose starvation, the expression was reversed, in which the Pab1prUTR reporter was translated at low levels versus Hsp30prUTR driven nLucPEST. These results replicated our S-35 pulldown data, in which Pab1 is translationally repressed during glucose starvation while Hsp30 is upregulated and readily expressed. To distinguish the role of the 5'UTR sequence from that of the promoter, we assessed a reporter with the Pab1 promoter but the 5'UTR of Hsp30 under the same conditions (Figure 2.4B). Expression during glucose starvation increases relative to the Pab1prUTR reporter but is still dramatically reduced relative to expression during log phase as well as Hsp30prUTR expression during glucose starvation. This

demonstrates that the difference in expression is not dependent on the 5'UTR sequence. We then tagged several endogenous genes with nLucPEST and sought to replicate our S^{35} findings for Pgk1 and Hsp30. nLucPEST was tagged downstream of a self-cleaving E2A viral peptide in order to avoid alterations to the endogenous protein half-lives (Souza-Moreira et al., 2018). Pab1 and Pgk1 expression are highly reduced during glucose starvation, while Hsp30 is induced (Figure 2.5). As we observed in Figure 2.3, Pgk1 and Hsp30 protein expression during glucose starvation are surprisingly similar despite the stark contrast we have observed in mRNA levels and ribosome occupancy.

We next sought to test the hypothesis that, in response to glucose-limited conditions, ribosomes slow down and build up on the downstream ends of CDSs because of decreased elongation by directly measuring elongation rate. To do this, we created a doxycycline-inducible reporter driving the expression of nLuc and a second reporter driving the expression of LacZ C-terminally tagged with nLuc. As LacZ has a long open reading frame (3072 bp), there will be a delay in luciferase signal versus nLuc alone. An analysis technique known as Schleif plotting factors in both initial time of reporter induction and the amount of time that elapses between expression of the nLuc and LacZ-nLuc reporters to calculate the average elongation rate necessary to translate through LacZ (Dai et al., 2016; Schleif et al., 1973).

During log phase growth, we calculated an elongation rate of ~4-5 amino acids per second, within the range of 3-10 amino acids per second observed in previous studies (Karpinets et al., 2006; Riba et al., 2019) (Figure 2.6). Glucose starvation resulted in a slower elongation rate of ~2-3 amino acids per second. We hypothesize that this rate is representative of more the preferentially translated proteins such as the heat shock genes. Since our dox-inducible reporter is transcribed after glucose starvation, we expect it will have a faster elongation rate than the pre-existing pro-growth mRNAs for which we observe very poor translational efficiencies. It is not possible to assess the elongation rate slowdown of ribosomes initiated prior to glucose starvation, which we hypothesize are responsible for the high ribosomal occupancy and poor translational efficiency of pro-growth mRNAs.

Since glucose starvation is a particularly acute stress, we also investigated the elongation rate change as yeast cultures approach the diauxic shift. As yeast divide rapidly during log phase, glucose is consumed in anaerobic respiration and converted into ethanol. Continued growth eventually depletes the remaining glucose and necessitates a metabolic shift towards aerobic respiration and the use of ethanol as the primary carbon source. This switch in metabolism is a more gradual adaptive process that yeast cells often face in their natural environment after rapid growth, rather than the abrupt removal of glucose from log phase cultures. We found that the elongation rate slows significantly to roughly 2 AA/sec in cells after the diauxic shift, representing a slowdown in elongation rate comparable to that during glucose starvation (Figure 2.6). Thus, the slowdown in elongation is a more general phenomenon not restricted to acute glucose starvation.

Finally, we sought to establish whether the ribosomes that slow or stall along CDSs during glucose starvation are competent to resume translation upon reintroduction of glucose to the environment. To do this, we again utilized both ribosome profiling and *in vivo* reporter assays. After acute glucose starvation, glucose was reintroduced and samples were collected for ribosome profiling, RNA-seq, and polysome profiling after one minute and five minutes. We were particularly interested in long genes which we expected to be poorly translated during glucose starvation but were earlier shown to remain associated with the polysome as assessed by qPCR (Figure 2.2).

Upon glucose readdition a ‘wave’ of increased RPF read density, suggestive of new initiation events, was detected near the start codon within the first minute (Figure 2.7A). By five minutes, this wave of newly initiated ribosomes was observed spanning the first approximately 2,200bp of mRNAs. To assess ribosome movement in response to glucose readdition in a gene-specific manner, we looked at the distribution of reads on two yeast genes that are particularly long, each over 6,000bp in log phase, starvation, and readdition conditions (Figure 2.7B). We wondered whether it would be possible to parse the engagements and movement of ribosomes that slowed on these mRNAs during starvation from those that were newly initiated. Intriguingly, the profile of ribosomes engaged during glucose starvation

appears to move down the transcript at the same time as new initiation events occur, resulting in a bimodal distribution of RPF reads at the 5' and 3' ends of these genes after 5 minutes of readdition. We hypothesized that there could be two populations of ribosomes on the CDSs: one population of ribosomes that underwent initiation during log phase, built up downstream during glucose starvation, and then resumed elongation and a second population that were newly initiated upon glucose readdition. This led us to wonder if we could directly test whether the former were actively elongating ribosomes and, furthermore, whether these ribosomes could finish translation and produce functional protein.

To test the potential for these ribosomes to resume translation upon relief of starvation, we tagged the long, endogenous *FAS1* and *URA2* genes with an E2A self-cleaving peptide followed by nLucPEST and monitored reporter expression in log phase, during glucose starvation, and following glucose readdition (Souza-Moreira et al., 2018) (Figure 2.7C). We estimated these mRNAs were long enough that any new translation events would take longer than five minutes to complete as the 'wave' of ribosome density we saw in Figure 2.7A would correspond to translation of proteins less than 1,000 amino acids. Additionally, once initiated, a ribosome would need to elongate at 7-8 amino acids per second to translate through these reporters within five minutes. This rate is faster than the elongation rates we observe even in log phase conditions (Figure 2.6) and faster than the rate we would predict from our ribosome profiling data. Even still, to separate translation events that arise due to new initiation after glucose readdition from translation events due to ribosomes that completed initiation prior to readdition, we developed an experimental approach that directly decoupled these two possibilities.

Specifically, we glucose starved cells expressing these reporters for 30 minutes, added glucose back, and then measured luciferase production in the presence (treated) and absence (untreated) of two different drugs: either CHX, a translation elongation inhibitor, or lactimidomycin (LTM), a translation inhibitor that preferentially inhibits initiation at the concentration used (Eisenberg et al., 2020; Schneider-Poetsch et al., 2010) (Figure 2.7D). Since CHX addition prevents ribosomes from completing

elongation and producing any functional luciferase, the difference in luciferase signal between the CHX-treated versus untreated samples represents all luciferase produced during signal measurement. In all conditions tested, there was a significant difference in luciferase signal with CHX treatment compared to untreated cultures, indicating expression was taking place in all conditions. As expected, expression was greatly reduced in glucose starvation conditions compared to log phase for both reporters.

Intriguingly, after five minutes of glucose readdition, there was no difference in protein expression due to LTM treatment compared to the untreated samples. This suggests the nLuc expression that took place did not depend on new initiation events. If it had, using an initiation inhibitor would have reduced luciferase production compared to the untreated sample. On the other hand, we found that upon 15 minutes of glucose readdition, significantly less protein was produced from both CHX and LTM treatments. This suggests new initiation events were contributing to expression after 15 minutes, unlike after five minutes. Taken together, we interpret these results to demonstrate that there is indeed a population of ribosomes bound to the CDSs of our reporters that underwent initiation prior to glucose readdition, resumed elongation upon readdition, and produced functional protein.

Our lab has demonstrated previously that the promoter directs both a mRNAs transcription and its subsequent subcellular localization in the cytoplasm during glucose starvation (Zid and O'Shea, 2014). During glucose starvation, there are two distinct sets of transcriptionally upregulated genes. Transcriptionally upregulated and well-translated mRNAs, such as those coding for heat shock proteins, remain diffusely localized in the cytoplasm and have high levels of ribosome occupancy. Another class of mRNAs is transcriptionally upregulated but poorly translated, instead localizing to stress granules. Intriguingly, these mRNAs appear to have a high concentration of ribosome occupancy on the start codon but are otherwise poorly associated with ribosomes. We were curious if these mRNAs were primed for translation upon the relief of starvation conditions. To assess this possibility, we

endogenously tagged two of these genes, Gsy1 and Hxk1, with our E2A-nLucPEST reporter and monitored their expression during glucose readdition (Figure 2.8).

Indeed, glucose readdition results in robust translation of these transcriptionally upregulated mRNAs. In addition, these mRNAs are more strongly induced when a quantity of glucose $1/10^{th}$ that of normal growth media of is added to cultures, below the concentration at which severe inhibition of translation and subsequent polysome collapse can be observed (Castelli et al., 2011). As time passes and cells recover from starvation, protein expression returns towards the low baseline expression measured during log phase growth.

Figure 2.1: *Glucose starvation alters ribosome engagement with mRNAs*
(A) RPF reads per million (rpm) by nucleotide position for the indicated genes during log phase (purple; left) and after 15 minutes of glucose starvation (orange; right). **(B)** Normalized read density plots for indicated gene categories in log phase (purple; top) and after 15 minutes of glucose starvation (orange; middle and bottom; red, respectively). To generate read density plots the aggregate number of reads per single nucleotide position across all genes >1000bp with > 25 reads per gene per library were included and normalized to enable inter-library comparison. **(C)** Plot of log2 RO calculated as RPF reads divided by mRNA reads per gene in glucose starvation conditions against log2 mRNA induction after 15 minutes of glucose starvation. Abundant log phase genes (purple markers) were the 150 transcripts with the highest mean TPM scores in two replicate ribosome profiling libraries. TPM = transcripts per million. For both B and C, genes with mRNA log2 fold change > 2.5 and RO log2 fold change > 0.09 were classified as upregulated in response to glucose starvation. **(D)** Percentage of all reads in the indicated libraries by category. 149 genes had >4-fold increase in mRNA reads after 15 minutes of glucose starvation compared to log phase (green). Abundant log phase mRNAs (blue) were the 150 mRNAs with the highest mean TPM scores in two replicate RNA-seq libraries. There is substantial overlap between the top 150 RFP TPM genes in C (purple markers) and the top 150 mRNA TPM genes in D (green) with 123 total shared.

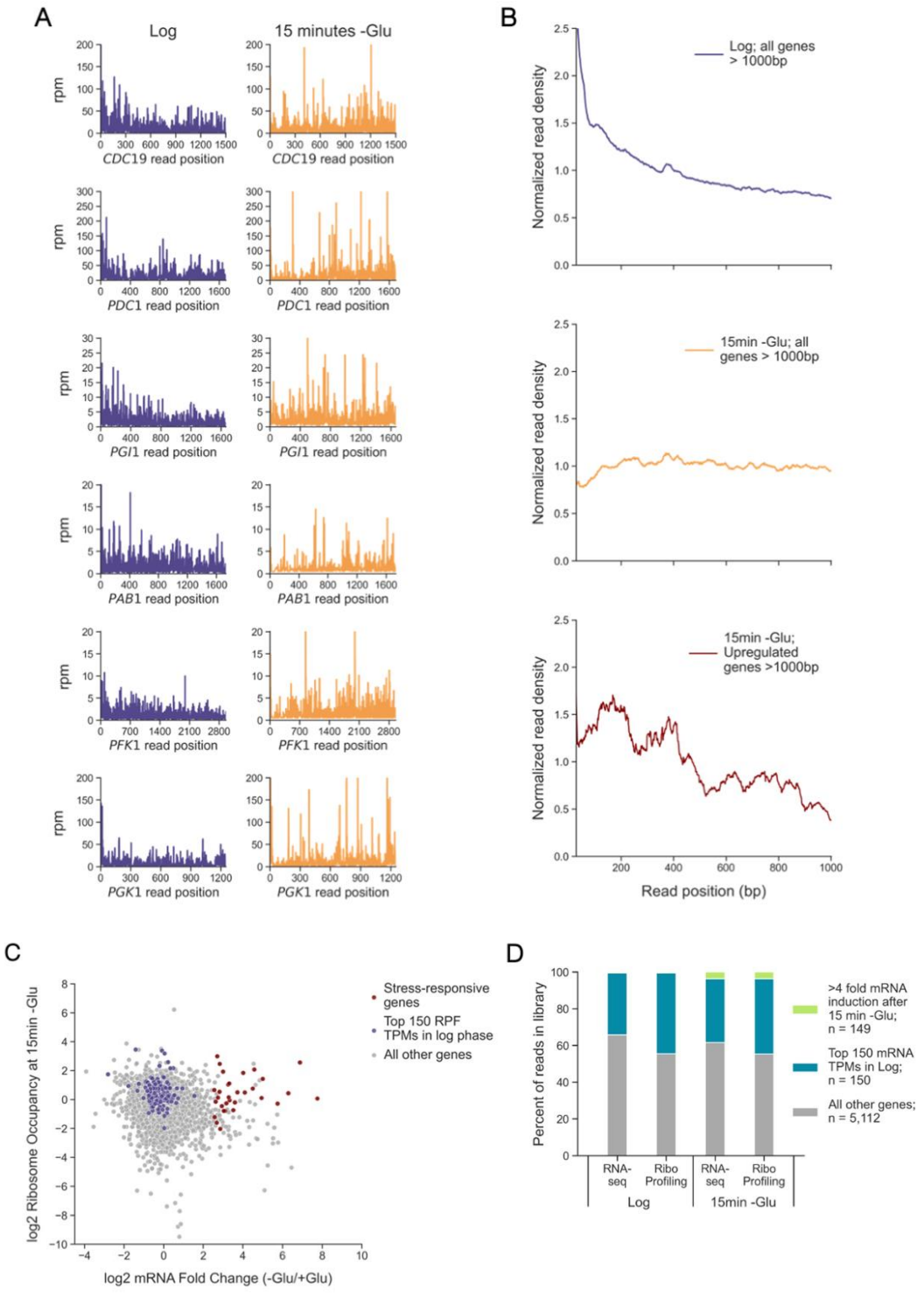
A
Log
15 minutes -Glu
rpm
CDC19 read position
PDC1 read position
PGI1 read position
PAB1 read position
PFK1 read position
PGK1 read position
B
Log; all genes > 1000bp
15min -Glu; all genes > 1000bp
15min -Glu; Upregulated genes >1000bp
Normalized read density
Read position (bp)
C
Stress-responsive genes
Top 150 RPF TPMs in log phase
All other genes
log2 Ribosome Occupancy at 15min -Glu
log2 mRNA Fold Change (-Glu/+Glu)
D
Percent of reads in library
>4 fold mRNA induction after 15 min -Glu; n = 149
Top 150 mRNA TPMs in Log; n = 150
All other genes; n = 5,112
RNA-seq
Ribo Profiling
Log
15min -Glu

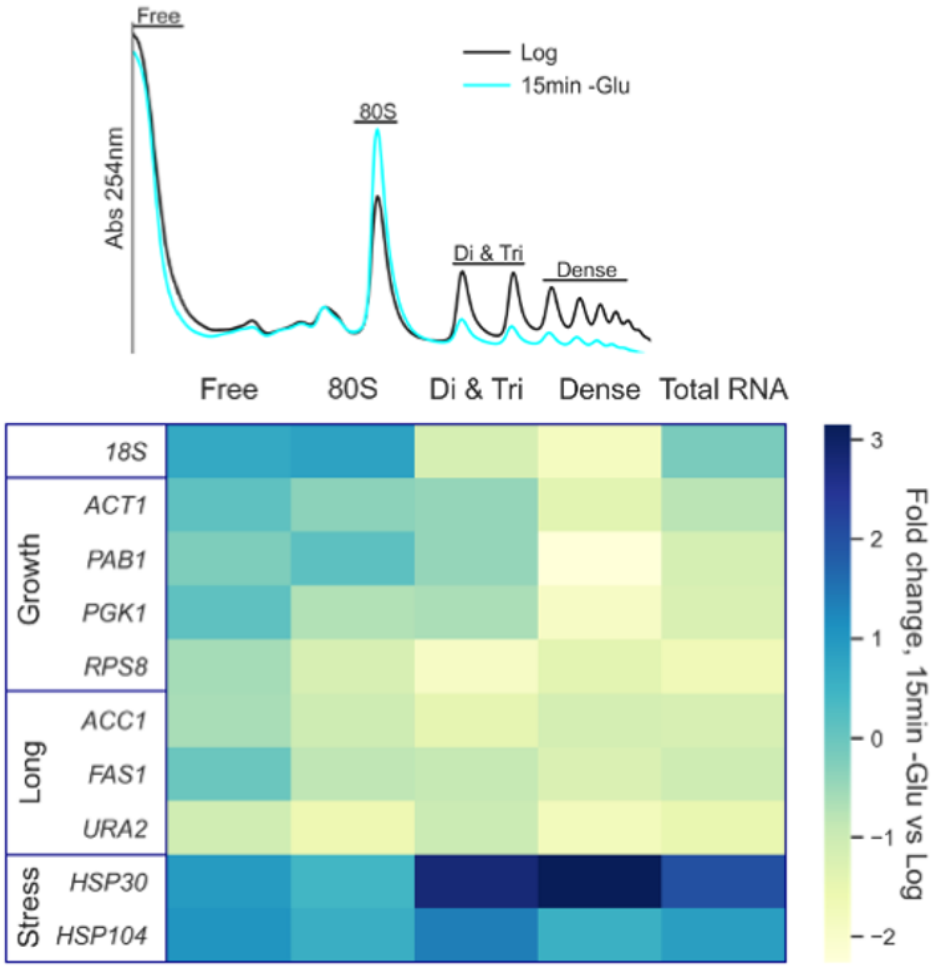

Figure 2.2: *Pre-existing mRNAs display incomplete runoff during glucose starvation*
Traces of polysome fractionation gradients showing what fractions were combined (top). Pooled fractions underwent RNA extraction and RT-qPCR to quantify the changes in transcript abundance in the indicated fraction after 15 minutes of glucose starvation compared to log phase (bottom). An exogenous, spike-in RNA was used for standardization to quantify abundance in each pool and the fold change in RNA abundance as assessed by ΔΔCt analysis is indicated in the heatmap for mRNAs grouped into the indicated categories.

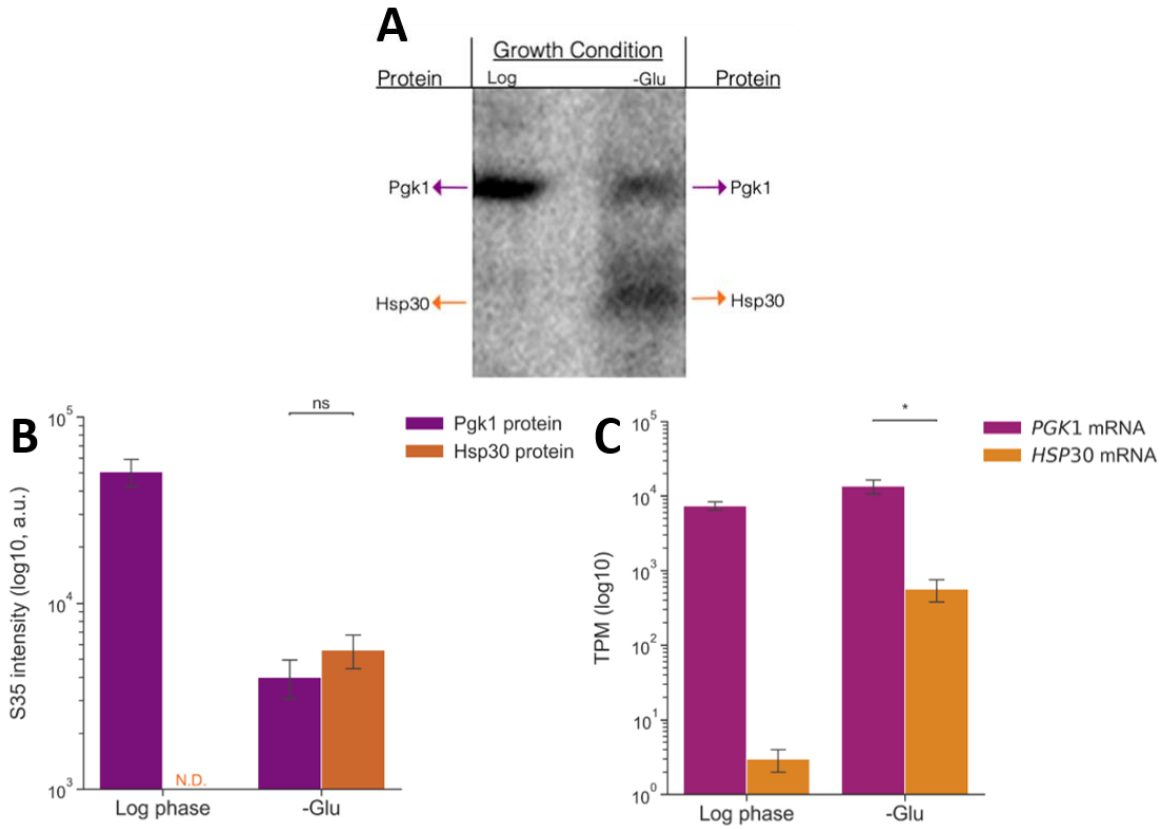

Figure 2.3: *Ribosomal occupancy on pre-existing mRNAs does not correlate with protein production* **(A)** Representative image of autoradiography exposure used to calculate radiolabeled S^{35} methionine incorporation in B. For each lane, immunoprecipitation was performed on the indicated TAP-tagged proteins from cell lysates grown to log phase and, for the right lane, glucose starved for 30 minutes. The volume of lysate loaded for the log phase sample (left lane) was $1/10^{th}$ the volume loaded of the glucose starved lysate. (**B)** S^{35} intensity from four biological replicates performed as described in C. (**C)** The TPM of ribosome protected fragment (RPF) reads from replicate log phase and glucose starvation ribosome profiling libraries plotted as mean ± sem. TPM = transcripts per million. a.u. = arbitrary units. For A and B values are plotted as mean ± sem from a minimum of four biological replicates. Statistical significance was assessed by unpaired Student's t-Test (***p<0.001; **p<0.01, * p<0.05, ns = not significant).

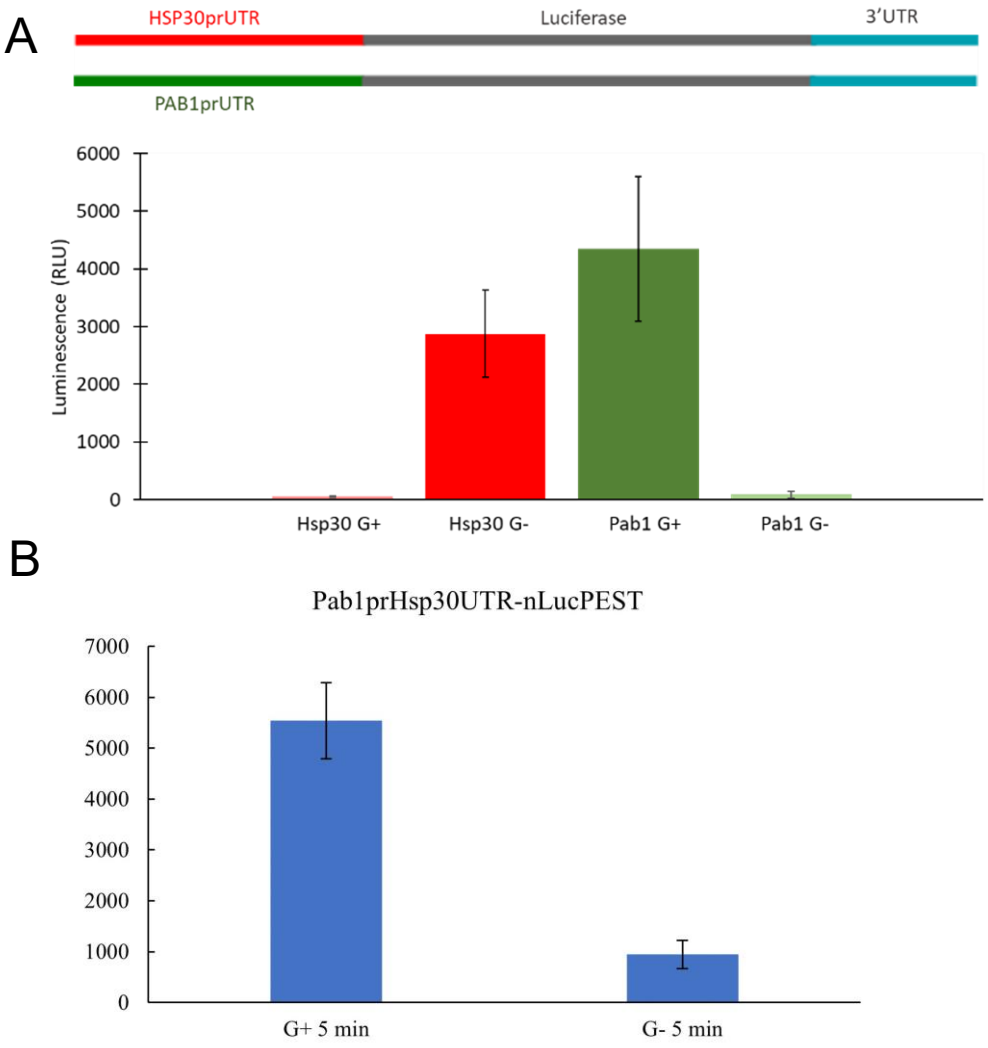

Figure 2.4: *Differential expression of nLucPEST during glucose starvation*
(A) Expression of nLucPEST reporters during early log phase and after 15 minutes of glucose starvation. **(B)** Expression of the nLucPEST reporter when downstream of the Pab1 promoter sequence and the Hsp30 5'UTR. Each bar represents the mean difference ± sem in luciferase signal detected during measurement between aliquots of untreated culture and the same culture treated with CHX.

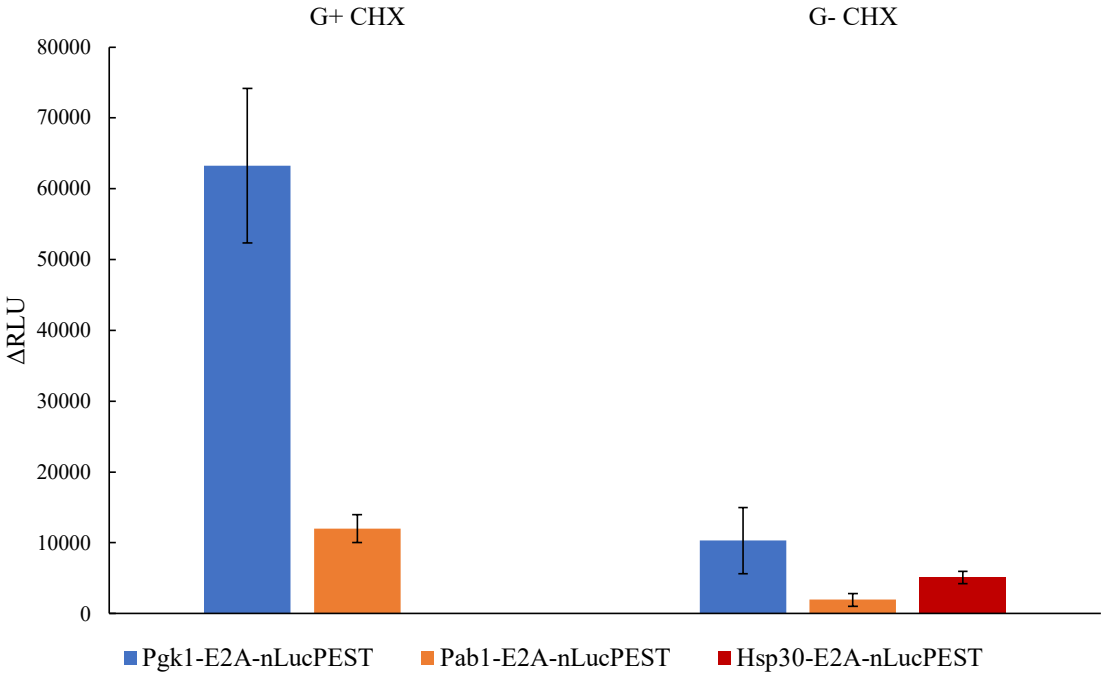

Figure 2.5: *nLucPEST tagged genes recapitulate the S^{35} data*
Expression of nLucPEST reporters C-terminally tagged to the endogenous genes investigated in Figure 2.3. Cultures were measured during early log phase and after 15 minutes of glucose starvation. Each bar represents the mean difference ± sem in luciferase signal detected during measurement between aliquots of untreated culture and the same culture treated with CHX.

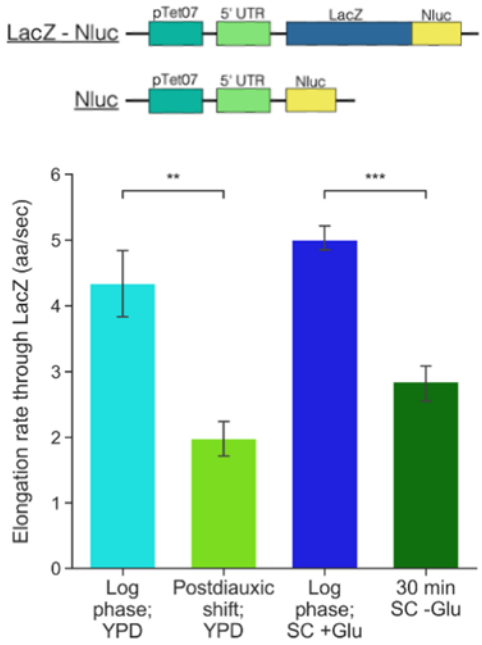

Figure 2.6: *Elongation rates drop during glucose starvation and the diauxic shift*
The elongation rate in amino acids per second (AA/sec) through LacZ calculated following reporter induction in the indicated growth and media conditions.

Figure 2.7: *Glucose readdition following starvation results in new initiation and continued elongation* **(A)** Normalized read density plots for glucose starved cultures after one minute (green; left) and five minutes (yellow; right) of glucose readdition. To generate read density plots the aggregate number of reads per nucleotide position across all genes >3000bp with > 25 reads per gene were included and normalized to enable inter-library comparison. (**B**) RPF reads per million by position for the indicated genes in log phase (purple), glucose starvation (orange), after one minute readdition (green), and five minutes readdition (yellow). **(C)** Schematic of reporters used to determine luciferase production in D. **(D)** Each bar represents the mean difference ± sem in luciferase signal detected during measurement between aliquots of untreated culture and the same culture treated with the indicated translation inhibitor from a minimum of six biological replicates. For log phase and 30 min -Glu conditions the signal was recorded after 5 minutes of treatment and the difference was calculated and plotted on the y-axis. For readdition, the signal difference was taken at the indicated time points and plotted. Statistical significance was assessed by paired Student's t-Tests for differences in luciferase production between cultures that underwent either LTM or CHX treatment, respectively, paired against luciferase production from the same culture without treatment (***$p<0.001$; **$p<0.01$, * $p<0.05$, ns = not significant).

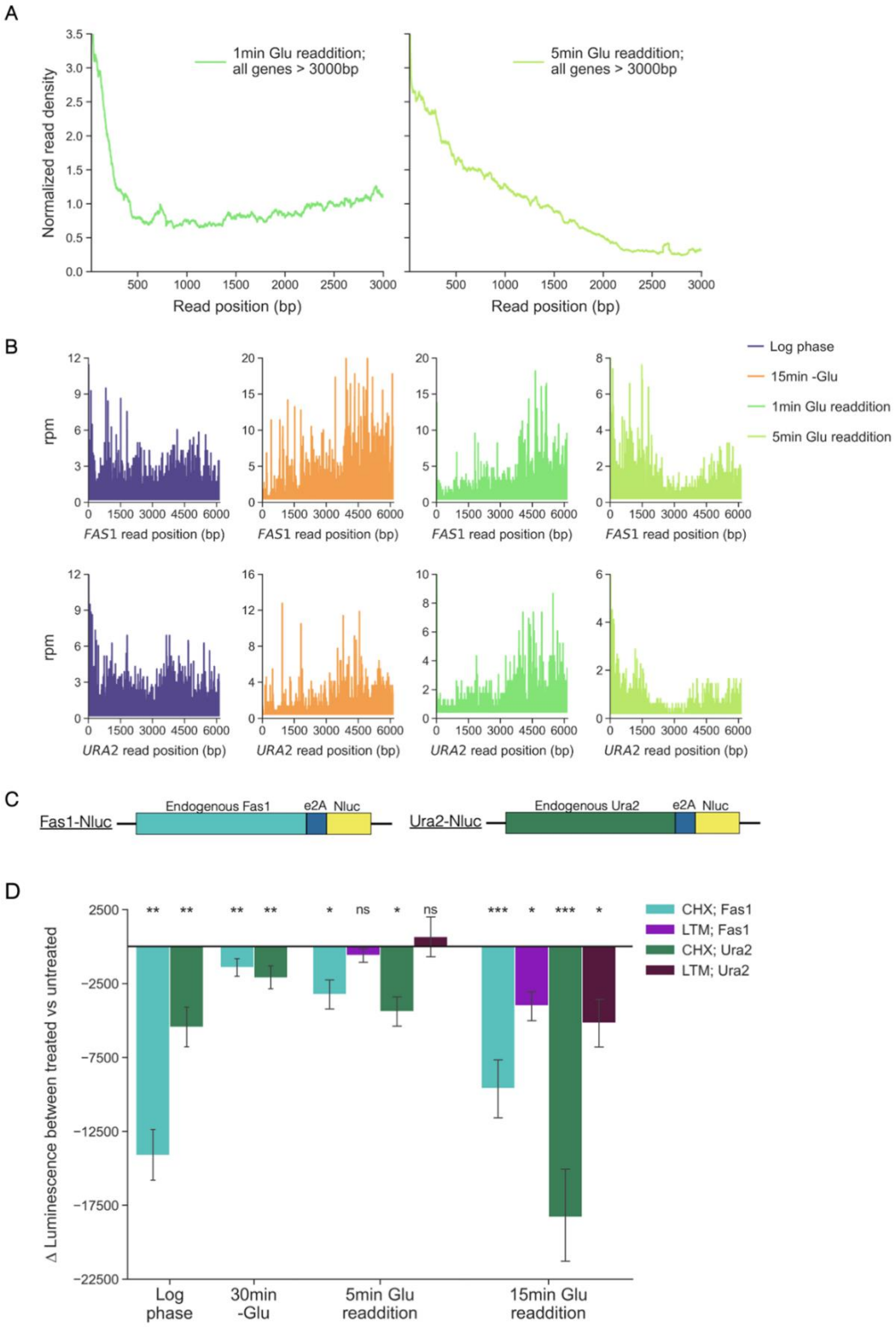
A
Normalized read density
1min Glu readdition;
all genes > 3000bp
5min Glu readdition;
all genes > 3000bp
Read position (bp)
Read position (bp)
B
rpm
FAS1 read position (bp)
URA2 read position (bp)
Log phase
15min -Glu
1min Glu readdition
5min Glu readdition
C
Fas1-Nluc
Endogenous Fas1
e2A
Nluc
Ura2-Nluc
Endogenous Ura2
D
Δ Luminescence between treated vs untreated
CHX; Fas1
LTM; Fas1
CHX; Ura2
LTM; Ura2
Log phase
30min -Glu
5min Glu readdition
15min Glu readdition

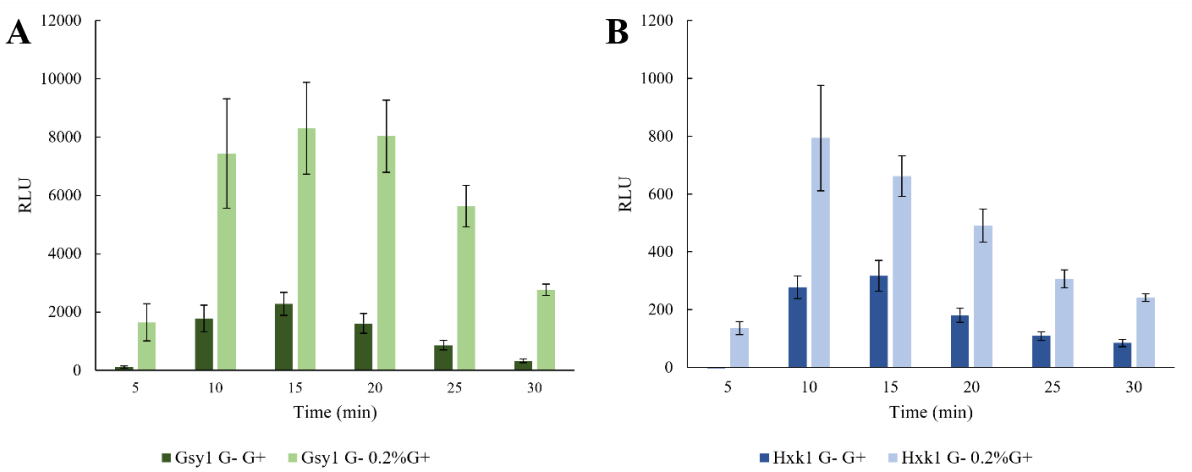

Figure 2.8: *A transient surge in protein expression occurs after glucose readdition for mRNAs transcribed during glucose starvation*

(A) Strains expressing Gsy1-E2A-nLucPEST were subjected to glucose starvation for 30 minutes. Glucose was returned to cultures at final concentrations of either 2% or 0.2% *(w/v)*. Protein expression was quantified relative to cultures concurrently treated with CHX. Assay measurements were taken at the corresponding timepoints following glucose readdition. **(B)** Glucose readdition of a strain expressing Hxk1-E2A-nLucPEST.

2.4 Discussion:

Here, we explored the distribution of ribosomes across yeast mRNAs during acute glucose starvation to better understand how yeast regulate protein synthesis during stress. Notably, we found that many pro-growth mRNAs retain relatively robust ribosome occupancy, but the distribution of these ribosomes skew towards the 3' end and they have positive polarity scores. These results contrast with those for well-translated stress-induced genes like *HSP30*. We hypothesize this altered ribosome distribution is driven by cessation of initiation followed by an elongation slowdown. Examining this observation concordantly with reports of polysome collapse during glucose starvation leads us to posit a nuanced interpretation of ribosome runoff in response to glucose starvation. Specifically, in the initial seconds following glucose removal, elongation continues at a rate comparable to pre-stress, log phase elongation. This rapid ribosome transit causes ribosomes to finish translating shorter genes, which we show are more likely to display a decrease in RO, as their short CDSs inherently require less time for runoff to take place. Then, as the duration of acute stress continues and seconds turn to minutes, ribosome transit slows more and more. This leads to an accumulation of downstream ribosome engagement on mRNAs of sufficient length such as *PGK1*. Meanwhile, shorter genes are more devoid of ribosomes. As the shortest yeast mRNAs tend to code for ribosomal proteins and ribosomal biogenesis genes, we conclude one way yeast responds to acute glucose starvation and downregulates bulk protein synthesis quickly is by reducing expression from these short transcripts. Conversely, comparatively longer, glycolytic genes like *PGK1* remain in the polysome to a larger degree, perhaps to retain their ability to quickly produce protein if glucose is reintroduced to the environment for subsequent, rapid metabolism.

In addition to ribosome profiling, we explored how glucose starvation impacts protein production in living cells. *In vivo* measurements of elongation rate using nLuc reporters showed elongation is slower during acute glucose starvation compared to log phase. Similar effects took place during the postdiauxic shift, a less acute manner of glucose starvation. While there has been a growing

appreciation in recent years for the importance of translation regulation at the step of elongation, much of this work has focused predominantly on codon-specific effects as it has been well-established that certain motifs cause ribosome elongation to stall and activate ribosome quality control pathways (Park and Subramaniam, 2019; Presnyak et al., 2015; Weinberg et al., 2016). Our findings are indicative of a more general phenomenon as elongation rates differ on the same LacZ-nLuc reporter in a condition-dependent manner. This is also apparent in the results of our promoter driven nLuc reporters. nLuc expressed from the Pab1 promoter is not readily translated during glucose starvation but is upregulated when driven by the Hsp30 promoter.

Our results also indicate that slowed and paused ribosomes are primed to resume elongation and finish translation if environmental conditions continue to fluctuate, but in a favorable way. Specifically, we show that long mRNAs can undergo translation from ribosomes bound before glucose readdition. Greater protein production was measured upon glucose readdition than would otherwise be expected from new initiation alone as samples treated with the initiation inhibitor LTM show no significant difference in protein expression during the first five minutes of glucose readdition. This indicates the expression detected comes from pre-existing ribosomes. We speculate that such pausing may allow for a population of mRNAs to remain bound to ribosomes for rapid continuation of growth once stress has been relieved, provided the duration of the stress is not too long. Additionally, the shift in ribosome distribution towards positive polarity which takes place upon the postdiauxic shift and acute glucose withdrawal suggests the general slowdown in elongation we identify during glucose starvation may play an important role in fine tuning translation during metabolic transitions to alternative carbon sources and metabolic pathways more generally, though this remains to be tested.

It would also be interesting to determine how this would relate at the individual cell level, as it has been demonstrated by single-cell microfluidics that subpopulations of cells exist prior to and during starvation, following a bimodal bet-hedging strategy (Bagamery et al., 2020). One population favors a rapid-growth state poorly prepared for adverse conditions, while others favor a more conservative

quiescent one more adaptive to stress but a reduced fitness in a glucose rich environment. Single-cell sequencing approaches are still in their infancy, but very recent advancements in ribosome profiling have also begun to probe the single-cell level. A recent study by (VanInsberghe et al., 2021) reported patterns of codon-specific translational pausing correlated to distinct stages of the cell-cycle. As the field develops, approaches at the single-cell level should provide further insight into the mechanistic responses to stress that are averaged together at our global point of view.

Additionally, we demonstrate that glucose readdition also results in the transient surge of mRNAs transcriptionally upregulated during glucose starvation but poorly translated. This surge is more pronounced when low levels of 0.2% (w/v) glucose are added, a concentration below the threshold of 0.6% (w/v) by which severe inhibition of translation occurs (Castelli et al., 2011). These findings agree with the gene ontology of these mRNAs, as this class of mRNAs is dominated by alternative glucose metabolism genes (Zid and O'Shea, 2014). During glucose starvation there is no available carbon source, which may lead the cell to prioritize the translation of more immediate stress response genes such as the heat shock proteins. Glucose limitation is more akin to the gradual depletion of glucose leading into the diauxic shift when these genes are expressed in the transition to respiratory growth. Intriguingly, ribosome profiling of these mRNAs during glucose starvation appears to show increased ribosome occupancy around the AUG start codon but not in the downstream open reading frame. Glucose readdition assays with LTM to inhibit initiation as performed previously are difficult, as the low ribosome count near the start codon would leave little signal above background. However, the mechanisms that lead to the differential localization and repressed translation of these stress-induced mRNAs remain interesting topics for future investigation.

It is important to note that, though we compared elongation rates along identical mRNA sequences, we did not simultaneously test how fast elongation takes place on populations of mRNAs transcribed prior to glucose starvation compared to mRNAs transcribed during glucose starvation. This is due to experimental limitations imposed by inducible reporters, an approach necessary to ensure that

elongation rate calculations were not muddled by detecting protein expression from pre-stress reporter transcription events while only intending to measure protein production that takes place during stress. Given the necessity of inducing reporter expression after stress to measure elongation rates during stress, we conjecture that our calculated elongation rate, though slower than it is during log phase, still overestimates the elongation rate that would be observed for ribosomes moving along mRNAs that were transcribed during log phase prior to the onset of stress. This is based on our observation that ribosome engagement with pre-existing mRNAs remains abundant, even during glucose starvation, though protein synthesis from them is greatly reduced. As such, we think the elongation rate of approximately two amino acids per second we calculated for LacZ in glucose starvation is more comparable to the elongation rate along a stress-responsive gene such as *HSP30*, which is both transcribed and translated in response to stress and is not pre-existing. The elongation rate on *PGK1*, a pre-existing transcript poorly translated during stress but with high ribosome occupancy, would be even slower. Future experimental approaches to parse the difference in elongation rate during stress on mRNAs transcribed pre-stress compared to mRNAs transcribed during stress would provide more insight into this nuance.

Finally, while our previous results indicate there is a strong dependence on the promoter sequence with respect to localization and competency for translation during stress (Zid and O'Shea, 2014), we cannot rule out that the timing of transcription itself is another key determinant in cytoplasmic RNA fate more generally. For example, it is possible that a copy of *PGK1* mRNA transcribed before stress would be somehow differentially marked or associated with proteins compared to a copy transcribed during stress. Those mRNAs, though coding the same gene, could be regulated in contrasting ways. Future work in this vein would further elucidate the importance of transcription timing with regards to acute stress and parse how important timing is for localization to either P-bodies or stress granules independent of mRNA sequence motifs. Additionally, further investigation is necessary to determine the mechanism or mechanisms that mediate the general slowdown in elongation we characterized in response to acute glucose starvation in yeast. Such a mechanism would have to

allow for discrimination between pre-existing and stress-induced genes. Indeed, mechanisms that facilitate the expression of stress-induced genes like heat shock proteins during severe stress have been a topic of extensive and detailed study for decades and understanding how they work in concert with repressive mechanisms will be crucial to fully understanding how organisms adapt gene expression in response to acute stress.

2.5 Materials and Methods

2.5.1 Yeast strain information

Yeast strains used are listed in Table 2.1. Strains with either TAP-tagged Hsp30 or Pgk1 were from the Yeast-TAP Tagged ORF library collection (Ghaemmaghami et al., 2003). For luciferase measurements during glucose readdition, the E2A-nLucPEST sequence was inserted into a pKT vector (Sheff and Thorn, 2004) containing a hygromycin selection marker. Endogenous genes were tagged with E2A-nLucPEST through the integration of PCR products including 40 bp overhangs homologous to the sequence immediately upstream and downstream of the 3'-end of the target gene. P_{TetO7}-LacZ-nLucPEST and P_{TetO7}-nLucPEST were assembled into a pRS305 integration vector with homology for the LEU2 locus. Polysome profiling was performed with strain ZY185. Plasmid pST1760 (Tanaka et al., 2015) was integrated in strain EY0690. Endogenous Dhh1 was C-terminally tagged by PCR amplification of a 3xmini auxin inducible degron from plasmid pST1932 (Tanaka et al., 2015) with homology for the 3'-end of Dhh1. Yeast transformations were performed using lithium acetate/PEG as previously described (Ito et al., 1983).

2.5.2 Polysome profiling

800mL cultures of strain ZY185 were inoculated in SC media and grown overnight to early log phase (0.4-0.6 OD_{600}). 400mL were rapidly filtered, washed, and resuspended in SC -G media to begin glucose starvation. The remaining half of the glucose replete culture was rapidly filtered, and the cell paste was scraped into liquid nitrogen for flash freezing. 1.2mL of polysome gradient lysis buffer (20mM Tris-Cl (pH 7.5), 140mM KCl, 2 mM $MgCl_2$, 100 µg/mL CHX, 20 U/mL SUPERase•In™ (Invitrogen), 1% Triton X-100) was flash frozen dropwise with the cell paste. After 15 minutes of glucose starvation, SC -G cultures were filtered down and the cell paste was flash frozen with 1.2mL of lysis buffer. Cell pastes were stored at -80°C. Cell lysis was performed by cryogenic ball milling for 4x3 minute cycles and cooled with liquid nitrogen between each cycle. The resulting lysates were gently thawed to room temperature in a water bath and treated with DNase I (12.5 U/mL). Lysates were

centrifuged at 4°C for 5 min at 3000xg and the supernatant was centrifuged once more for 10 min at 20,000xg. Approximate concentrations were estimated by A_{260} measurements.

A 7-47% sucrose gradient in polysome gradient buffer without Triton X-100 was prepared with a gradient maker. Clarified supernatants were added and centrifuged at 4°C for 3 hours at 35,000RPM in a Beckman SW41Ti rotor. The gradient was fractionated into 1 mL aliquots using a gradient fractionator and UA-6 detector (Isco/Brandel). Polysome traces were monitored through absorbance measurements at 254nm. 2 ng of *in vitro* transcribed renilla luciferase (rLuc) RNA was added to each aliquot as a spike-in control. Transcription reactions were performed with a mMESSAGE mMACHINE™ T7 Transcription Kit according to manufacturer's instructions and RNA was purified with acid phenol:cholorform extraction (Invitrogen). After adding the rLuc spike-in, 600µL of Guanidine HCl and 600µL isopropanol were added to 400uL of each fraction and incubated overnight at -20°C. Fractions were centrifuged at 10,000g for 25 minutes to isolate RNA pellets. Samples were washed with 70% EtOH and resuspended in 400µL of TE buffer. Cleanup was performed by precipitation with 40 µL of NaOAC and 2.5 volumes of 100% EtOH. Samples were centrifuged for 25 min @ 10,000xg, pellets were washed with 70% EtOH, dried, and resuspended. Fractions corresponding to free RNA, 80S, disome/trisome, and dense polysomes were pooled and the RNA was then treated with RQ1-DNase (Promega) and reverse transcribed with Protoscript® II Reverse Transcriptase (NEB), both according to manufacturer's instructions. qPCR measurements with SYBR green were performed with the cDNA libraries and primers designed for each respective gene. The 18S rRNA primer set was adopted from (Cankorur-Cetinkaya et al., 2012). CT values for the rLuc spike-in were used to normalize variance in cDNA concentration arising due to sample cleanup and RT efficiency.

2.5.3 S^{35} methionine and autoradiography

15mLs of tap-tagged strains were grown in SC media lacking histidine (SC -His) to an OD_{600} of 0.4. Two cultures of *HSP30-TAP* and *PGK1-TAP* of equal OD were then mixed to make 30mLs. Cultures were pelleted, resuspended, and grown in SC -His and 0.01x methionine for 30 minutes. To

15mLs of this combined culture, 0.2 mCi of [^{35}S] methionine-cysteine (EXPRESS[^{35}S] protein labeling mix; Perkin-Elmer) was added and incubated at 30°C for 30 minutes. To the remaining 15mLs, cells were pelleted and resuspended in SC -G, -His, 0.01x Met + 0.2 mCi [^{35}S] and incubated at 30°C for 30 min. Labeled cells were pelleted and lysed in 400uL RIPA buffer (50mM Tris pH 8, 1% NP-40, 0.1% SDS, 0.5% Sodium Deoxycholate, 150 mM NaCl) with glass beads. Supernatants were isolated before being applied to immunoprecipitation with IgG-coupled beads. Dynabeads M270 Epoxy were coupled with IgG as described previously (https://commonfund.nih.gov/sites/default/files/Conjugation-of-Dynabeads.pdf).

Supernatants were incubated with Dynabeads for 30 minutes at RT, then washed 3 times with RIPA buffer. The Dynabeads were then resuspended in 25µl of 1× loading buffer (50mM Tris, pH 7.0, 2.5% sodium dodecyl sulfate [SDS], 0.02% bromophenol blue, 10% glycerol), and TAP-tagged proteins were eluted from the beads with moderate heat treatment at 65°C for 10 min. Loading buffer was transferred to a new tube, and 2-β-mercaptoethanol was added to a final concentration of 200mM. Samples were boiled for 5 min, and 20µl was loaded and resolved on 4-20% polyacrylamide gradient gels followed by autoradiography and quantitation with a PhosphorImager (Molecular Dynamics). Signal intensity was quantified using background subtraction and the 'rectangles' option in Quantity One software (Bio-Rad).

2.5.4 Nanoluciferase Reporter Assays

nLuc assays were adapted from methods previously described (Masser et al., 2016). Briefly, cells were grown in SC media and added to a 96-well plate. Promega Nano-Glo® substrate was diluted 1:100 with PBS and added 1:10 to each well immediately prior to measurement. Luminescence was measured every 30 seconds with a Tecan Infinite® 200 PRO plate reader. For glucose starvation, cells were sedimented by centrifugation, washed 2x with SC -G media, and resuspended in SC G- media for 30 minutes of incubation at 30°C with rotating. 20% glucose was added with the substrate to monitor expression upon glucose readdition. For CHX-treated samples, 10 mg/mL CHX in deionized H_2O was

added to achieve a final concentration of 100 µg/mL. For LTM-treated samples, 3.5mM LTM in DMSO was added to achieve a final concentration of 3.5µM. To measure elongation rates during the diauxic shift log phase cultures were inoculated in YPD media at 0.1 OD_{600} and incubated overnight. Assays were performed on the cultures at the indicated timepoints afterwards using the same methods described above.

2.5.5 Elongation Measurements

Doxycycline was added to a final concentration of 10 mg/ml to induce transcription of the LacZ-nLuc and nLuc reporters in liquid culture. Luciferase expression was monitored as described in the preceding section. Data was linearized using Schleif plots to estimate the minimum reaction time required for complete translation (Dai et al., 2016; Schleif et al., 1973).The reaction time of the nLuc reporter was subtracted from the reaction time of LacZ-nLuc to calculate the time required for translation of the LacZ sequence alone. An RNA transcription speed of 2000nt/min was used to calculate the estimated time required to transcribe the LacZ sequence (Mason and Struhl, 2005). Subtracting the transcription time from the LacZ reaction time provides the elongation rate for LacZ.

2.5.6 Yeast growth and glucose starvation for RNA-seq and ribosome profiling

Ribosome profiling experiments were performed with strain BY4741 grown in batch culture at 30°C with shaking at 250rpm to OD600 between 0.4-0.6 for all log phase samples. Synthetic complete (SC) media with 2% (w/v) glucose was used to grow cells for all acute starvation experiments. Glucose starvation was performed in SC media prepared without glucose (SC -G). For each starvation sample, half the volume of a culture was filtered for transfer to SC -G media while the other half remained incubating in glucose replete media in log phase, non-stressed conditions. Cells were collected with a vacuum filtration apparatus onto cellulose filter membranes. For glucose starvation, the cells were collected, quickly rinsed in 50-100mL of pre-warmed SC -G media, re-filtered, and resuspended in prewarmed SC -G with continued rotation at 30°C for either 1 minutes, 5 minutes, 10 minutes, 15 minutes, 20 minutes, or 30 minutes, as indicated. Log phase cells still in SC media were harvested while

starvation samples were incubating in SC -G. For glucose readdition experiments, cultures that underwent starvation were supplemented with a 2% (w/v) final concentration of glucose added back to the media with continued shaking at 30°C for the indicated times prior to harvest. For the multi-day growth experiments, yeast was grown in liquid YPD (2% peptone, 1% yeast extract, 2% dextrose). Samples were collected at log phase (0 day), postdiauxic shift (1 day), and stationary phase (5 day) conditions as in 60. Following vacuum filtration, all cells were flash frozen in liquid nitrogen and stored at -80°C until library preparation.

2.5.7 RNA-seq and ribosome profiling library preparation

For CHX-pretreatment log phase, glucose readdition, and glucose starvation samples, libraries were prepared in (Zid and O'Shea, 2014). Briefly, prior to harvesting, CHX was added to a final concentration of 100µg/mL for 1 min with continued shaking at 30°C. Cells were pulverized under cryogenic conditions, extracts were digested with RNase I, and RPFs were isolated from monosome fractions via sucrose gradient sedimentation. Then, 28mer RPFs were selected, polyadenylated, and reverse transcribed. RNA-seq libraries from these samples were prepared following or poly(A)+-selected RNA using Oligo(dT) Dynabeads (Invitrogen), also as described in (Zid and O'Shea, 2014).

Libraries that did not undergo CHX-pretreatment, including log phase, acute glucose starvation, postdiauxic shift, and stationary phase samples, were prepared according to previously published methods 61 with minor modifications. Briefly, after cells were flash frozen, they were ground with yeast footprint lysis buffer (20 mM Tris-Cl (pH8.0), 140 mM KCl, 1.5 mM MgCl2, 1% Triton X-100) via cryogenic ball milling with boiling in liquid nitrogen between cycles. Lysates were thawed, digested with RNase I (Epicentre), and monosomes were isolated with size exclusion chromatography 62. RPFs were separated and size-selected via TBE-Urea PAGE. Next, footprints underwent dephosphorylation with T4 PNK and linker ligation with T4 enzyme Rnl2(tr) K227Q (NEB). Ligation reactions were excised following separation and size-selection on a TBE-Urea gel and pooled. Next, pools underwent reverse transcription with Protoscript II (NEB), circularization with CircLigase II (Lucigen),

quantification with qPCR, and PCR amplification. Libraries were sequenced at the Institute for Genomic Medicine sequencing core at UC San Diego on an Illumina HiSeq 4000.

2.5.8 Ribosome profiling bioinformatic analysis

For libraries prepared with CHX-pretreatment, read trimming and alignment took place as described in (Zid and O'Shea, 2014). For libraries prepared without CHX-pretreatment, read trimming and alignment took place as follows. First, unprocessed fastq files were trimmed with Cutadapt 63 to remove the adapter sequence AGATCGGAAGAGCAC. Reads less than 17bp or without adapters were discarded. For files that required manual demultiplexing, Cutadapt was used again to demultiplex with a custom fasta containing the barcode sequence corresponding to a given biological sample. Next, Cutadapt output files had their unique molecular identifiers (UMIs) removed from the read line of the fastq and appended to the header line with a custom python script for subsequent deduplication of PCR artifacts. Next, reads were aligned to S. cerevisiae ncRNA using bowtie 64 with the following flags: -k 1 --best -t -S -q. Reads that did not align to ncRNA were filtered to remove low quality reads based on Phred score with fastqx_toolkit (http://hannonlab.cshl.edu/fastx_toolkit/). Those that passed this quality control step were aligned against the S. cerevisiae genome. Index files generated via bowtie were from genome assembly R64-1-1 (SGD). Next, files were deduplicated with custom python scripts. Read features were counted using htseq-count 65, feature files were also obtained from SGD using genome assembly R-64-1-1. To calculate polarity scores per gene custom python scripts were run based on (Schuller et al., 2017). All scripts are available upon request and sequencing data has been deposited at the NCBI GEO database with accession number ***.

2.5.9 Yeast gene length calculations

Median yeast gene length was calculated from information retrieved from the Saccharomyces genome database (SGD) on June 21st, 2021 (https://yeastmine.yeastgenome.org/yeastmine/bagDetails.do?scope=all&bagName=Verified_ORFs). The median length was calculated from the list of 5,195 genes categorized as verified ORFs.

Table 2.1: *Yeast strains used in this study*

Strain	Genetic Background	Reference source
BY4741	MATa his3Δ1 leu2Δ0 met15Δ0 ura3Δ0	Euroscarf
EY0690	(W303) MATa trp1-1 leu2-3 ura3-1 his3-11 can1-100	
P_{TetO7}-nLuc only reporter	BY4741, P_{ERV14}-rtTA::URA3, P_{TetO7}-NlucPEST-MS2(v4)::HIS3	This study
P_{TetO7}-LacZ-nLuc reporter	BY4741, P_{ERV14}-rtTA::URA3, P_{TetO7}-LacZ-NlucPEST-MS2(v4)::HIS3	This study
Pgk1 TAP tag	S288C: (ATCC 201388: MATa his3Δ1 leu2Δ0 met15Δ0 ura3Δ0)	Yeast-TAP Tagged ORF library collection (Horizon Discovery)
Hsp30 TAP tag	S288C: (ATCC 201388: MATa his3Δ1 leu2Δ0 met15Δ0 ura3Δ0)	Yeast-TAP Tagged ORF library collection (Horizon Discovery)
ZY185	EY0690, HIS3 OsTIR1, tTA, TetR'-SSN6, Dhh1-3xmini-AID-5xFlag-KanMX	This study
Fas1-E2A-nLucPEST	EY0690, Fas1::E2A-nLucPEST::HIS3	This study
Gsy1-E2A-nLucPEST	EY0690, Gsy1::E2A-nLucPEST::HIS3	This study
Hxk1-E2A-nLucPEST	EY0690, Hxk1::E2A-nLucPEST::HIS3	This study
Pab1-E2A-nLucPEST	EY0690, Pab1::E2A-nLucPEST::HIS3	This study
Ura2-E2A-nLucPEST	EY0690, Ura2::E2A-nLucPEST::HIS3	This study

Table 2.2: *qPCR primers used in this study*

qPCR Gene and Primer Set	Forward Primer	Reverse Primer
18S rRNA (ZO995/996)	AATCATCAAAGAGTCCGAAGACATTG	CCTTTACTACATGGTATAACTGTGG
Acc1 (ZO1014/1015)	TTTCTGCCATTTTCTCTACTCC	TGTTCAGTTCTTTCCTTGACC
Act1 (ZO83/84)	CTGCCGGTATTGACCAAACT	CGGTGATTTCCTTTTGCATT
Fas1 (ZO787/788)	CGCTGCATCATTCTCTCAAG	TTGACGATTTCAACCAACCA
Hsp30 (OS262/263)	TTGGACTGGTGTTCAAGCTG	CAGGACAAGAACCAGGCAAT
Hsp104 (OS803/804)	CGACGCTGCTAACATCTTGA	CACTTGGTTCAGCGACTTCA
Pab1 (ZO95/96)	TCTCTGTGTTTGGTGACATCTT	TTGGCAGCACCTTCTTCTT
Pgk1 (OS773/774)	GGACAAGCGTGTCTTCATCA	CGTTTCTTTCACCGTTTGGT
RPS8A (ZO952/953)	TCAACCAGCCAACACCAAG	CAGAAGCCCAAGAAAAGTTACC
Ura2 (ZO1018/1019)	ATTCCCCGCTTACACGAAC	AACACCAGAACCCAAGACC
nLuc (ZO553/554)	TGGTGATCAAATGGGTCAAA	CCTTCATAAGGACGACCAAA

Acknowledgements

Chapter 2, in part, consists of material from a manuscript submitted for publication as it may appear in RNA Biology, 2022, entitled “Differential translation elongation directs protein synthesis in response to acute glucose deprivation in yeast,” by Anna R. Guzikowski, Alexander T. Harvey, Jingxiao Zhang, Shihui Zhu, Kyle Begovich, Cohn, M.H.; James E. Wilhelm, and Brian M. Zid. The dissertation author is the second author of this work.

Chapter 3: Quantification of elongation rate effects through synonymous codons

3.1 Abstract

Ribosomal pauses are a critical part of co-translational events including protein folding and localization. However, extended ribosome pauses can lead to ribosome collisions, resulting in the activation of ribosome rescue pathways and turnover of protein and mRNA. While this relationship has been known, the specific threshold between permissible pausing versus activation of rescue pathways has not been quantified. We have taken a method used to measure elongation time and adapted it for use in *S. cerevisiae* to quantify the impact of elongation stalls. We find that in transcripts containing a strong, localized stall, a Hel2-mediated dose-dependent decrease in protein and mRNA expression and increase in elongation delay. In transcripts containing synonymous substitutions to nonoptimal codons, we find a decrease in protein and mRNA expression and similar increase in elongation delay but through a non-Hel2-mediated mechanism. This indicates that different distributions of poor codons in a transcript will activate different rescue pathways despite similar elongation stall durations. Finally, we find that Dhh1 selectively increases protein expression, mRNA expression, and elongation rate. Taken together, these results provide new quantitative mechanistic insight into the surveillance of translation and the roles of Hel2 and Dhh1 in mediating ribosome pausing events.

3.2 Introduction

Production of cellular proteins through translation is crucial for maintaining homeostasis and adapting to changing environmental conditions. Translation can be broken down into three sequential steps: initiation, during which ribosomes assemble at the initiation site on an mRNA, elongation, during which ribosomes translocate across the mRNA and build upon a nascent peptide, and termination, during which ribosomes are removed from the mRNA, recycled, and the newly synthesized protein is released. Cells dedicate many resources to the monitoring, regulation, and quality control of protein synthesis as dysregulation may lead to aberrant cellular function and neurological diseases such as ALS (Bosco, 2018; Wang et al., 2016).

Each step in the translation process is governed by various regulatory steps. Initiation has long been known to be the primary rate-limiting step of translation and subject to intense regulation (Shah et al., 2013; Sonenberg and Hinnebusch, 2009). Recent studies have focused on elongation as another important regulatory step in protein synthesis. Indeed, modulation of elongation speed has been shown to serve a functional role in both proper protein folding (Hartl et al., 2011; Pechmann and Frydman, 2013; Spencer et al., 2012; Yu et al., 2015; Zhao et al., 2021) and localization (Alamo et al., 2011; Mason et al., 2000; Ogg and Walter, 1995; Tsuboi et al., 2020). These examples give credence to the notion that ribosome pausing is essential for certain cellular processes. Recent reports using ribosome profiling to analyze disome peaks have estimated that upwards of 10% of translating ribosomes are engaged in the disome state (Arpat et al., 2020; Han et al., 2020; Zhao et al., 2021), indicating the commonplace occurrence of ribosome collisions.

The functional and necessary nature of ribosome stalls, however, makes it challenging for cellular machinery to distinguish between beneficial stalls and situations requiring ribosome rescue. Ribosomes that undergo translation on an aberrant mRNA, such as on a truncated mRNA, stall in place and are unable to be disassembled by translation termination machinery (Buskirk and Green, 2017; Joazeiro, 2017; Yip and Shao, 2021). Upon extended stalling events, translating ribosomes may collide

with stalled ribosomes, resulting in a ribosome collision which can eventually lead to further accumulation of collided ribosomes. Two pathways may be activated upon the detection of these collision events: (1) ribosome quality control (RQC), which leads to the rescue and recycling of stalled ribosomes, and (2) no-go decay (NGD), which leads to the endonucleolytic cleavage and subsequent degradation of the aberrant transcript (Ferrin and Subramaniam, 2017; Park and Subramaniam, 2019; Simms et al., 2017). Both pathways are triggered by the ribosome collision sensor Hel2(yeast)/ZNF598(mammals) which detects disome formations which form as a result of prolonged ribosome stalling (Ikeuchi et al., 2019; Juszkiewicz et al., 2018). In RQC, Hel2 ubiquitinates the small ribosomal subunit which leads to activation of the RQC trigger (RQT) complex in yeast, ultimately resulting in ribosome disassembly and degradation of the nascent peptide (Buskirk and Green, 2017; Joazeiro, 2017; Yip and Shao, 2021). Concurrently, Hel2 activation also leads to the activation of the NGD pathway which results in mRNA degradation primarily through the endonuclease Cue2 and the exonucleases Xrn1 and Ski7 (Buskirk and Green, 2017; D'Orazio et al., 2019; Navickas et al., 2020). Hel2 and other sensors of elongation quality must maintain a balance between permitting transient and functional stalls while at the same time engaging rescue pathways to prevent the buildup of ribosomes on problematic mRNA.

How elongation quality sensors can distinguish between functional stalls and those requiring rescue pathways remains unclear. It has been proposed that the severity of ribosome collision may determine which cellular response is activated in response to a collision event (Meydan and Guydosh, 2021). In support of this model, a recent study by Goldman and colleagues found that clearance of stalled ribosomes was far slower than elongation and termination and proposed that slow ribosome clearance allows cells to distinguish between transient and deleterious stalls (Goldman et al., 2021). While this model may explain how functional stalls and detrimental stalls either resume elongation or initiate RQC using the same surveillance pathways, respectively, the definition of "severity" in this context remains vague. Are the distinguishing factors the time duration of the stall, the number of

ribosome collisions (Goldman et al., 2021), the specific location and context of where the stall occurs on a transcript, or a combination of all these factors and more? It is from this lack of understanding of how cellular surveillance machinery can distinguish between these two opposing outcomes that necessitates reliable, quantitative methods to describe the various aspects of ribosome stalling events.

One important factor that contributes to elongation speed is codon optimality, a metric that describes the translational efficiency of the 61 amino acid specifying codons. The redundancy of the genetic code, which utilizes 61 codons to encode for only 20 amino acids, provides an additional layer of information by which cells can modulate the translation rates of otherwise similar polypeptide sequences (D'Onofrio and Abel, 2014). Codon optimality, unique to each species, takes into account various factors implicated in elongation rate, including tRNA availability and demand, frequency of use in the genome, GC content, and interactions with the ribosome exit tunnel (Gardin et al., 2014; Pechmann and Frydman, 2013; Presnyak et al., 2015; Reis et al., 2004). Furthermore, codon optimality has been found to correlate with elongation speed and mRNA decay, with transcripts enriched in "optimal" codons associated with faster elongation speed and lower mRNA decay rates and those enriched in "nonoptimal" codons associated with slower elongation speed and higher mRNA decay rates (Chu et al., 2011; Gardin et al., 2014; Hanson and Coller, 2018; Harigaya and Parker, 2016; Hussmann et al., 2015; Ingolia, 2014; Ingolia et al., 2009; Koutmou et al., 2015; Radhakrishnan et al., 2016; Saikia et al., 2016; Weinberg et al., 2016). While many studies, both *in vivo* and *in vitro*, have assessed the impact of synonymous codon substitutions on protein expression, mRNA decay, and ribosome pausing, quantification of the impact on elongation time has not been widely available.

In this study, we describe the development of an *in vivo* quantitative luciferase-based assay to measure elongation time. We assessed the time delay associated with acute stalls caused by the inclusion of repeats of the nonoptimal arginine codon CGA and find that elongation time increases in a dose-dependent manner. Surprisingly, we find that no-go mRNA decay reaches a maximum level at a specific stall length despite increasing translation elongation times and protein expression continuing to

decrease. Furthermore, we assessed the effect of synonymous codon substitutions on elongation time of a standardized ORF and identified the leucine codon CTT as a strong driver of elongation delay. CTT's effect on elongation time is dependent on its inclusion in the 5' end of the ORF. The development of this assay and our findings provide steps towards a detailed understanding of the triggers of ribosome quality control pathways.

3.3 Results

Although many studies have investigated the effects of synonymous codons on mRNA stability and protein expression, the quantification of the elongation rate for individual synonymous codons has not been well characterized. To create a quantitative elongation duration reporter assay, we utilized a tetracycline-inducible promoter to control mRNA induction of a bioluminescent nanoluciferase (nLuc) reporter downstream of open reading frames (ORFs) of interest. The nLuc reporter has been previously studied in yeast under the control of a stress-inducible promoter and its bioluminescent output faithfully recapitulates induced mRNA levels after heat shock (Masser et al., 2016). To test this system, we developed a series of constructs in which we varied the length of the upstream ORF by insertion of yeast-optimized yellow fluorescent protein (YFP) or yeast-optimized monomeric infrared red fluorescent protein (miRFP) ORFs upstream of nLuc (Figure 3.1A). nLuc protein expression was collected for each construct over 60 minutes and normalized to OD600 measured at T=0 min. Elongation time was calculated using a Schleif plot (Dai et al., 2016; Schleif et al., 1973) and adjusted based on an average mRNA transcription time of 1500 nucleotides per second (Mason and Struhl, 2005) (Edwards et al. 1991).

We find a delay in the first appearance of nLuc upon the addition of optYFP and a further delay in the longer miRFP-optYFP-nLuc reporter (Figure 3.1B). We then used these measured delays to calculate the translation elongation rate of optYFP and miRFP ORFs as approximately 4 AA/sec and 3 AA/sec (Figure 3.1C), respectively, which is consistent with bulk elongation rate measurements of 3-10 AA/sec (Karpinets et al., 2006; Riba et al., 2019). We do not find a significant difference in elongation rate between the two optimized ORFs. This implies that our reporter can quantify the in vivo translation rates of our reporters.

To quantify the duration of elongation pauses and assess their impact on gene expression, we classified elongation stalls into two categories: (1) acute stalls, which are characterized by a strong, localized internal stall made of nonoptimal codons within the ORF and (2) distributed stalls, which are

characterized by nonoptimal codons distributed throughout the ORF. To measure the effect of acute stalls on elongation time and gene expression, we developed a series of constructs in which we inserted between 2 and 6 tandem CGA repeats between the yeast-optimized YFP ORF and nLuc reporter ORF shown previously (Figure 3.2A). CGA codons have been previously shown to induce ribosomal stalling and reduce protein expression (Letzring et al., 2010; Veltri et al., 2021). First, we tested the protein expression of our induced constructs and found a dose-dependent exponential decline in protein production as the number of CGA codons increased, similar to a previous study by (Letzring et al., 2010) (Figure 3.2B). We, however, did not see an impact on protein expression until 3 CGA codons were included. Next, we measured mRNA expression and found that mRNA expression significantly decreased with the addition of 3 CGA codons but mRNA levels remained constant around 40% of our control construct regardless of additional CGA codons (Figure 3.2C). We then measured the elongation delay in each of our constructs by comparing to a control reporter lacking any CGA codons (Figure 3.2D). We found that elongation delay increased in a dose-dependent manner beginning at 3xCGAs, with 6xCGA causing an ~4.5 minute extension of the translation duration. There was a relatively linear relationship between CGA stall number after 3 CGAs and elongation time which allowed us to calculate that each CGA adds approximately 76 seconds to the overall elongation time.

We then asked whether the impact on gene expression seen in our CGA-containing strains was a result of Hel2-mediated effects. Hel2 is a translation surveillance factor that senses ribosome collisions and activates the ribosome rescue pathways of ribosome quality control (RQC) and no-go decay (NGD) which result in protein and mRNA turnover, respectively. We measured protein expression in our constructs containing 2, 4, and 6 CGAs in a *hel2Δ* background and we compared it to their wild type (WT) counterparts (Figure 3.3A). We found that deletion of Hel2 partially rescued protein expression in the 4xCGA and 6xCGA. We next measured RNA expression in our 2xCGA, 4xCGA, and 6xCGA strains and found that RNA expression was increased in our 4xCGA and 6xCGA-containing strains but there was no change in the 2xCGA strain (Figure 3.3B). Together, these results

imply Hel2-mediated RQC and NGD are partially responsible for the observed decrease in protein and RNA expression, respectively, in the wild-type strains. Lastly, we sought to measure the impact of Hel2 on elongation time. A recent review by Meydan and Guydosh proposed two non-mutually exclusive models of Hel2's activity on the stability of ribosome collisions: (1) Hel2 is necessary to rescue stalled ribosomes and Hel2 deletion would result in further buildup of collided ribosomes and (2) Hel2 stabilizes collided ribosomes and Hel2 deletion would result in reduced ribosomal pausing (Meydan and Guydosh, 2021). To assess the effect of Hel2 on ribosome pausing and distinguish between these two models, we compared the elongation time of our control, 4xCGA, and 6xCGA strains between WT and *hel2Δ* backgrounds and found no significance in our control strain but a decrease in overall elongation time in our 4xCGA and 6xCGA strains when expressed in a *hel2Δ* background (Figure 3.3C). This suggests that Hel2 functions to slow down elongation in our CGA-containing strains and is consistent with the second proposed model in which Hel2 stabilizes collided ribosomes.

Next, we asked how distributed slowdowns of non-optimal codons impact gene expression and elongation time. To study the impact of distributed non-optimal codons, we used our optYFP-nLuc construct and synonymously substituted the first 20 of 21 leucines for a nonoptimal leucine variant (Table 3.1). First, we wanted to determine the impact of these synonymous substitutions on overall elongation time. We measured the elongation time in each of our strains and compared it to the optimized strain to determine the elongation time delay associated with each synonymous substitution (Figure 3.4A). We found that substitution of the optimal leucine codon TTG for the nonoptimal codons CTC and CTT resulted in a significant delay in elongation time of approximately 0.5 and 2.5 minutes, respectively. Due to the statistically significant differences in elongation time, we selected both the CTC and CTT-containing constructs for further study. Next, we measured the impact of codon substitution on protein and RNA expression (Figure 3.4B-C). We compared the protein and RNA expression of our YFP[CTT] and optYFP constructs 60 minutes post-mRNA induction. Relative to optYFP, we found that substitution with CTC codons reduced both protein and RNA expression by approximately 20% while

substitution with CTT codons reduced protein and RNA expresion by 50%. As both protein and mRNA expression dropped to approximately the same normalized level, we reasoned that the drop in protein expression could be explained by the decrease in mRNA levels.

Subsequently, we sought to determine whether the increase in elongation time and decrease in protein expression observed was either contributed equally by each non-optimal codon or due to the specific placement of non-optimal codons in the YFP ORF. To assess this, we created a set of chimeric reporters in which the first 10 leucines of the YFP ORF were either optimal or nonoptimal followed by the next 10 leucines of the opposite optimality. We hypothesized that if each codon contributed equally to elongation time, the elongation time delay of our chimeric constructs would be half of the delay between optYFP and YFP[CTT]. Instead, we found that both the elongation delay and protein expression of our chimeric YFP[CTT/TTG] closely resembled YFP[CTT] and that our chimeric YFP[TTG/CTT] closely resembled YFP[TTG] (Figures 3.5A-B, left panels). This provides evidence that substitution of leucines to a nonoptimal variant in the 5' half of the YFP ORF is sufficient to drive protein expression and elongation time outcomes.

A recent study by Chu and colleagues showed that poor codons in the 5' region of a transcript could negatively affect translation initiation through ribosome buildup preventing initiation from occurring upstream, thereby reducing overall translational output (Chu et al., 2014; Hanson and Coller, 2018). To test if the observed decrease in protein expression was a result of interference with initiation, we inserted a yeast-optimized miRFP (315 amino acids) upstream of our optYFP-nLuc and YFP[CTT]-nLuc constructs. We hypothesized that, if initiation was negatively impacted by ribosome buildup, the addition of a long yeast-optimized ORF upstream of the nonoptimal YFP[CTT] would rescue protein expression as compared to the optimal construct. Instead, we found that a statistically significant difference remained between the optimal and CTT-containing nonoptimal constructs (Figure 3.5B, right panel). Furthermore, we assessed the impact on elongation time and found that elongation time was not rescued back to WT levels and the magnitude of delay is similar to the YFP[CTT] construct (Figure

3.5A, right panel). This suggests that the decrease in protein expression in YFP[TTG] is a result of the specific placement of the nonoptimal CTT codons within the 5' half of the YFP ORF, but is not dependent on close proximity to the initiation start site.

Subsequently, we wanted to investigate if Hel2 or other translation sensors were responsible for the negative impacts on gene expression in our nonoptimal codon substituted constructs. Of particular interest was the RNA binding protein Dhh1, a conserved DEAD-box helicase previously shown to have roles in mRNA decapping and translational repression (Carroll et al., 2011; Coller and Parker, 2005; Coller et al., 2001; Fischer and Weis, 2002; Tseng-Rogenski et al., 2003). Importantly, it has been shown to bind preferentially to mRNA with low codon optimality and has also been proposed to slow down ribosome movement (Radhakrishnan et al., 2016; Sweet et al., 2012). We hypothesized that the negative impacts on gene expression observed in YFP[CTC] and YFP[CTT] compared to the optYFP control may be a result of either Hel2 or Dhh1 influence. To test this, we transformed our optYFP, YFP[CTC], and YFP[CTT] constructs into either a *dhh1Δ* or *hel2Δ* strain.

First, we assessed the impact of protein expression on our constructs in a *dhh1Δ* or *hel2Δ* background (Figure 3.5A). Based on Dhh1's role in mediating translation repression of transcripts enriched with nonoptimal codons, we expected to see no impact in optYFP expression and a rescue of protein expression for YFP[CTC] and YFP[CTT]. Instead, we found differing effects for each construct; deletion of Dhh1 slightly increased protein expression of our optYFP construct, decreased protein expression of our YFP[CTC] construct, and had no statistically significant impact on our YFP[CTT] construct. We also found that Hel2 deletion had no statistically significant effect on protein expression for any of our constructs. This suggests that the drop in protein expression seen in the nonoptimal constructs was not due to a Hel2-mediated mechanism and is distinct from our acute CGA-containing constructs. Next, we examined the effect of Dhh1 on mRNA expression by comparing WT and *dhh1Δ* mRNA levels (Figure 3.5B). We found that deletion of Dhh1 decreased mRNA expression in our YFP[CTC] construct but had no statistically significant difference in the other constructs. The negative

impact of Dhh1 deletion in our YFP[CTC] construct was of similar magnitude in both protein and mRNA expression. This suggests that Dhh1 increases the mRNA levels of our YFP[CTC] construct which leads to increased protein production.

Lastly, wanted to determine the impact of the *dhh1Δ* and *hel2Δ* backgrounds on the elongation time of our substituted leucine constructs. We measured elongation delay by comparing the elongation times of our constructs in each deletion strain relative to the WT background (Figure 3.5C). We found that deletion of Dhh1 increased elongation delay in our optYFP and YFP[CTC] strains, suggesting that Dhh1 functions to speed up elongation for these constructs. However, we found no statistically significant difference in elongation time for our YFP[CTT] construct. Additionally, we found no statistically significant difference in elongation times in our *hel2Δ* strains. This is consistent with the *hel2Δ* protein expression data and supports the idea that a non-Hel2-mediated pathway is responsible for the negative impact on gene expression in our substituted leucine constructs.

Based upon our previous study of YFP[CTT], we were curious if the elongation rate slowdown for CTC codons in the *dhh1Δ* background was also dependent on the first 10 leucine codons. We created a set of chimeric reporters for CTC and assessed them in both the wildtype and the *dhh1Δ* strain (Figure 3.6A). Unlike the impaired translation driven by CTT codons in the wildtype background, there does not appear to be a strong dependence on nonoptimal leucine codons located in the first half of the YFP ORF Both YFP[TTG/CTC] and YFP[CTC/TTG] have large elongation delays compared to optYFP. Intriguingly, there is also not a significant difference between the chimeric reporters and YFP[CTC], suggesting that at least 10 CTC codons are required to impair YFP translation but additional CTC codons are not additive to this defect. This effect is also not observed in the wildtype strain, as the small elongation delay of YFP[CTC] is much reduced for YFP[TTG/CTC] and retained for YFP[CTC/TTG].

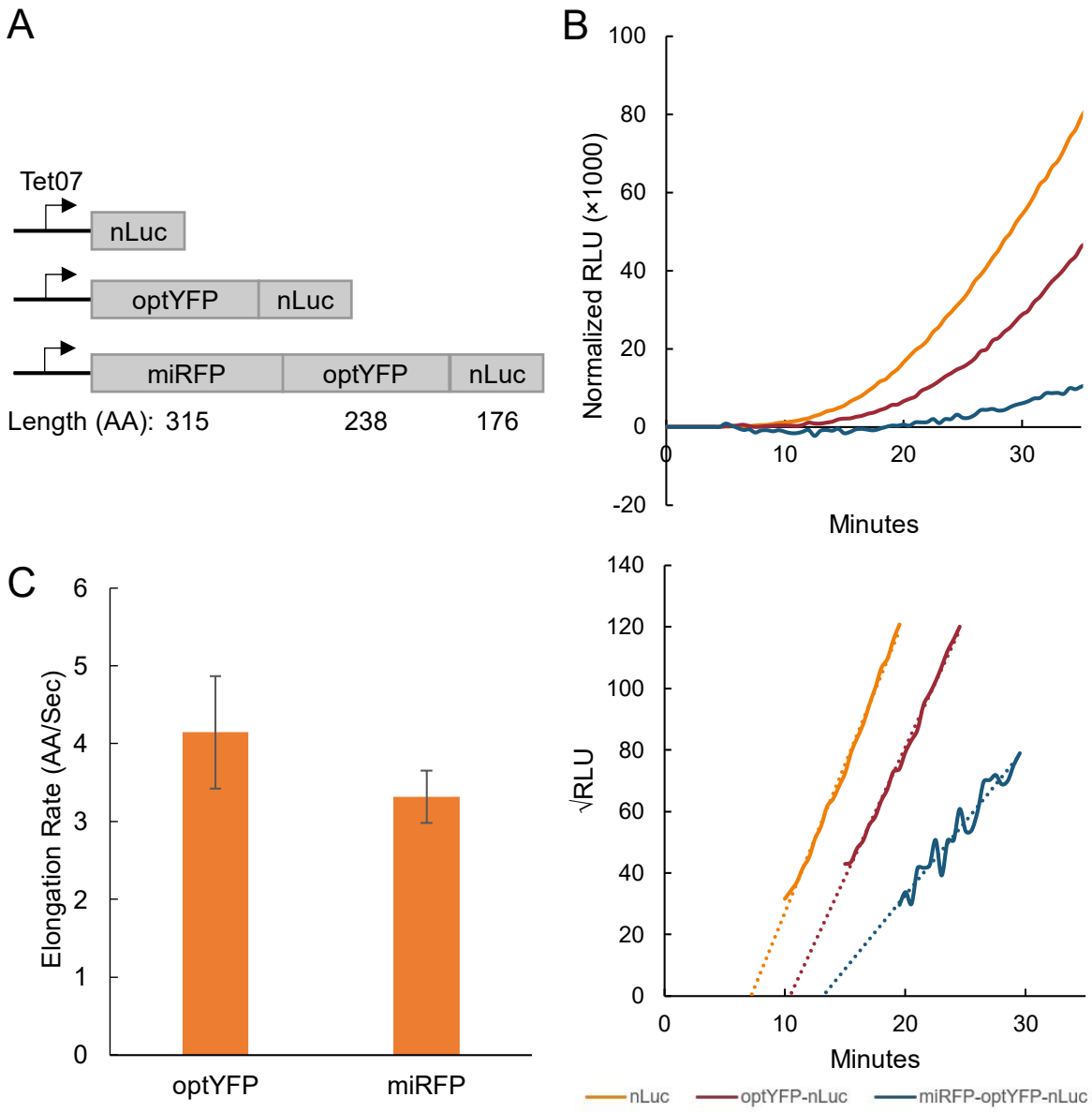

Figure 3.1: *Assay validation via elongation rate measurements*
(A) Diagram of yeast-optimized constructs of various lengths. Optimized YFP (optYFP) or both optYFP and optimized miRFP (miRFP) are set upstream of a nanoluciferase (nLuc) reporter. Constructs are expressed from an inducible Tet07 promoter. **(B)** (Top) Representative assay data of relative light units (RLU) of each construct over time normalized to OD600. (Bottom) Schleif plot and associated trendlines of the top graph. **(C)** Calculated elongation rate measurements of optYFP (n=9) and miRFP (n=4) ORFs. Error bars indicate SEM.

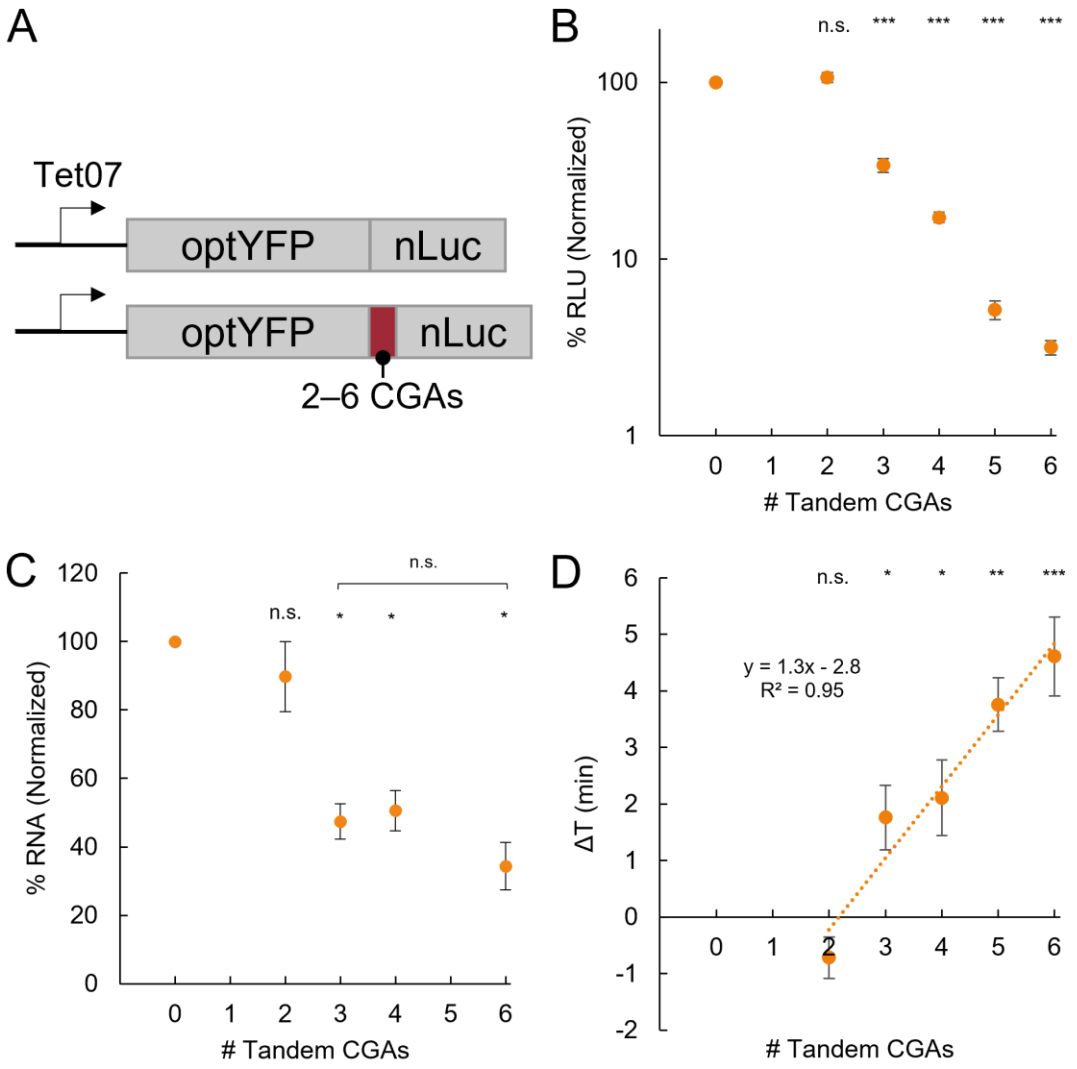

Figure 3.2: *CGA-derived acute stalls negatively impact gene expression in a dose-dependent manner* **(A)** Diagram of optimal and CGA-containing constructs. Between 2 and 6 CGAs are inserted between the optYFP and nLuc ORFs. **(B)** Protein expression of CGA constructs at T=60 min normalized to optimized control (2xCGA n=10, 3xCGA n=8, 4xCGA n=10, 5xCGA n=5, 6xCGA n=10). **(C)** mRNA expression of CGA constructs at T=60 min normalized to optimized control. (n=3). **(D)** Elongation delay of CGA-containing constructs compared to optimized control. (n=3). All error bars indicate SEM. All statistical significances were calculated for each construct using two-tailed paired Student's t-Test against optYFP control).

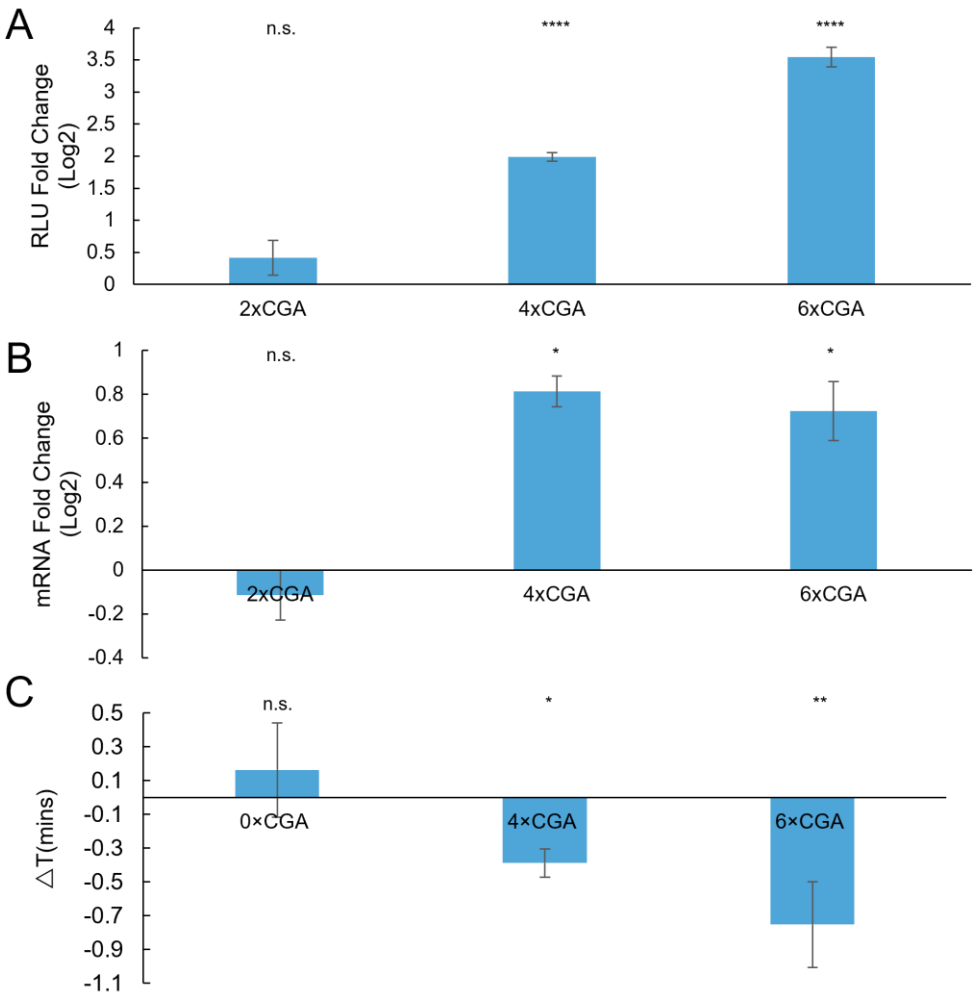

Figure 3.3*: Hel2 deletion rescues protein expression, mRNA expression, and elongation time.* **(A)** Protein expression fold change of CGA constructs in a *hel2Δ* vs WT background (2xCGA n=2, 4xCGA n=7, 6xCGA n=7). **(B)** mRNA expression fold change of CGA constructs in a *hel2Δ* vs WT background (n = 3). **(C)** Elongation delay of CGA constructs in a *hel2Δ* vs WT background (n = 3). All error bars indicate SEM. All statistical significances were calculated for each construct using two-tailed paired Student's t-Test against WT control.

Table 3.1: *tAI scores of leucine codons used in this study*

Leucine Codon	TAI	Use	Construct
TTG	0.754	0.29	optYFP
CTC	0.062	0.06	YFP[CTC]
CTA	0.185	0.14	YFP[CTA]
CTT	0.027	0.13	YFP[CTT]
CTG	0.059	0.11	YFP[CTG]

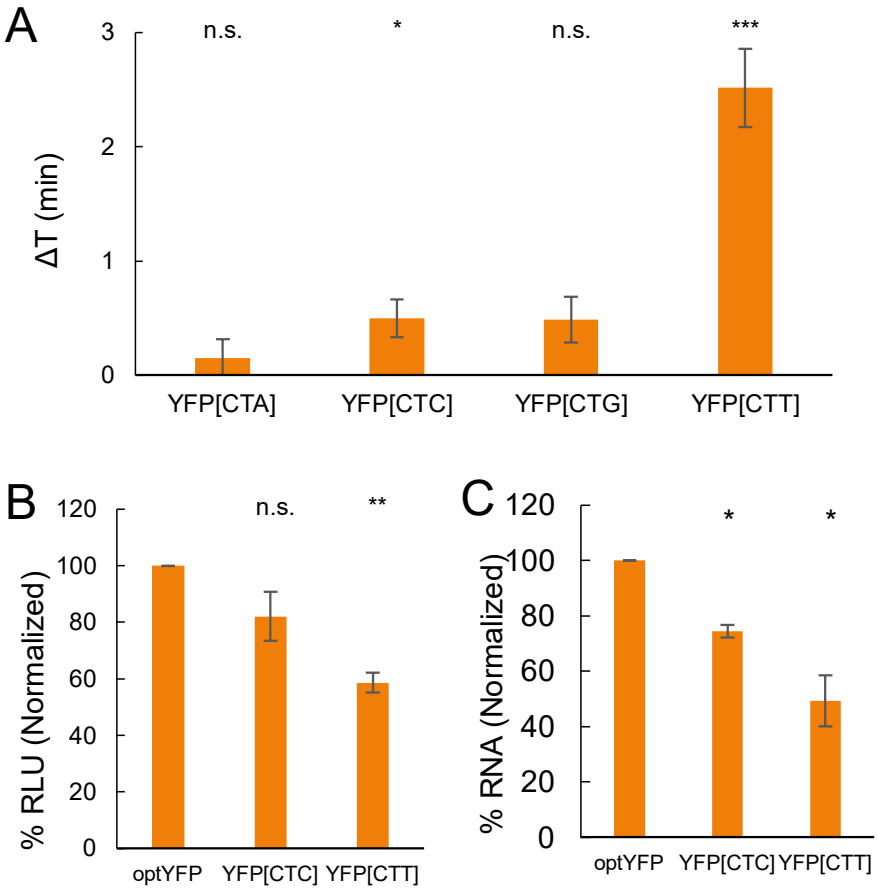

Figure 3.4: *Distributed stalls in the YFP ORF decrease protein expression, mRNA expression, and delay elongation time*

(A) Elongation delay of distributed stall constructs compared to optYFP (CTA n=6, CTC n=6, CTG n=5, CTT n=7). The first 20 out of 21 total optimal TTG leucine codons in optYFP are synonymously substituted to a nonoptimal codon specified in brackets. **(B)** Protein expression of distributed stall constructs normalized to optYFP control (n=4). **(C)** mRNA expression of distributed stall constructs normalized to optYFP control (n=3). All error bars indicate SEM. All statistical significances were calculated for each construct using two-tailed paired Student's t-Test against optYFP control unless otherwise specified (***p<0.001; **p<0.01, * p<0.05, n.s. = not significant).

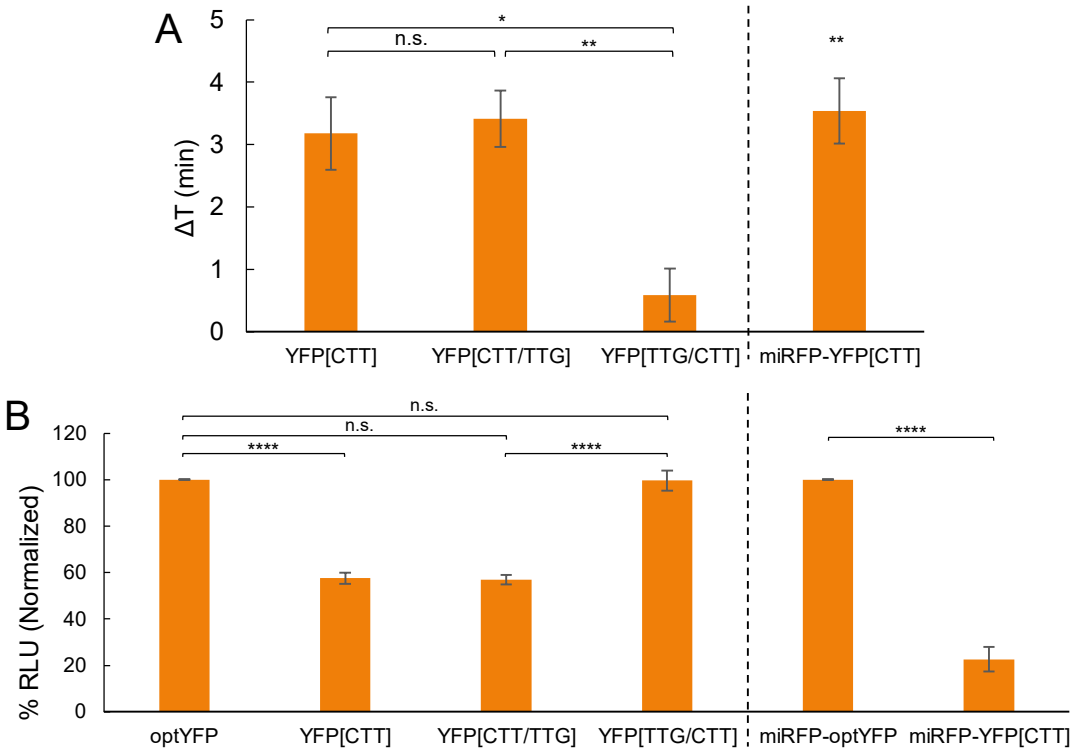

Figure 3.5: *CTT codons slow elongation rate independently of proximity to the 5'end*
(A) (Left) Elongation delay measurements of chimeric constructs normalized to optYFP control (n=9). (Right) Elongation delay measurements of miRFP-YFP[CTT] normalized to miRFP-optYFP control (n=6). **(B)** (Left) Protein expression chimeric constructs normalized to optYFP control (n=5). (Right) Protein expression of miRFP-YFP[CTT] normalized to miRFP-optYFP control (n=6). All error bars indicate SEM. All statistical significances were calculated for each construct using two-tailed paired Student's t-Test against optYFP control unless otherwise specified (***p<0.001; **p<0.01, * p<0.05, n.s. = not significant).

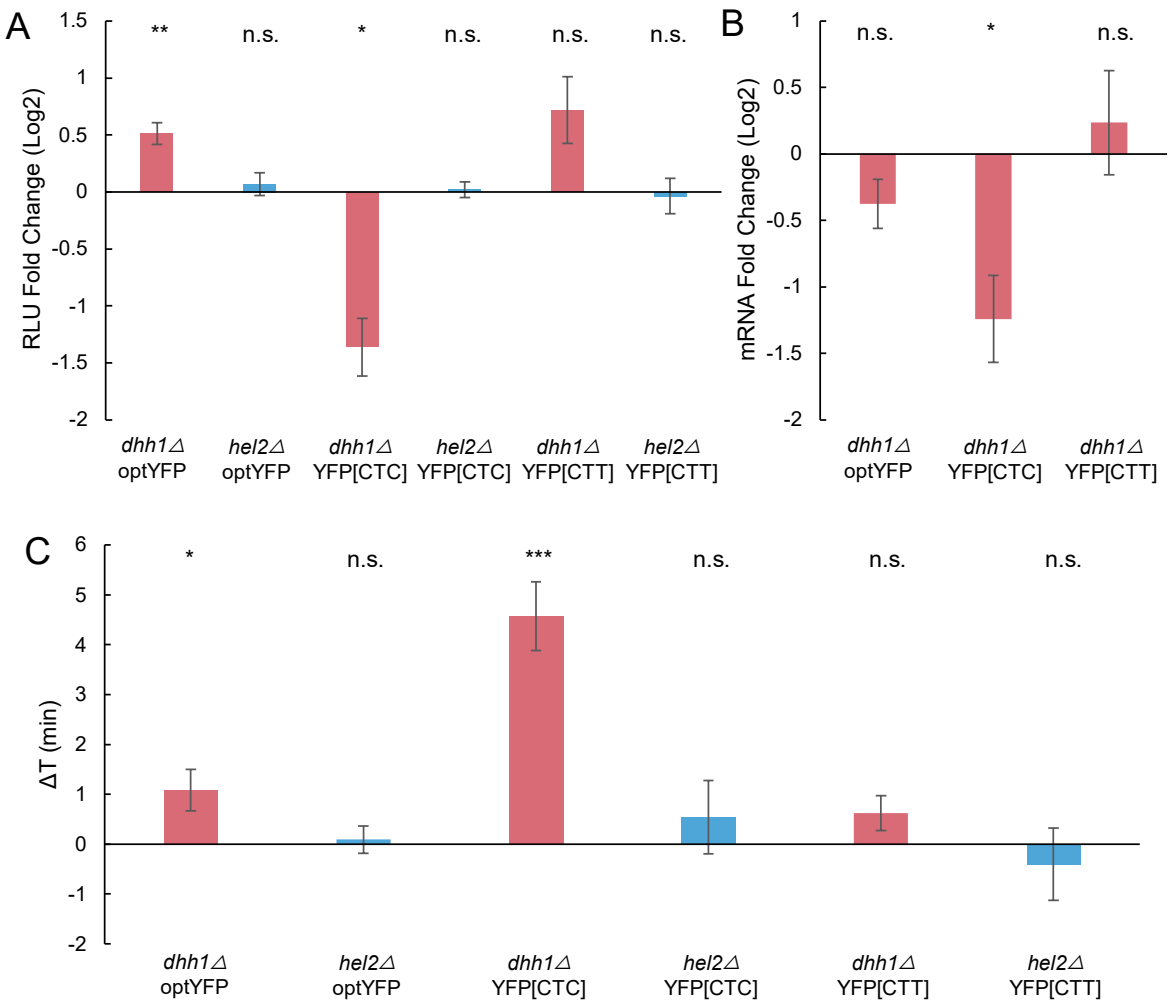

Figure 3.6: *Dhh1 deletion decreases the elongation rate for YFP[CTC] and reduces both mRNA and total protein levels*

(A) Protein expression of distributed stall constructs in *dhh1Δ* or *hel2Δ* background vs WT (n=5, n=4, n=4, n=5, n=7, n=3, respectively). **(B)** mRNA expression fold change of distributed stall constructs in a *dhh1Δ* vs WT background (optYFP=5, CTC=4, CTT=7). RNA was extracted from cell pellets collected 60 minutes after ATC induction. RNA was reverse-transcribed and measured by qPCR. **(C)** Elongation delay of distributed stall constructs in *dhh1Δ* or *hel2Δ* background vs WT (n=19, n=4, n=18, n=6, n=9, n=5, respectively). Total nLuc luminescence was measured 60 minutes after ATC induction and used as a proxy for relative protein production. All error bars indicate SEM. All statistical significances were calculated for each construct using two-tailed paired Student's t-Test against WT control (***p<0.001; **p<0.01, * p<0.05, n.s. = not significant).

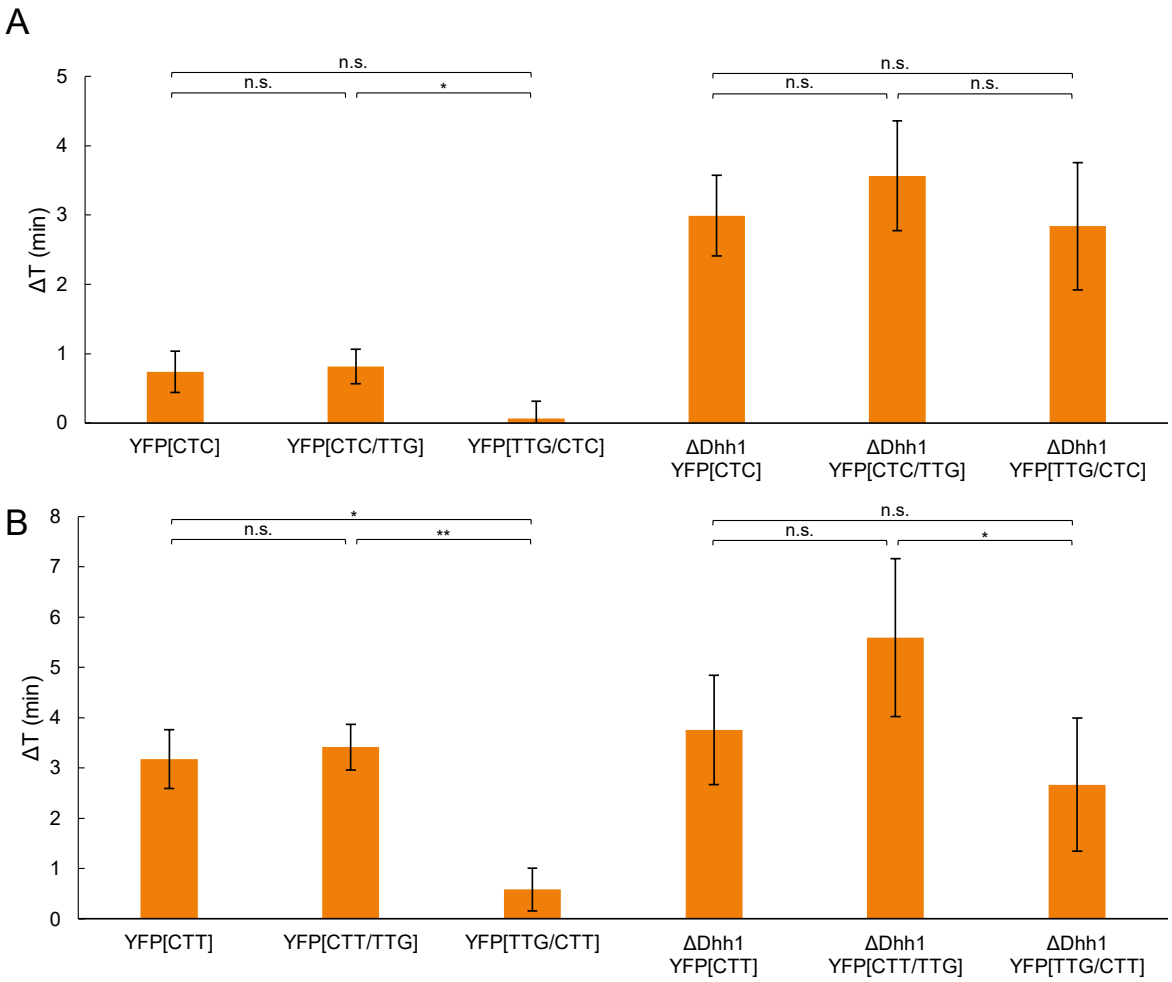

Figure 3.7: *Dhh1 deletion decreases the elongation rate of both CTC chimeric reporters* **(A)** Elongation delay measurements of CTC chimeric constructs normalized to optYFP control (Wildtype n=12, *dhh1Δ* n=8). **(B)** Elongation delay measurements of CTT chimeric constructs normalized to optYFP control (Wildtype n=9, *dhh1Δ* n=4). All error bars indicate SEM. All statistical significances were calculated for each construct using two-tailed paired Student's t-Test against optYFP control unless otherwise specified (***p<0.001; **p<0.01, * p<0.05, n.s. = not significant).

3.4 Discussion

Ribosome stalling and the connected quality control pathways are important for recognizing faulty and damaged mRNAs, yet quantitative measurements of how these stalls impact translation duration have been lacking. In this study, we developed a reporter assay to quantify the *in vivo* elongation time of various constructs containing stalling sequences in *S. cerevisiae*. Using CGA stalling reporters we find that total elongation time increases in a dose-dependent manner corresponding with the number of tandem CGA repeats while protein expression decreases logarithmically with increasing CGA repeats. Strikingly, we find that mRNA levels stabilize upon reaching a specific stall length, suggesting that the stall-activated NGD pathway rescues a maximum decay rate at 3xCGA. Interestingly, the ~50% reduction in mRNA levels is very similar to the mRNA reduction reported for a completely independently designed reporter containing 12xCGA (Veltri et al., 2021) and other reporters containing 10xAAG (rare poly-lysine codon) or 8xCCG (rare poly-proline codon) stalling sequences (Park and Subramaniam, 2019), further supporting NGD may be saturated at relatively shorter translational stalls.

From our synonymous leucine substitution constructs, we find that the nonoptimal codon CTT causes substantial delays in elongation time on the order of minutes. The elongation delay of ~ 150s for the CTT reporter is very similar to the elongation delay for our 4xCGA stalling reporter. Yet these two reporters behave very differently as the decrease in protein expression due to CTT could be explained completely by decreased mRNA levels, while the 4xCGA decreased protein levels to an even larger extent then the ~50% decrease in mRNA levels. This pointed to the induction of RQC, which reduces protein expression on the CGA stalls through ribosome rescue. Further supporting this induction of RQC on CGA stalls but not CTT stalls, deletion of the RQC factor could partially rescue the mRNA levels and protein production of CGA stalls, yet it had no significant effect on protein production and elongation times due to non-optimal CTT codons. These data point to further differentiation of ribosome stalling beyond just stall duration timing.

While 20 synonymous Leu codons were changed to poor CTT codons, not all non-optimal codons contribute equally to the elongation slowdown. Instead, the second set of 10 Leu codons had no measurable effect on elongation or protein production, while the first 10 Leu were sufficient to impact elongation and protein production. This appear to be caused by local sequence effects and not specifically the poor codons being in the 5' end of the ORF, as adding an upstream miRFP ORF was not able to rescue the translation slowdown and reduced protein production. This argues that local sequence context is important for determining the effects of codon optimality on gene expression. This fits with reports showing that specific combinations of codons modulate translation efficiency and mRNA decay (Burke et al., 2021; Gamble et al., 2016).

We found that CGA stalls added ~76s per CGA codon to the translation duration of the reporter after 3xCGAs. This led to an almost 5 minute lengthening of translation duration for a 6xCGA construct. A recent paper by Goldman and colleagues examined ribosomal clearance times on mRNA containing difficult-to-translate polyA-containing stretches and found it took approximately 10 and 13 minutes for ribosomes to clear off 50% of transcripts containing poly(A)36 and poly(A)60 stretches, respectively (Goldman et al., 2021). Their finding on delays lasting on the order of minutes is consistent with our findings and represents an intriguing observation considering that the average half-life of yeast mRNAs is ~10 minutes, suggesting that a significant portion of an mRNA's half-life can be spent engaged in a ribosomal stall (Chan et al., 2018). Furthermore, we were surprised that substitution of a relatively small percentage of codons (20 out of 176 coding codons in YFP; approximately 11%) was sufficient to increase elongation time by minutes. Considering ribosome pauses and their role in co-translational protein folding, recognition of localization signals on nascent proteins, and overall protein output, inclusion of these significantly-slowing codons may be a useful mechanism to add an extended pause on the order of seconds when necessary during elongation with a single codon.

Previous research suggests that Hel2 senses stalled ribosomes and mediates surveillance pathways such as RQC and NGD. Throughout RQC and NGD pathways, nascent peptides and

detrimental mRNA will be degraded respectively to help cells survive. Theoretically, within a Hel2-depletion strain, both protein production and mRNA expression will be rescued since we kill RQC and NGD pathways. We found Hel2 deletion rescues mRNA level back to WT levels, while partially rescuing protein expression, which proposes that protein production is influenced by multifaceted ways.

It is well-confirmed that Hel2 is a necessary factor mediating RQC and NGD pathways however its effects on ribosome stalling have been unclear. Two non-mutually exclusive models have been proposed: first, since Hel2 is needed to promote the rescue of the stalled ribosome in a collision complex, deletion of Hel2 will slow ribosome rescue, resulting in accumulated collided ribosomes, which increases elongation delay; In second model, we propose that Hel2 is able to sense and stabilize stalled ribosomes to prevent further translation. In this scenario, deletion of Hel2 would destabilize collided ribosomes, resulting in rescued elongation and shorter elongation delay. In this paper, we quantitatively measure the change of elongation delay after Hel2 depletion and find a reduction in the translation duration of CGA stalled sequences. This is distinct from mammalian cells, where depletion of the mammalian homolog of Hel2, ZNF598, causes further delays in the clearing of ribosomes.

It has been previously reported that Dhh1 plays a role in degradation of mRNA enriched in nonoptimal codons. However, Dhh1 deletion does not rescue mRNA levels of the YFP[CTT] construct and in fact decreases the expression of the YFP[CTC] construct. As the YFP constructs used in this study are all yeast codon-optimized apart from the leucine codons, it is possible that Dhh1 deletion would only be beneficial for mRNAs highly enriched in poor codons. Previous work demonstrates a negligible effect of Dhh1 deletion on mRNA half-life for primarily optimal mRNA (Radhakrishnan et al., 2016). The Dhh1 deletion background also presents a slowdown in growth rate compared to the wild type (120 minutes per doubling time versus 90 minutes for the wildtype background). This general slowdown in growth may result in a small slowdown of elongation that, in combination with the slowdown due to CTC codons, results in the YFP[CTC] construct slowing down sufficiently to cause

increased ribosome collisions and reductions in mRNA stability independently of direct effects due to the Dhh1 deletion.

Although most studies have investigated Dhh1 with regards to its role in mRNA decay and translational repression, Dhh1 has also been shown to promote the translation of certain proteins as well. It has been previously demonstrated that a subset of mRNAs that contain highly-structured 5'UTRs and coding sequences require Dhh1 helicase activity for efficient expression (Jungfleisch et al., 2017). The increased GC content of CTC codons may contribute to motifs more reliant on Dhh1-specific helicase and the analysis of mRNA secondary structure with RNAfold does predict changes in the location of probable secondary structure within the early ORF region previously reported by (Jungfleisch et al., 2017), however specific structures reliant on Dhh1 are unclear, as the CTC chimeric reporters were not significantly different in elongation rate.

Furthermore, Dhh1 can shift roles in a condition-dependent manner. During nitrogen starvation, Dhh1 is required for the efficient expression of autophagy-related proteins Atg1 and Atg13, but when nutrients are plentiful Dhh1 encourages ATG mRNA degradation (Liu et al., 2019). Overall, this argues that Dhh1 may play context specific roles in translation elongation and may be able to speed up elongation in specific sequence contexts.

3.5 Materials and Methods

3.5.1 Plasmid preparation and integration

All plasmids used in this study are listed in Table 3.2. Plasmids containing synonymous leucine codon substituted YFP (TTG, CTA, CTC, CTG, and CTT) and a single-copy yeast integrating plasmid containing a pTet07 promoter were provided as a kind gift from Dr. Arvind R. Subramaniam at the Fred Hutchinson Cancer Research Center in Seattle, Washington. Fragments containing pTet07, YFP variants, and yeast-optimized nanoluciferase (Masser et al., 2016) were amplified using PCR and cloned into the *XhoI* and *HindIII*-digested single-copy yeast integrating plasmid using Gibson assembly.

The pAG306-pTet07-YFP[CTT/TTG]-nLuc and pAG306-pTet07-YFP[TTG/CTT]-nLuc split strains were generated by PCR amplification of the entire backbone of the previous pAG306-pTet07-optYFP-nLuc plasmid beginning at nLuc and ending with pTet07, and PCR amplification of the first (1-377 bp from CDS start) and second (378-714 bp from CDS start) halves of the TTG and CTT YFP variants between the 10th and 11th leucine codons. These fragments were combined using Gibson assembly.

All plasmids were linearized using *NotI* and integrated into yeast by homologous recombination. Integrations were screened by growing transformed yeast on synthetic complete (SC) dropout plates lacking uracil. These were then frozen down for long-term storage in YPD containing 15% v/v glycerol.

3.5.2 Yeast strains, growth, and media

The background yeast strain w303 (EY0690) was used for all experiments. Yeast Dhh1 and Hel2 deletion strains were created by deleting the endogenous Dhh1 and Hel2 loci, respectively, using pRS315 (Addgene Plasmid #3974) and screened by growing transformed yeast on SC dropout plates lacking leucine. Specific oligos used are listed in Supplementary Table S2. Yeast strains were frozen down in YPD containing 15% v/v glycerol.

For cells cultured for use in our reporter assay, cells were streaked out from frozen stocks onto YPD Agar plates and grown at 30 °C for two days. These plates were stored at 4 °C for up to one month.

3.5.3 Luciferase-based elongation reporter assay

Liquid cultures were started from single colonies and allowed to grow overnight at 30 °C with shaking until an approximate OD600 of 0.3-0.5 after which cultures were divided into two tubes. For one of the tubes, 1 µL of a stock solution of anhydrotetracycline (250 µg/mL of ATC dissolved in EtOH) was added per mL of culture. Both tubes were returned to 30 °C with shaking for five to ten minutes. 90 µL of each culture was added to a 96-well white flat-bottom plate (Grainger) and to each well, 10 uL of furimazine (10 mM furimazine stock solution dissolved in DMSO diluted 1:200 in YPD), was added. Immediately after sample loading, the plate was placed in a 30 °C prewarmed Tecan Infinite® 200 PRO plate reader. The following program was used and luminescence measurements were taken every 30 or 60 seconds: (1) Kinetic Cycle: [Cycle Duration: 60 minutes, Kinetic Interval: 30 or 60 seconds], (2) Shaking: [Duration: 3 seconds, Mode: Orbital, Amplitude 2 mm], (3) Luminescence: [Attenuation: Automatic, Integration Time: 1000 ms, Settle Time: 0 ms].

3.5.4 Schlief plot and elongation delay measurements

The Schlief plot methodology was adapted from (Schleif et al., 1973) and slightly modified to assume a non-constant basal expression protein level. For each sample, ATC-induced protein expression was calculated by subtracting the -ATC samples from the corresponding +ATC samples across all measured timepoints. Samples were then normalized to an OD600 of 1.0 by dividing their protein expression over time by their respective ODs. The square root of each value was calculated and plotted against time. Values that produced an error due to the square root of a negative value were set as “N/A” and avoided in our analysis. From this Schlief plot, we identified regions of linearity across our samples and selected a 10-15 minute window for analysis. Ideally, these regions of linearity are parallel between each sample and contain a minimal amount of noise. For each time window, we created a trendline and

calculated the X-intercept of the trendline which represented the calculated elongation time of the sample. The calculated elongation time of the samples in a single assay were then compared to a control to determine elongation delay. These elongation delay measurements were then compared across assays and aggregated to determine the average elongation delay associated with the specific construct.

3.5.5 RNA Extraction and real time qPCR

Yeast pellets were collected from samples 60-minutes post-ATC addition by spinning 1-1.5 mL of liquid culture at 3000 *x g* for 2 minutes and discarding the supernatant. These yeast pellets were then flash frozen in liquid nitrogen and stored at -80 °C until RNA extraction. RNA was extracted from yeast pellets using the MasterPure™ Yeast RNA Purification Kit (Lucigen Cat. No. MPY03100) according to the manufacturer's instructions. RNA quality and concentration was assessed using a Nanodrop. RNA samples were subjected to DNase digestion using RQ1 RNase-free DNase (Promega) according to the manufacturer's instructions. cDNA was prepared from equal amounts of RNA from each sample using Protoscript II Reverse Transcriptase (New England Biolabs Cat. No. M0368X) and an oligodT(18) primer according to the manufacturer's instructions. RT-qPCR was done using a home-brew recipe with SYBR Green at a final concentration of 0.5X (Thermo Fisher S7564). Primers specific for nanoluciferase and actin are described in Supplementary Table S2. mRNA levels were normalized to *ACT1* abundance and fold change was calculated by a standard Ct analysis.

Table 3.2: *Plasmids used in this study*

Construct Name	Identifier	Plasmid
nLuc	ZP427	pAG306- P_{TetO7}-nLuc
LacZ	ZP478	pAG306- P_{TetO7}-LacZ-nLuc
optYFP	ZP436	pAG306- P_{TetO7}-YFP[TTG]-nLuc
2xCGA	ZP464	pAG306- P_{TetO7}-YFP[TTG]-2xCGA-nLuc
3xCGA	ZP486	pAG306- P_{TetO7}-YFP[TTG]-3xCGA-nLuc
4xCGA	ZP465	pAG306- P_{TetO7}-YFP[TTG]-4xCGA-nLuc
5xCGA	ZP487	pAG306- P_{TetO7}-YFP[TTG]-5xCGA-nLuc
6xCGA	ZP466	pAG306- P_{TetO7}-YFP[TTG]-6xCGA-nLuc
YFP[CTA]	ZP432	pAG306- P_{TetO7}-YFP[CTA]-nLuc
YFP[CTC]	ZP433	pAG306- P_{TetO7}-YFP[CTC]-nLuc
YFP[CTG]	ZP435	pAG306- P_{TetO7}-YFP[CTG]-nLuc
YFP[CTT]	ZP434	pAG306- P_{TetO7}-YFP[CTT]-nLuc
YFP[CTC/TTG]	ZP512	pAG306- P_{TetO7}-YFP[CTC/TTG]-nLuc
YFP[TTG/CTC]	ZP514	pAG306- P_{TetO7}-YFP[TTG/CTC]-nLuc
YFP[CTT/TTG]	ZP513	pAG306- P_{TetO7}-YFP[CTT/TTG]-nLuc
YFP[TTG/CTT]	ZP515	pAG306- P_{TetO7}-YFP[TTG/CTT]-nLuc
miRFP-optYFP	ZP531	pAG306- P_{TetO7}-miRFP-YFP[TTG]-nLuc
miRFP-YFP[CTT]	ZP530	pAG306- P_{TetO7}-miRFP-YFP[CTT]-nLuc

Table 3.3: *qPCR primers used in this study*

qPCR Gene and Primer Set	Forward Primer	Reverse Primer
Act1 (ZO83/84)	CTGCCGGTATTGACCAAACT	CGGTGATTTCCTTTTGCATT
nLuc (ZO553/554)	TGGTGATCAAATGGGTCAAA	CCTTCATAAGGACGACCAAA

Acknowledgements

Chapter 3, in part, consists of material from a manuscript that will be submitted for publication, 2022, entitled “Quantification of elongation stalls and impact on gene expression in yeast”, by Vince Harjono, Wanfu Hou, Alexander T. Harvey, Arvind R. Subramaniam, and Brian M. Zid. The dissertation author is the third author of this work.

Chapter 4: Investigation of Dhh1 as a potential mechanism for elongational pausing

4.1 Abstract

Protein synthesis is energetically expensive and its rate is influenced by factors including cell type and environment. Suppression of translation is a canonical response observed during stressful changes to the cellular environment. Inhibition of the initiation step of translation has been highlighted as the key control step in stress-induced translational suppression as mechanisms that quickly suppress initiation are well-conserved across organisms and stressors. This is particularly true during acute glucose starvation, which results in a rapid collapse in translation. In Chapter 2, we observed a widespread slowdown of elongation through both direct elongation rate measurements and an incomplete runoff of ribosomes from housekeeping pro-growth mRNAs that are translationally repressed during glucose starvation. Additionally, we observe the ability of these ribosomes to continue elongation upon readdition of glucose. This phenomenon cannot be explained by the canonical inhibition of ribosome initiation rates alone, but any regulatory mechanism to control elongation rates is yet unknown. In this study, we investigated the role of the proposed translation sensor Dhh1 in elongation control during glucose starvation. We correlated ribosome polarity with Dhh1 association and present the results of a conditional Dhh1 knockdown on the polysome association of several classes of mRNAs. We demonstrate a reduction in the expression of a luciferase reporter during Dhh1 knockdown. Altogether, our results are inconclusive on the role of Dhh1 and we determine no causal link between Dhh1 and slowed elongation rate during glucose starvation.

4.2 Introduction

During glucose starvation in yeast, a rapid collapse in global translation is observed within the first minute (Ashe et al., 2000). Rapid inhibition of RNA-binding by initiation factors such as eIF4A results in a global drop in translation initiation as the loss of 40S ribosome scanning factors prevents translation initiation downstream of the formation of the 43S preinitiation complex (Bresson et al., 2020; Castelli et al., 2011). Exact mechanisms that regulate this rapid shutdown are unknown and do not appear to be the result of previously characterized pathways of translational control (Ashe et al., 2000; Bresson et al., 2020). Despite the global downregulation of protein expression, some stress response mRNAs can evade this phenomenon and proceed with translation. Prior research has investigated the role of factors such as sequence GC content, mRNA secondary structure, internal ribosome entry sites (IRESes), posttranscriptional modifications, and the remodeling of RNA-binding proteins, in cellular stress responses, though the exact sequence of mechanisms during glucose starvation is undetermined (Arribere et al., 2011; Castelli et al., 2011; Gilbert et al., 2007; Iserman et al., 2020; Tardu et al., 2019; Zid and O'Shea, 2014).

The potential for regulatory mechanisms at the elongation stage of translation are less well characterized. Although there is a rapid inhibition of ribosome initiation that results in the runoff of most actively translating ribosomes at the start of glucose starvation, there is evidence that a subset of housekeeping mRNAs appear to remain associated with ribosomes despite producing very little protein (Brengues et al., 2005; Zid and O'Shea, 2014). In Chapter 2, we observed a widespread slowdown of elongation through both direct elongation rate measurements and an incomplete runoff of ribosomes from housekeeping pro-growth mRNAs that are translationally repressed during glucose starvation. Additionally, we observe the ability of these ribosomes to continue elongation upon readdition of glucose. Shutdown of initiation alone should allow these ribosomes to finish translation and be released from these transcripts on the order of several minutes for most mRNAs, but a regulatory pathway to pause ribosomes for prolonged durations during glucose starvation is unknown.

Dhh1, a DEAD-box helicase that is the homolog of mammalian DDX6, has been previously investigated as a factor promoting the decapping and degradation of non-optimally coded mRNA sequences. These sequences correlate with slow-moving ribosomes and it was proposed that Dhh1 may be a sensor for codon optimality (Hanson and Coller, 2018; Radhakrishnan et al., 2016). Dhh1 was previously implicated as a decapping activator involved in P-body formation and translational repression (Carroll et al., 2011; Coller and Parker, 2005). Tethering of Dhh1 to mRNAs has also been reported to increase the localization of the target mRNA to dense polysome fractions while also leading to impaired translation and increased mRNA decay of the target mRNA (Sweet et al., 2012). Although the direct binding of Dhh1 to ribosomal components has not been demonstrated, the correlations between both translational repression and polysome accumulation make it an intriguing target of study in the regulation of ribosomal elongation.

In this study, we determine a correlation between increased ribosome polarity from our ribosome profiling dataset and increased enrichment of Dhh1 in a previously published CLIP-seq dataset. We performed polysome profiling on a conditional knockdown of Dhh1 and detail the shift in ribosome association for different classes of mRNAs in response to glucose starvation. Additionally, we use a luciferase reporter to investigate protein expression before and after glucose starvation.

4.3 Results

Dhh1 is a DEAD-box helicase that is the homolog of mammalian DDX6 that plays a well-established role in mRNA-decapping and degradation (Coller and Parker, 2005). Interestingly, previous work has associated Dhh1 translation repression and has shown that Dhh1 preferentially binds to mRNAs with low codon optimality (Carroll et al., 2011; Radhakrishnan et al., 2016), while the tethering of Dhh1 to mRNA reporters has also been reported to increase enrichment in dense polysome fractions and result in impaired translation (Sweet et al., 2012).

By analyzing the polarity of ribosome distribution on all mRNAs during glucose starvation, we believe we can use this measure as a proxy for identifying mRNAs with slowly elongating ribosomes. A negative polarity corresponds to a weighted average of ribosome occupancy biased towards the 5' end of a particular mRNA, while positive polarity is a weighted average biased towards the 3' end (Schuller et al., 2017). During log phase growth, the global polarity score is slightly biased towards the 5' end. Intriguingly, during glucose starvation, the global polarity score is skewed towards the 3' end (Figure 4.1). We believe this phenomenon is indicative of the repression of new initiation and the movement of translating ribosomes further down the open reading frame. As we had previously observed a high ribosome occupancy on many pro-growth mRNAs that are poorly translated during glucose starvation, we believe these ribosomes are dramatically slowed or paused after the initial runoff that occurs immediately after glucose starvation.

Based upon the strong shift in global polarity we observed, we were curious if Dhh1 would be enriched on mRNAs that undergo large polarity shifts during glucose starvation. To do this, we performed an analysis of previously published CLIP-Seq data from (Cary et al., 2015) and related Dhh1 enrichment with the shift in ribosome polarity we observe between log phase and glucose starvation. We found that Dhh1-depleted mRNAs show a lower average shift in ribosome polarity towards the 3'end when compared with the global average (Figure 4.2). In contrast, Dhh1-enriched mRNAs show a higher average shift in polarity during glucose starvation. As we observe increased polarity towards the 3'end

for mRNAs that appear translationally repressed, this trend is indicative that Dhh1 may be involved in regulating elongation rates on these mRNAs.

Additionally, a positive enrichment of Dhh1 association during glucose starvation has a strong positive correlation with increasing mRNA length (Figure 4.3). We found this promising as longer mRNAs would have increased space for ribosomal loading and would take a longer time to finish the elongation stage of translation. This would result in a longer amount of time required for ribosomal runoff upon glucose starvation, allowing a longer window of opportunity for Dhh1 to slowdown ribosomes on these mRNAs.

To ascertain Dhh1's possible role in slowing ribosomal elongation, it was decided to test the effects of a Dhh1 knockdown strain on ribosomal occupancy. Unfortunately, we found that the *dhh1*Δ strain was slow growing (120 minutes vs 90 minutes) and exhibited an ~8-fold increase in mRNA induction of the stress-response gene Hsp30 versus the wildtype strain during normal log phase growth. Additionally, the *dhh1*Δ strain exhibited a ~2-fold lower induction after 15 minutes of glucose starvation, indicating a weakened stress response to starvation. To minimize the potential confounding effects due to this growth defect, we decided to conditionally knockdown Dhh1 by C-terminally tagging it with an inducible auxin degron (AID) (Tanaka et al., 2015). Upon addition of the plant hormone auxin, the protein TIR1 mediates the targeted ubiquitination and subsequent degradation of proteins tagged with the degron amino acid sequence (Nishimura et al., 2009). The Dhh1-AID strain exhibited a growth rate doubling time closer to the that of the wildtype background (100 minutes vs 90 minutes) and comparable Hsp30 induction after 15 minutes of glucose starvation. Addition of the auxin indole-3-acetic acid (IAA) for 30 minutes resulted in an effective knockdown of Dhh1 protein by roughly ~80% of the starting concentration (Figure 4.4).

To assess Dhh1's effects on ribosomal occupancy, we knocked down Dhh1 and performed polysome profiling during log phase and after 15 minutes of glucose starvation. As was hoped, the polysome traces of both the control and the knockdown conditions are highly similar, indicative of a

healthier phenotype than the *dhh1*Δ strain (Figure 4.5). Although this is the case, it appears that there is still a small difference in the polysome profile during glucose starvation. The IAA treated sample appears to result in more pronounced light polysome fractions. For example, there are larger disome/trisome peaks after Dhh1 knockdown, while the densest fractions appear roughly equivalent to or slightly decreased relative to the control.

We proceeded to pool fractions into four groups for subsequent RNA extraction and RT-qPCR, a free RNA pool, a monosome pool, a light polysome pool corresponding to disomes and trisomes, and a dense polysome pool. IAA treated cultures during log phase growth experienced a drop in enrichment for mRNAs in the dense and disome/trisome fractions (Figure 4.6). A reduction in polysome fractions was not surprising as the constitutive *dhh1*Δ strain displayed growth defects. After 15 minutes of glucose starvation, IAA treated cultures retained a larger concentration of mRNA associated with ribosomal fractions than the control (Figure 4.7). However, it appeared that the 18SrRNA measurements were approximately 2-fold higher during IAA treatment across all fractions. It is expected that 15 minutes of glucose starvation would not be a sufficient length of time to result in large changes in ribosomal autophagy (Ashe et al., 2000; Kraft et al., 2008). Since the distribution of ribosomes between the 80S and polysomal fractions was otherwise unchanged, it could be a discrepancy in sample loading.

To account for this, the results were reanalyzed by normalizing for 18SrRNA (Figure 4.8). After normalization, IAA treatment during glucose starvation reduces the concentration of most mRNAs we assessed by qPCR, with the exceptions of *PGK1* and *HSP104*. During log phase growth, stress response related *HSP30* and *HSP104* remain the only mRNAs that increase fold change enrichment in the dense polysome fraction after Dhh1 knockdown. When comparing the fold change during glucose starvation for each condition, there does not appear to be a distinct difference in the 18S normalized dense fractions for most mRNAs (Figure 4.9). *HSP30* and *HSP104* have a ~2-fold drop in induction upon glucose starvation in IAA treated samples as there is an increase in expression during log phase due to

IAA treatment. The long mRNA *ACC1* also displays a ~2-fold drop in relative enrichment, but other pre-existing mRNAs have small changes.

We decided to further assess the effect of Dhh1 knockdown by monitoring the protein expression of our nLucPEST reporters. The Hsp30 promoter nLucPEST reporter showed no difference in protein production upon Dhh1 knockdown (Figure 4.10). The Pab1 promoter nLucPEST reporter showed some reduced translation during log phase conditions, but no difference during glucose starvation. If Dhh1 was slowing ribosomes on the pre-existing Pab1pr-nLucPEST reporter, it is expected that there would be an increase in translation during glucose starvation. A limitation of these reporters is their relatively short length, as mRNA length is positively correlated with Dhh1 enrichment and increased polarity during glucose starvation.

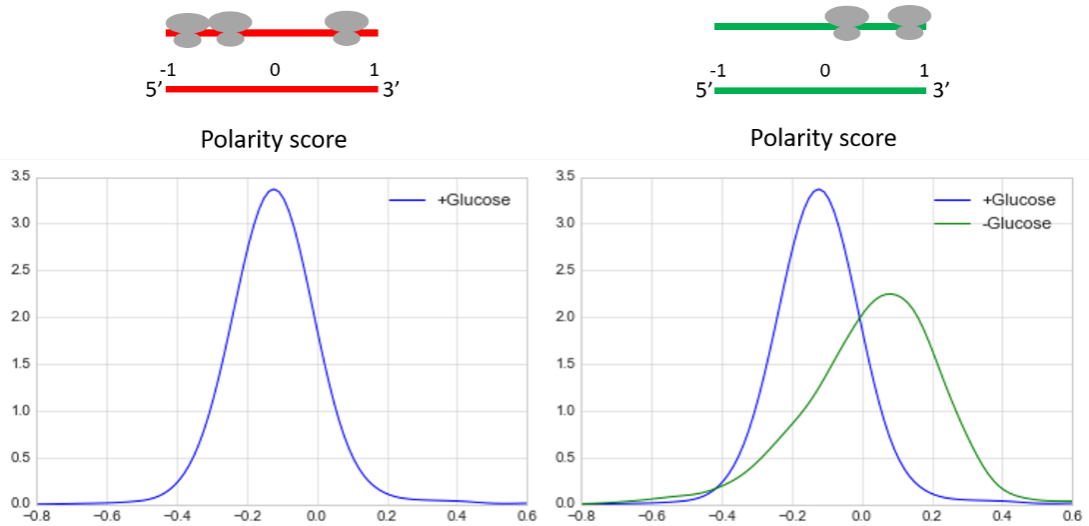

Figure 4.1: *Gene specific changes in ribosome polarity during glucose starvation*
Per-gene polarity scores were calculated and included in further analysis from all yeast genes that had > 25 reads per ribosomal profiling library. Plots were generated from the distribution of these scores. RPF reads on the 5’ half of a transcript contribute to negative polarity such while reads on the 3’ half of a transcript contribute to positive polarity. Densities of polarity score distributions from pre- and post-acute glucose starvation (right).

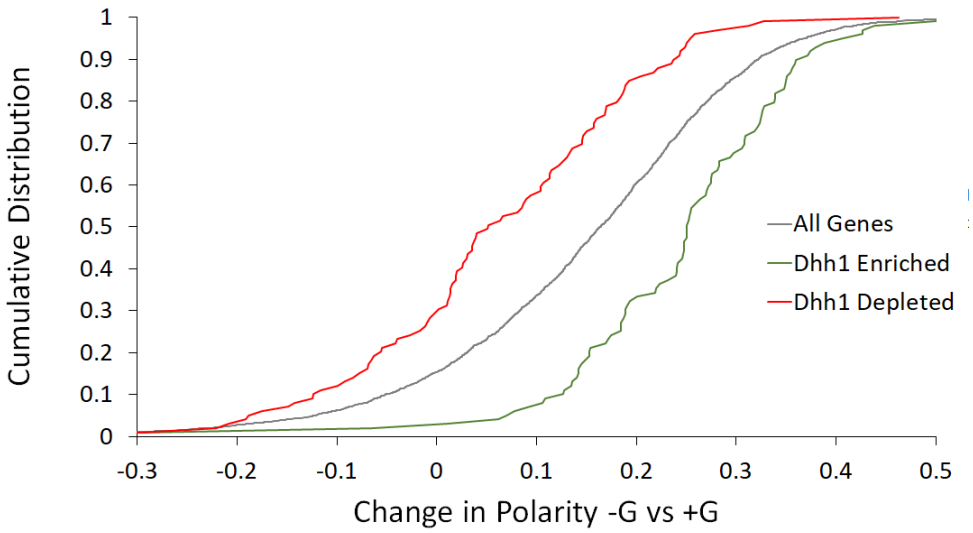

Figure 4.2: *The shift in ribosomal polarity upon glucose starvation is correlated with Dhh1 enrichment*
The change in polarity was calculated by subtracting the per-gene polarity scores. Dhh1 CLIP-Seq data from (Cary et al., 2015) was used to measure Dhh1 enrichment on mRNAs. Gene distribution is plotted versus the shift in ribosome polarity observed during 15 min glucose starvation relative to log phase.

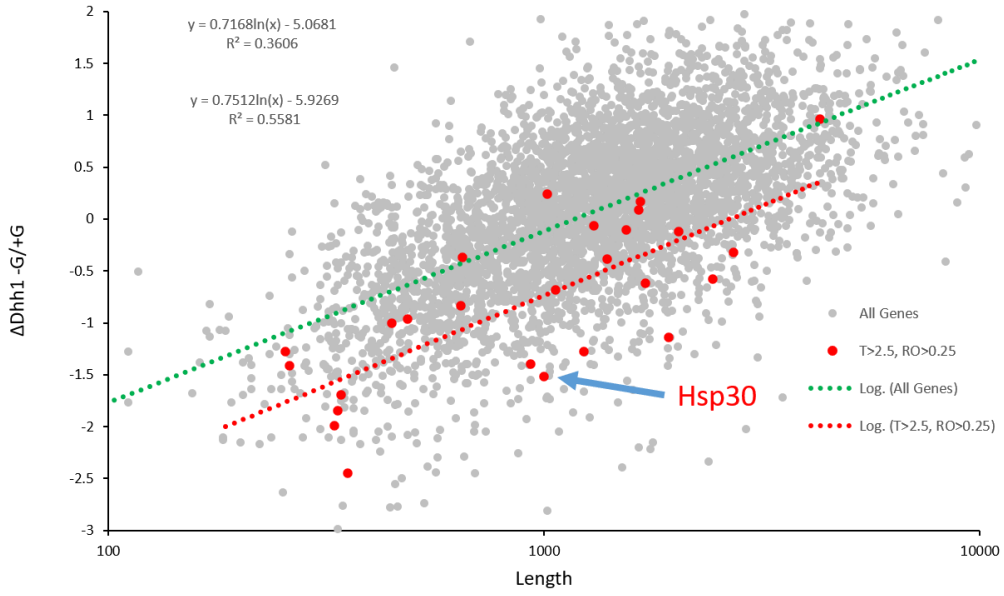

Figure 4.3: *Dhh1 shows a length dependent recruitment during glucose starvation*
The shift in Dhh1 enrichment from pre- to post- acute glucose starvation was calculated for each gene and plotted versus mRNA length. mRNAs transcriptionally upregulated during glucose starvation that have increased ribosome occupancy are plotted in red.

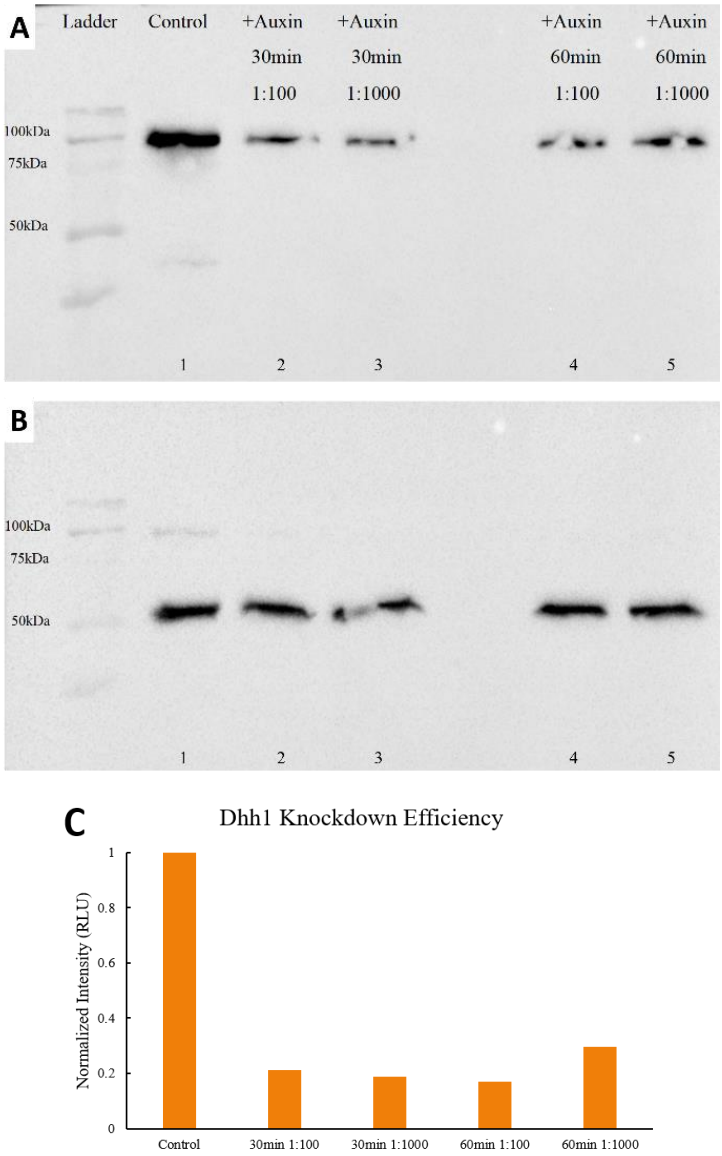

Figure 4.4: *Auxin addition is effective in degrading Dhh1*

(A) Western blot analysis of Dhh1-3xFLAG-AID probed by α-FLAG antibody. 50 mg/mL indole-3-acetic acid (IAA) was added to log phase yeast cultures at a 1:100 or 1:1000 dilution ratio. Samples were taken after 30 minutes and 60 minutes of treatment. (**B)** The Western blot from A was stripped and reprobed for Tubulin as a loading control. (**C)** Fraction of Dhh1 remaining after IAA treatment. Chemiluminescence intensity was quantified for each blot and normalized to the control. Tubulin signal intensity was used to correct values for sample loading.

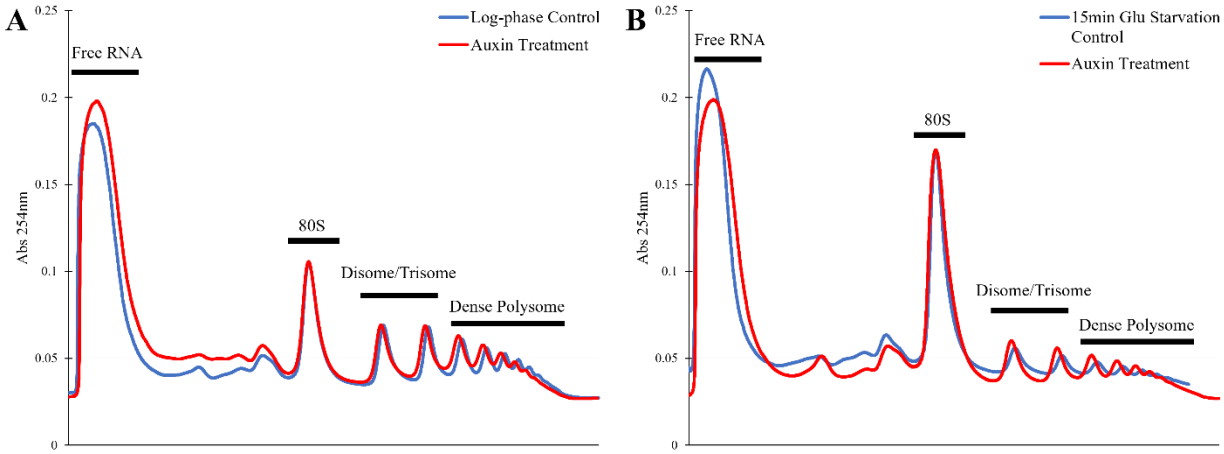

Figure 4.5: *Polysome traces during log phase and glucose starvation*
(A) Dhh1-AID cultures were treated with IAA (50 µg/mL) for 30 minutes during mid log phase. Extracts of both control and auxin-treated samples were fractionated over a high-density sucrose gradient. Absorbance values presented are normalized 1:1 between conditions by monosome peak absorbance. **(B)** Dhh1-AID cultures were treated with IAA (50 µg/mL) for 30 minutes during mid log phase, the subjected to glucose starvation for 15 minutes in media with IAA. Extracts were fractionated over a high-density sucrose gradient. Absorbance values presented are normalized 1:1 between conditions by monosome peak absorbance.

Dhh1-knockdown Vs Wildtype, Log-phase Enrichment (Log2)

		Free	80S	Di & Tri	Dense
	18S	0.61	0.78	-0.41	-0.53
Growth	ACT1	0.27	0.02	0.02	-0.74
Growth	PAB1	-0.32	-0.38	0.01	-0.94
Growth	PGK1	0.13	0.44	0.41	-0.65
Growth	RPS8	-0.31	-0.44	-0.58	-1.20
Long	ACC1	0.74	0.55	0.30	-0.43
Long	FAS1	0.23	-0.10	-0.25	-1.02
Long	URA2	0.21	-0.07	-0.24	-0.99
Stress	HSP30	-0.33	-0.73	-0.26	0.09
Stress	HSP104	0.88	1.29	1.43	1.39

Figure 4.6: *Dhh1 knockdown reduces dense polysome fractions during log phase*
Pooled fractions from Figure 4.6A underwent RNA extraction and RT-qPCR to quantify the changes in transcript abundance in the indicated fraction after 30 minutes of IAA treatment compared to the control. An exogenous, spike-in RNA was used for standardization to quantify abundance in each pool and the fold change in RNA abundance as assessed by ΔΔCt analysis is indicated in the heatmap for mRNAs grouped into the indicated categories.

Dhh1-knockdown Vs Wildype, 15min starvation Fold Change (Log2)

		Free	80S	Di & Tri	Dense
	18S	0.38	1.24	0.97	1.01
Growth	ACT1	0.34	1.25	0.60	0.66
Growth	PAB1	-0.18	0.55	0.19	0.25
Growth	PGK1	0.92	1.41	1.18	1.45
Growth	RPS8	0.57	1.11	0.22	0.20
Long	ACC1	0.89	0.78	0.58	0.21
Long	FAS1	0.13	0.74	-0.14	0.11
Long	URA2	0.94	0.94	0.29	0.33
Stress	HSP30	0.02	0.79	0.09	0.75
Stress	HSP104	0.23	1.73	1.45	2.00

Figure 4.7: *Dhh1 knockdown increases enrichment of dense polysome fractions during glucose starvation*
Pooled fractions from Figure 4.6B underwent RNA extraction and RT-qPCR to quantify the changes in transcript abundance in the indicated fraction after 30 minutes of IAA treatment compared to the control. An exogenous, spike-in RNA was used for standardization to quantify abundance in each pool and the fold change in RNA abundance as assessed by ΔΔCt analysis is indicated in the heatmap for mRNAs grouped into the indicated categories.

Dhh1-knockdown Vs Wildtype, Log-phase Fold Change (Log2) 18SrRNA Normalized

		Free	80S	Di & Tri	Dense
	18S	0.00	0.00	0.00	0.00
Growth	ACT1	-0.34	-0.76	0.43	-0.21
Growth	PAB1	-0.93	-1.16	0.42	-0.40
Growth	PGK1	-0.48	-0.34	0.82	-0.12
Growth	RPS8	-0.92	-1.22	-0.17	-0.67
Long	ACC1	0.13	-0.23	0.71	0.10
Long	FAS1	-0.38	-0.88	0.16	-0.49
Long	URA2	-0.40	-0.85	0.16	-0.45
Stress	HSP30	-0.94	-1.52	0.14	0.63
Stress	HSP104	0.27	0.51	1.84	1.92

Dhh1-knockdown Vs Wildtype, 15min starvation Fold Change (Log2) 18SrRNA Normalized

		Free	80S	Di & Tri	Dense
	18S	0.00	0.00	0.00	0.00
Growth	ACT1	-0.04	0.01	-0.37	-0.35
Growth	PAB1	-0.56	-0.69	-0.78	-0.77
Growth	PGK1	0.55	0.17	0.21	0.44
Growth	RPS8	0.19	-0.13	-0.75	-0.81
Long	ACC1	0.51	-0.46	-0.39	-0.80
Long	FAS1	-0.25	-0.51	-1.11	-0.90
Long	URA2	0.56	-0.30	-0.68	-0.68
Stress	HSP30	-0.36	-0.45	-0.88	-0.27
Stress	HSP104	-0.15	0.49	0.48	0.99

Figure 4.8: *18SrRNA normalization*

qPCR analysis from Figure 4.6 & 4.7 normalized by the fold change in 18S rRNA. The fold change in RNA abundance as assessed by ΔΔCt analysis is indicated in the heatmap for mRNAs grouped into the indicated categories.

Wildtype, 15min G- Vs Log-Phase Fold Change (Log2) 18S Normalized

		Free	80S	Di & Tri	Dense
	18S	0.00	0.00	0.00	0.00
Growth	ACT1	-0.62	-0.87	1.08	0.17
Growth	PAB1	0.64	-0.84	0.75	0.27
Growth	PGK1	0.13	-1.35	0.60	0.28
Growth	RPS8	-0.44	-2.09	-0.86	-0.42
Long	ACC1	-2.22	-2.59	-0.12	0.72
Long	FAS1	-1.23	-2.10	0.59	0.50
Long	URA2	-1.65	-2.77	-0.13	0.05
Stress	HSP30	-0.12	0.09	4.15	4.75
Stress	HSP104	1.21	-0.70	2.02	2.05

Dhh1-knockdown, 15min G- Vs Log-Phase Fold Change (Log2) 18S Normalized

		Free	80S	Di & Tri	Dense
	18S	0.00	0.00	0.00	0.00
Growth	ACT1	0.23	-0.49	-0.07	-0.18
Growth	PAB1	1.12	-0.33	-0.48	-0.13
Growth	PGK1	1.31	-0.87	0.15	0.57
Growth	RPS8	1.02	-1.07	-1.35	-0.55
Long	ACC1	-0.83	-2.81	-1.25	-0.26
Long	FAS1	-0.92	-1.75	-0.87	0.01
Long	URA2	-0.70	-1.92	-0.67	0.03
Stress	HSP30	0.64	0.73	2.83	3.93
Stress	HSP104	0.76	-0.79	0.60	1.19

Figure 4.9: *mRNA fold change during glucose starvation*

RNA abundance after 15 minutes of glucose starvation compared to log phase was calculated for auxin addition and the control. The fold change in RNA abundance as assessed by ΔΔCt analysis is indicated in the heatmap for mRNAs grouped into the indicated categories.

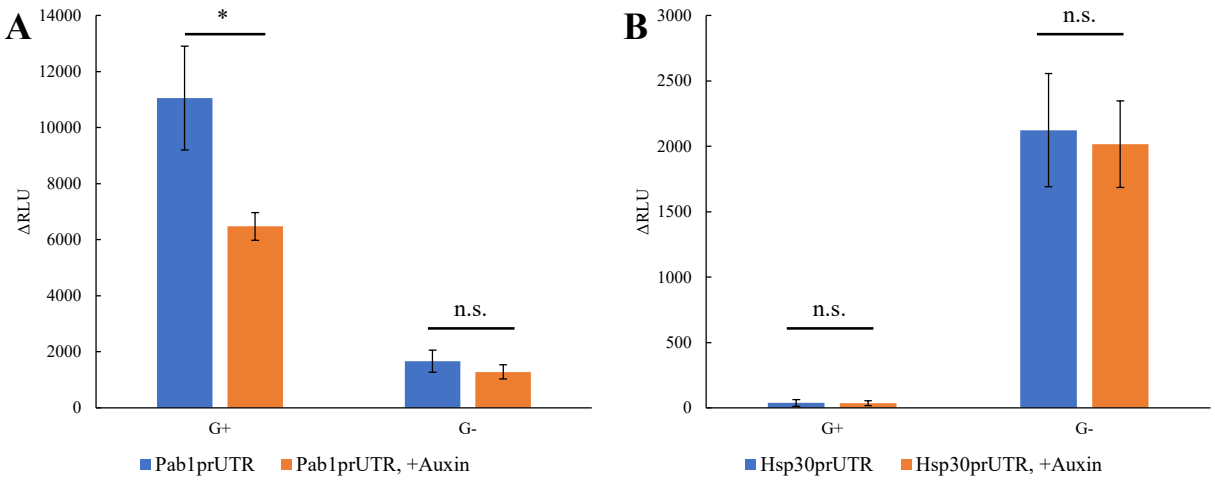

Figure 4.10: *nLucPEST induction during Dhh1 knockdown*

(A) Dhh1-AID cultures expressing Pab1prUTR-nLucPEST were treated with IAA (50 µg/mL) for 30 minutes during mid log phase, then subjected to glucose starvation for 30 minutes in media with IAA. Each bar represents the mean difference ± sem in luciferase signal detected during measurement between aliquots of untreated culture and the same culture treated with CHX. For log phase and 30 min -Glu conditions the signal was recorded after 5 minutes of treatment and the difference was calculated and plotted on the y-axis. **(B)** Dhh1-AID cultures expressing Hsp30prUTR-nLucPEST were treated with IAA (50 µg/mL) for 30 minutes during mid log phase, then subjected to glucose starvation for 30 minutes in media with IAA. Statistical significance was assessed by paired Student's t-Tests for differences in luciferase production between cultures that underwent auxin treatment paired against luciferase production from the same culture without treatment (***p<0.001; **p<0.01, * p<0.05, n.s. = not significant).

4.4 Discussion

Prior work has shown that Dhh1 is associated with nonoptimal codon sequences and that overexpression of Dhh1 results in an increase in the ribosome occupancy of nonoptimal mRNAs but no difference in the occupancy of highly optimal mRNAs (Radhakrishnan et al., 2016). Our analysis of Dhh1 CLIP-Seq data from (Cary et al., 2015) reveals that Dhh1 is enriched on mRNAs with an increased positive shift in polarity during glucose starvation and it is depleted for mRNAs with either negative or below average positive shifts in polarity. As we find that mRNAs with low translational efficiency during glucose starvation are correlated with positive shifts in ribosome polarity, these results also suggest Dhh1 recruitment to slow codon sequences.

Polysome profiling demonstrates that a knockdown of Dhh1 results in a moderate impairment in polysome levels and the induction of a mild stress response. We observe a drop in mRNA enrichment to polysome fractions for the pro-growth and long mRNAs tested in the Dhh1 knockdown condition. Ribosome levels as indicated by 18SrRNA levels are also moderately lower in the polysome fractions and moderately higher in the monosome fraction, representing some reduction in the pool of active ribosomes. Mild stress versus the control is evident by the simultaneous enrichment of *HSP104* to the polysome fraction and the maintenance of *HSP30* levels as both mRNAs are upregulated during a stress-response. Furthermore, normalization of mRNA levels by the change in 18SrRNA relative to wildtype indicates *HSP30* is enriched relative to polysome concentration in the Dhh1 knockdown. It is also clear that *RPS8* levels, representative of mRNA encoding for either Rps8A or its paralog Rps8B, drop in relative enrichment more than any of the other growth and long mRNAs assessed. As Rps8 is a protein component of the 40S ribosomal subunit, it appears that ribosomal protein synthesis is particularly sensitive to downregulation during Dhh1 knockdown. As the synthesis of ribosomes is tightly-coordinated and the most energy-intensive process in the cell, it is highly responsive to stressors and also indicates a broader impact on cellular growth in the knockdown strain (de la Cruz et al., 2018).

During glucose starvation, initial results indicated the Dhh1 knockdown increased concentrations of nearly all mRNAs across fractions as well as a ~2-fold increase in 18SrRNA in the monosome, disome/trisome, and dense polysome fractions. Ribosomes are generally stable and changes in autophagy induced during starvation occur on the timescale of hours versus the 15 minute treatment of glucose starvation performed (Ashe et al., 2000; Kraft et al., 2008; Martinez et al., 2004). Thus, solely mRNA fold change normalized by 18SrRNA appears reliable for interpretation as the raw results are likely due to differences in sample loading. When normalized, the Dhh1 knockdown results in a ~1.5-2-fold decrease in most growth and long mRNAs. The highly abundant mRNA *PGK1* is the only housekeeping mRNA enriched in the polysome fractions relative to the control. HSP30 appears to have slightly reduced polysome association while HSP104 is enriched ~2-fold in the dense polysome fraction.

It appears feasible that the broad decrease in the normalized concentration of housekeeping mRNAs during Dhh1 knockdown could result from increased elongation rates of the ribosomes we observe on pre-existing but translationally downregulated mRNAs. If new initiation remains repressed, the runoff of these previously paused ribosomes would remove these mRNAs from the polysome fractions. mRNAs such as *HSP104* that are readily translated during glucose starvation could appear enriched in the polysome fractions as a higher proportion of remaining polysomes would be translationally active.

However, as the Dhh1 knockdown appears to drop ribosome occupancy in the log phase data set prior to starvation, the decrease in housekeeping mRNAs could also occur if the Dhh1 knockdown impairs translation. When the fold change in mRNA enrichment during glucose starvation is calculated for auxin and control conditions separately, there are not clear shifts in polysome enrichment for most mRNAs. The shift in polysome association of the long mRNA *ACC1* during glucose starvation does appear to be a magnitude of ~2-fold lower when Dhh1 is knocked down but the other housekeeping mRNAs have shifts in polysome association during glucose starvation that are largely unchanged in the

Dhh1 knockdown. The stress mRNAs have a ~2-fold lower increase in enrichment to polysome fractions when glucose starved in the Dhh1 knockdown, but this is likely a result of the increased induction that occurs in log phase conditions prior to starvation.

Deletion of Dhh1 slows cellular growth rate, which may explain the additional slowdown in elongation. While the knockdown strain displayed a healthier phenotype than the deletion background, there was still a small yet noticeable lag in growth rate versus wildtype. Alternatively, our results are also compatible with a role in which Dhh1 enhances translation rather than slowing elongation rates. For example, the Dhh1 knockdown appears to result in decreased translation of our Pab1prUTR-nLucPEST reporter during log phase conditions. Additionally, in Chapter 3, the *dhh1*Δ strain heavily decreased the elongation rate of our YFP[CTC] reporter and to a lesser extent our optYFP reporter. The YFP[CTT] reporter was unaffected relative to wildtype but the large slowdown in elongation rate was not rescued by the removal of Dhh1.

Although most studies have investigated Dhh1 with regards to its role in mRNA decay and translational repression, Dhh1 has also been shown to promote the translation of certain proteins as well. It has been previously demonstrated that a subset of mRNAs that contain highly-structured 5'UTRs and coding sequences require Dhh1 helicase activity for efficient expression (Jungfleisch et al., 2017). A highly structured region 50-120 nucleotides after the start codon was particularly predictive of translational activation by Dhh1. Furthermore, Dhh1 can shift roles in a condition-dependent manner. During nitrogen starvation, Dhh1 is required for the efficient expression of autophagy-related proteins Atg1 and Atg13, but when nutrients are plentiful Dhh1 encourages ATG mRNA degradation (Liu et al., 2019). Overall, this argues that Dhh1 may play context specific roles in translation elongation any may be able to speed up elongation in specific sequence contexts.

If Dhh1 enhances translation, it may be the case that the mRNAs enriched in polysome fractions after Dhh1 knockdown are the easiest to translate. Pgk1 encodes for the most abundant mRNA assessed and has a steady-state protein concentration ~7-8 fold higher than for any of the other tested genes (Ho

et al., 2018). This may explain the increase in *PGK1* association with polysomes as it is a highly optimized and efficiently translated mRNA that may be less reliant on Dhh1 driven effects on translation. *HSP30* and *HSP104* are stress response mRNAs robustly translated during glucose starvation and other stresses that require a reprogramming of translation. For example, during heat shock, the condensation of the DEAD-box RNA helicase Ded1 has been shown to impair the translation of housekeeping mRNAs such as Pab1 while Hsp30 and Hsp104 remain well translated due to the minimal secondary structure of their 5'UTRs (Iserman et al., 2020). Should Dhh1 helicase activity play a related role in enhancing translation, the reduced secondary structure of these mRNAs relative to many housekeeping mRNAs may explain their increased association with polysomes during glucose starvation relative to the pro-growth and long mRNAs we measured and the decreased association of Dhh1 on these mRNAs in the CLIP-Seq analysis.

This hypothesis is also compatible with the results of our nLuc assays during Dhh1 knockdown. The expression of the Pab1prUTR-nLucPEST reporter during log phase is reduced relative to wildtype strains but the expression of the Hsp30prUTR-nLucPEST reporter during glucose starvation is unaffected. It is possible that the slowdown in elongation we observe for YFP[CTC] in the *dhh1*Δ background is due to changes in local RNA secondary structure of the YFP coding sequence. Dhh1 helicase activity may be required for efficient translation of the YFP[CTC] coding sequence whereas the optYFP and YFP[CTT] do not have the same unique secondary structure specific for Dhh1. The analysis of mRNA secondary structure with RNAfold does predict changes in the location of probable secondary structure within the early ORF region previously reported by (Jungfleisch et al., 2017) and the increased GC content of CTC codons may contribute to motifs more reliant on Dhh1-specific helicase activity. Specific structures reliant on Dhh1 are unclear, as the CTC chimeric reporters were not significantly different in elongation rate.

Although initial research reported an association of Dhh1 with slow moving polysomes, more recent work has found that the Ccr4-Not complex appears to recruit Dhh1 to polysome fractions through

interaction with Not5 (Buschauer et al., 2020). In the absence of Not5, Dhh1 was not found to directly associate with ribosomes. Other groups have also studied the complex's intricate role in translational repression (Allen et al., 2021; Preissler et al., 2015). For example, another component, Not4, has also been shown to be vital for translational repression during stress response (Preissler et al., 2015). During acute glucose starvation, Not4 deletion prevented the global repression of translation and demonstrated continued S35-methionine incorporation (Preissler et al., 2015). Additionally, previous research supporting Dhh1's role in repressing translation by slowing ribosomes did so by tethering Dhh1 to mRNAs and monitoring Dhh1 association with polysome fractionation (Sweet et al., 2012). As only the highest density fractions were enriched during Dhh1-tethering, it is possible that this enrichment could be due in part to RNP granule association rather than an association with dense polysomes fraction. Dhh1 is a constitutive mRNA processing-body component and is known to accumulate in stress granules which contain a number of pre-initiation complex components (Swisher and Parker, 2010). As tethering Dhh1 results in a significant drop in mRNA level, a large pool of the mRNA detected in sucrose fractions may have been pulled by Dhh1 into dense RNP granules for decapping and decay. For example, a previous study detected a high accumulation of the mRNA *FBA1* inside P-bodies when Dhh1 was tethered to it and RNA decapping was inhibited (Carroll et al., 2011). Similarly, the correlation we observe between ribosome polarity and Dhh1 enrichment could be due to mRNA recruitment to RNP granules. Increased association of Dhh1 with the pool of free mRNA will not be accurately reflected by ribosome polarity.

Our polysome profiling focused broadly on ribosome association in the light and heavy polysomes to detect bulk changes in ribosome runoff, but this approach lacks the sensitivity that fractionation into a larger number of samples could provide. A more granular approach may be taken in future investigations to further elucidate the subtleties behind Dhh1's mode of action. Additionally, as the Dhh1 knockdown only partially rescued the growth defects of the constitutive *dhh1*Δ strain, it may be beneficial to perform polysome profiling during glucose starvation with a tighter knockout strain.

This could be improved through the use of the iAID system, the addition of a Tet-OFF promoter to shut off transcription in tandem with protein degradation by the AID tag (Tanaka et al., 2015). A more effective knockout could allow for a shorter incubation than the 30 minute auxin treatment used previously, resulting in a shortened exposure of cells to the *dhh1*Δ phenotype prior to the beginning of glucose starvation.

Additionally, while we have assessed elongation rates when Dhh1 is deleted, it could be informative to pair the Dhh1 knockdown with our elongation reporter assay to obtain a direct measure of elongation rates during glucose starvation and during log phase. While we have measured elongation rates of the constitutive deletion strain during log phase, it has a slower growth rate than the knockdown strain and may present much different results. We have thus far studied the effects of Dhh1 deletion, but it would also be informative to measure the elongation rate when Dhh1 is tethered to our elongation reporter. While previous studies tethering Dhh1 to mRNAs have measured effects such as polysome association and total protein and mRNA expression levels to implicate Dhh1 in translational repression and ribosomal slowdown, they have not measured ribosome elongation rates directly (Carroll et al., 2011; Radhakrishnan et al., 2016; Sweet et al., 2012). The mechanism by which Dhh1 affects these reporter mRNAs could be further investigated by tethering mutant forms of Dhh1, such as the ATPase-domain mutant Dhh1^{DQAD}, to these mRNAs instead, as previous studies have reported that the ATPase and helicase domains are required for enhanced translation, but that it is unnecessary for tethered Dhh1 to inhibit translation (Carroll et al., 2011; Jungfleisch et al., 2017; Liu et al., 2019; Pause and Sonenberg, 1992).

4.5 Materials and Methods

4.5.1 Dhh1 knockdown

3-Indoleacetic acid (IAA, Sigma-Aldrich) was dissolved in 100% ethanol at 50 mg/mL. IAA was added to cultures at a final concentration of 50 μg/mL. Cultures were incubated for 30 minutes during early log phase (0.4-0.6 OD_{600}) prior to 15 minutes of glucose starvation.

4.5.2 Western blotting

Cell lysates were prepared and separated by SDS-PAGE. Proteins were transferred to a nitrocellulose membrane utilizing semidry transfer buffer (Bjerrum and Schafer-Nielsen transfer buffer) for 1 hour. Blots were blocked with 2% (w/v) non-fat milk for 1 hour at room temperature. Blots were incubated with the primary antibody, monoclonal mouse anti-FLAG M2 (F3165, Sigma-Aldrich©) then detected with a goat anti-mouse HRP-conjugated secondary antibody. Western blots were prepared for restaining as described in "Western blot membrane stripping for restaining protocol" by Abcam©. Blots were incubated in mild stripping buffer (15 mg/mL glycine, 1 mg/mL SDS, 100 μL/mL Tween 20, pH 2.2) at room temperature for two intervals of 10 minutes, exchanging for fresh buffer in between intervals. Blots were washed twice for 10 minutes in PBS and subsequently twice for 5 minutes in TBST. Western blotting was repeated for detection of tubulin by mouse monoclonal anti-α -tubulin (12G10, Developmental Studies Hybridoma Bank, University of Iowa, Iowa City, IA).

4.5.3 Polysome profiling

800 mL cultures of strain ZY185 were inoculated in SC media and grown overnight to early log phase (0.4-0.6 OD_{600}). 400 mL were rapidly filtered, washed, and resuspended in SC -G media to begin glucose starvation. The remaining half of the glucose replete culture was rapidly filtered, and the cell paste was scraped into liquid nitrogen for flash freezing. 1.2 mL of polysome gradient lysis buffer (20 mM Tris-Cl (pH 7.5), 140 mM KCl, 2 mM $MgCl_2$, 100 μg/mL CHX, 20 U/mL SUPERase•In™ (Invitrogen), 1% Triton X-100) was flash frozen dropwise with the cell paste. After 15 minutes of glucose starvation, SC -G cultures were filtered down and the cell paste was flash frozen with 1.2 mL of

lysis buffer. Cell pastes were stored at -80°C. Cell lysis was performed by cryogenic ball milling for 4x3 minute cycles and cooled with liquid nitrogen between each cycle. The resulting lysates were gently thawed to room temperature in a water bath and treated with DNase I (12.5 U/mL). Lysates were centrifuged at 4°C for 5 min at 3000xg and the supernatant was centrifuged once more for 10 min at 20,000xg. Approximate concentrations were estimated by A_{260} measurements.

A 7-47% sucrose gradient in polysome gradient buffer without Triton X-100 was prepared with a gradient maker. Clarified supernatants were added and centrifuged at 4°C for 3 hours at 35,000RPM in a Beckman SW41Ti rotor. The gradient was fractionated into 1 mL aliquots using a gradient fractionator and UA-6 detector (Isco/Brandel). Polysome traces were monitored through absorbance measurements at 254nm. 2 ng of *in vitro* transcribed renilla luciferase (rLuc) RNA was added to each aliquot as a spike-in control. Transcription reactions were performed with a mMESSAGE mMACHINE™ T7 Transcription Kit according to manufacturer's instructions and RNA was purified with acid phenol:cholorform extraction (Invitrogen). After adding the rLuc spike-in, 600µL of Guanidine HCl and 600µL isopropanol were added to 400uL of each fraction and incubated overnight at -20°C. Fractions were centrifuged at 10,000g for 25 minutes to isolate RNA pellets. Samples were washed with 70% EtOH and resuspended in 400µL of TE buffer. Cleanup was performed by precipitation with 40 µL of NaOAC and 2.5 volumes of 100% EtOH. Samples were centrifuged for 25 min @ 10,000xg, pellets were washed with 70% EtOH, dried, and resuspended. Fractions corresponding to free RNA, 80S, disome/trisome, and dense polysomes were pooled and the RNA was then treated with RQ1-DNase (Promega) and reverse transcribed with Protoscript® II Reverse Transcriptase (NEB), both according to manufacturer's instructions. qPCR measurements with SYBR green were performed with the cDNA libraries and primers designed for each respective gene. The 18S rRNA primer set was adopted from (Cankorur-Cetinkaya et al., 2012). CT values for the rLuc spike-in were used to normalize variance in cDNA concentration arising due to sample cleanup and RT efficiency.

4.5.4 Nanoluciferase Reporter Assays

nLuc assays were adapted from methods previously described (Masser et al., 2016). Briefly, cells were grown in SC media and added to a 96-well plate. Promega Nano-Glo® substrate was diluted 1:100 with PBS and added 1:10 to each well immediately prior to measurement. Luminescence was measured every 30 seconds with a Tecan Infinite® 200 PRO plate reader. For glucose starvation, cells were sedimented by centrifugation, washed 2x with SC -G media, and resuspended in SC G- media for 30 minutes of incubation at 30ºC with rotating. For CHX-treated samples, 10 mg/mL CHX in deionized H_2O was added to achieve a final concentration of 100 µg/mL.

Chapter 5: Conclusion

In Chapter 2, we demonstrate that ribosomal runoff for growth mRNAs is incomplete during glucose starvation and explore a previously underappreciated role of slowed ribosomal elongation in response to acute glucose starvation. Ribosome profiling identifies high ribosome occupancy rates for highly expressed pre-stress mRNAs and a shift in ribosome polarity towards the 3'end of mRNAs. We quantify a direct slowdown in the elongation rate for an *in vivo* luciferase reporter, supporting the presence of a more general slowdown in elongation independent of coding sequence. Additionally, we find that these ribosomes remain poised to resume translation and produce functional proteins once glucose is returned, producing functional protein independently of new initiation.

A key limitation we encountered in quantifying elongation rates was the necessity of inducing transcription of our reporters immediately prior to running the assays. This is not an issue during steady state growth conditions, but it is unclear how the elongation rate during glucose starvation would differ if our reporters were transcribed prior to starvation. An alternative approach that would allow us to decouple the time of transcription from the translation of our reporters would be immensely valuable for an accurate representation of the housekeeping mRNAs transcribed pre-stress.

In Chapter 3, we utilize an in vivo luciferase reporter to directly quantify elongation rate and provide quantitative measurements of ribosome stalls. We quantify the dose-dependent effects of poly-CGA induced stalls and link these stalls to a Hel2-mediated RQC pathway. We also demonstrate the large effects distributed synonymous codon substitutions can have on the elongation rates of otherwise optimized mRNAs. The substitution of the optimal leucine codon TTG with the nonoptimal codon CTT results in a significant elongation delay for YFP on the order of minutes rather than seconds. We link this delay to local sequence effects driven by a Hel2-independent mechanism.

Additionally, we find this elongation delay is independent of the proposed translation sensor Dhh1. The elongation delay and impaired mRNA stability we observe due to CTT codons are not rescued by the deletion of Dhh1, and Dhh1 deletion may in fact result in the further slowdown of

translation. The elongation rates of YFP[CTC] and, to a much lesser degree, optYFP, are slowed, and protein and mRNA expression is dramatically impaired by the use of CTC codons.

We speculate this may be due to the slowed growth rate of the deletion strain, but direct effects of Dhh1 on these reporters cannot be ruled out. To determine if Dhh1 plays a direct role, a future approach investigating the elongation rate over CTC codons in a $Dhh1^{DQAD}$ mutant, which eliminates helicase activity, may prove informative.

In Chapter 4 we observe a correlation between high ribosomal polarity, which we previously linked to ribosome slowdown, and increased association with Dhh1. However, we were unable to demonstrate a causal relationship between the two. Combined with our findings from Chapter 3, it appears that Dhh1 may play a role in enhancing translation. It remains unclear how the cell maintains the active translation of some stress response mRNAs while selectively slowing elongation for pre-existing mRNAs.

Although Dhh1 does not appear responsible for the accumulation of ribosomes we observe in glucose starvation, future studies on the role of the Ccr4-Not complex during glucose starvation appear promising. Recent findings have implicated the Ccr4-Not complex as a sensor for ribosomes translating nonoptimal codon sequences and demonstrated that recruitment of Dhh1 to polysomes was dependent on the Not5 subunit (Allen et al., 2021; Buschauer et al., 2020). The Ccr4-Not complex may play a similar role in monitoring ribosome slowdown during glucose starvation conditions. The recruitment of Dhh1 to polysomes by the Ccr4-Not complex could explain the correlation we observe between Dhh1 enrichment and increased ribosome polarity during glucose starvation.

References

Advani, V.M., Ivanov, P., 2019. Translational Control under Stress: Reshaping the Translatome. BioEssays 41, 1900009. https://doi.org/10.1002/bies.201900009

Alamo, M. del, Hogan, D.J., Pechmann, S., Albanese, V., Brown, P.O., Frydman, J., 2011. Defining the Specificity of Cotranslationally Acting Chaperones by Systematic Analysis of mRNAs Associated with Ribosome-Nascent Chain Complexes. PLOS Biology 9, e1001100. https://doi.org/10.1371/journal.pbio.1001100

Allen, G.E., Panasenko, O.O., Villanyi, Z., Zagatti, M., Weiss, B., Pagliazzo, L., Huch, S., Polte, C., Zahoran, S., Hughes, C.S., Pelechano, V., Ignatova, Z., Collart, M.A., 2021. Not4 and Not5 modulate translation elongation by Rps7A ubiquitination, Rli1 moonlighting, and condensates that exclude eIF5A. Cell Reports 36. https://doi.org/10.1016/j.celrep.2021.109633

Arpat, A.B., Liechti, A., Matos, M.D., Dreos, R., Janich, P., Gatfield, D., 2020. Transcriptome-wide sites of collided ribosomes reveal principles of translational pausing. Genome Res. 30, 985–999. https://doi.org/10.1101/gr.257741.119

Arribere, J.A., Doudna, J.A., Gilbert, W.V., 2011. Reconsidering Movement of Eukaryotic mRNAs between Polysomes and P Bodies. Molecular Cell 44, 745–758. https://doi.org/10.1016/j.molcel.2011.09.019

Ashe, M.P., De Long, S.K., Sachs, A.B., 2000. Glucose Depletion Rapidly Inhibits Translation Initiation in Yeast. MBoC 11, 833–848. https://doi.org/10.1091/mbc.11.3.833

Bagamery, L.E., Justman, Q.A., Garner, E.C., Murray, A.W., 2020. A Putative Bet-Hedging Strategy Buffers Budding Yeast against Environmental Instability. Current Biology 30, 4563-4578.e4. https://doi.org/10.1016/j.cub.2020.08.092

Bosco, D.A., 2018. Translation dysregulation in neurodegenerative disorders. PNAS 115, 12842–12844.

Brengues, M., Teixeira, D., Parker, R., 2005. Movement of Eukaryotic mRNAs Between Polysomes and Cytoplasmic Processing Bodies. Science. https://doi.org/10.1126/science.1115791

Bresson, S., Shchepachev, V., Spanos, C., Turowski, T.W., Rappsilber, J., Tollervey, D., 2020. Stress-Induced Translation Inhibition through Rapid Displacement of Scanning Initiation Factors. Molecular Cell 80, 470-484.e8. https://doi.org/10.1016/j.molcel.2020.09.021

Burke, P.C., Park, H., Subramaniam, A.R., 2021. A Nascent Peptide Code for Translational Control of mRNA Stability in Human Cells. https://doi.org/10.1101/2021.12.01.470782

Buschauer, R., Matsuo, Y., Sugiyama, T., Chen, Y.-H., Alhusaini, N., Sweet, T., Ikeuchi, K., Cheng, J., Matsuki, Y., Nobuta, R., Gilmozzi, A., Berninghausen, O., Tesina, P., Becker, T., Coller, J., Inada, T., Beckmann, R., 2020. The Ccr4-Not complex monitors the translating ribosome for codon optimality. Science 368, eaay6912. https://doi.org/10.1126/science.aay6912

Buskirk, A.R., Green, R., 2017. Ribosome pausing, arrest and rescue in bacteria and eukaryotes. Philosophical Transactions of the Royal Society B: Biological Sciences 372, 20160183. https://doi.org/10.1098/rstb.2016.0183

Cankorur-Cetinkaya, A., Dereli, E., Eraslan, S., Karabekmez, E., Dikicioglu, D., Kirdar, B., 2012. A Novel Strategy for Selection and Validation of Reference Genes in Dynamic Multidimensional Experimental Design in Yeast. PLOS ONE 7, e38351. https://doi.org/10.1371/journal.pone.0038351

Carroll, J.S., Munchel, S.E., Weis, K., 2011. The DExD/H box ATPase Dhh1 functions in translational repression, mRNA decay, and processing body dynamics. Journal of Cell Biology 194, 527–537. https://doi.org/10.1083/jcb.201007151

Cary, G.A., Vinh, D.B.N., May, P., Kuestner, R., Dudley, A.M., 2015. Proteomic Analysis of Dhh1 Complexes Reveals a Role for Hsp40 Chaperone Ydj1 in Yeast P-Body Assembly. G3 Genes|Genomes|Genetics 5, 2497–2511. https://doi.org/10.1534/g3.115.021444

Castelli, L.M., Lui, J., Campbell, S.G., Rowe, W., Zeef, L.A.H., Holmes, L.E.A., Hoyle, N.P., Bone, J., Selley, J.N., Sims, P.F.G., Ashe, M.P., 2011. Glucose depletion inhibits translation initiation via eIF4A loss and subsequent 48S preinitiation complex accumulation, while the pentose phosphate pathway is coordinately up-regulated. MBoC 22, 3379–3393. https://doi.org/10.1091/mbc.e11-02-0153

Chan, L.Y., Mugler, C.F., Heinrich, S., Vallotton, P., Weis, K., 2018. Non-invasive measurement of mRNA decay reveals translation initiation as the major determinant of mRNA stability. eLife 7, e32536. https://doi.org/10.7554/eLife.32536

Chu, D., Barnes, D.J., von der Haar, T., 2011. The role of tRNA and ribosome competition in coupling the expression of different mRNAs in Saccharomyces cerevisiae. Nucleic Acids Research 39, 6705–6714. https://doi.org/10.1093/nar/gkr300

Chu, D., Kazana, E., Bellanger, N., Singh, T., Tuite, M.F., von der Haar, T., 2014. Translation elongation can control translation initiation on eukaryotic mRNAs. The EMBO Journal 33, 21–34. https://doi.org/10.1002/embj.201385651

Coller, J., Parker, R., 2005. General Translational Repression by Activators of mRNA Decapping. Cell 122, 875–886. https://doi.org/10.1016/j.cell.2005.07.012

Coller, J.M., Tucker, M., Sheth, U., Valencia-Sanchez, M.A., Parker, R., 2001. The DEAD box helicase, Dhh1p, functions in mRNA decapping and interacts with both the decapping and deadenylase complexes. RNA 7, 1717–1727. https://doi.org/10.1017/S135583820101994X

Costello, J.L., Kershaw, C.J., Castelli, L.M., Talavera, D., Rowe, W., Sims, P.F.G., Ashe, M.P., Grant, C.M., Hubbard, S.J., Pavitt, G.D., 2017. Dynamic changes in eIF4F-mRNA interactions revealed by global analyses of environmental stress responses. Genome Biol 18, 201. https://doi.org/10.1186/s13059-017-1338-4

Crawford, R.A., Pavitt, G.D., 2019. Translational regulation in response to stress in Saccharomyces cerevisiae. Yeast 36, 5–21. https://doi.org/10.1002/yea.3349

Dai, X., Zhu, M., Warren, M., Balakrishnan, R., Patsalo, V., Okano, H., Williamson, J.R., Fredrick, K., Wang, Y.-P., Hwa, T., 2016. Reduction of translating ribosomes enables Escherichia coli to maintain elongation rates during slow growth. Nat Microbiol 2, 1–9. https://doi.org/10.1038/nmicrobiol.2016.231

de la Cruz, J., Gómez-Herreros, F., Rodríguez-Galán, O., Begley, V., de la Cruz Muñoz-Centeno, M., Chávez, S., 2018. Feedback regulation of ribosome assembly. Curr Genet 64, 393–404. https://doi.org/10.1007/s00294-017-0764-x

Dever, T.E., Dinman, J.D., Green, R., 2018. Translation Elongation and Recoding in Eukaryotes. Cold Spring Harb Perspect Biol 10, a032649. https://doi.org/10.1101/cshperspect.a032649

Dever, T.E., Green, R., 2012. The Elongation, Termination, and Recycling Phases of Translation in Eukaryotes. Cold Spring Harb Perspect Biol 4, a013706. https://doi.org/10.1101/cshperspect.a013706

Diaz-Ruiz, R., Rigoulet, M., Devin, A., 2011. The Warburg and Crabtree effects: On the origin of cancer cell energy metabolism and of yeast glucose repression. Biochimica et Biophysica Acta (BBA) - Bioenergetics, Bioenergetics of Cancer 1807, 568–576. https://doi.org/10.1016/j.bbabio.2010.08.010

D'Onofrio, D.J., Abel, D.L., 2014. Redundancy of the genetic code enables translational pausing. Frontiers in Genetics 5.

D'Orazio, K.N., Wu, C.C.-C., Sinha, N., Loll-Krippleber, R., Brown, G.W., Green, R., 2019. The endonuclease Cue2 cleaves mRNAs at stalled ribosomes during No Go Decay. eLife 8, e49117. https://doi.org/10.7554/eLife.49117

Eisenberg, A.R., Higdon, A.L., Hollerer, I., Fields, A.P., Jungreis, I., Diamond, P.D., Kellis, M., Jovanovic, M., Brar, G.A., 2020. Translation Initiation Site Profiling Reveals Widespread Synthesis of Non-AUG-Initiated Protein Isoforms in Yeast. Cell Systems 11, 145-160.e5. https://doi.org/10.1016/j.cels.2020.06.011

Ferrin, M.A., Subramaniam, A.R., 2017. Kinetic modeling predicts a stimulatory role for ribosome collisions at elongation stall sites in bacteria. eLife 6, e23629. https://doi.org/10.7554/eLife.23629

Fischer, N., Weis, K., 2002. The DEAD box protein Dhh1 stimulates the decapping enzyme Dcp1. The EMBO Journal 21, 2788–2797. https://doi.org/10.1093/emboj/21.11.2788

Gamble, C.E., Brule, C.E., Dean, K.M., Fields, S., Grayhack, E.J., 2016. Adjacent Codons Act in Concert to Modulate Translation Efficiency in Yeast. Cell 166, 679–690. https://doi.org/10.1016/j.cell.2016.05.070

Gardin, J., Yeasmin, R., Yurovsky, A., Cai, Y., Skiena, S., Futcher, B., 2014. Measurement of average decoding rates of the 61 sense codons in vivo. eLife 3, e03735. https://doi.org/10.7554/eLife.03735

Gerashchenko, M.V., Lobanov, A.V., Gladyshev, V.N., 2012. Genome-wide ribosome profiling reveals complex translational regulation in response to oxidative stress. PNAS 109, 17394–17399.

Ghaemmaghami, S., Huh, W.-K., Bower, K., Howson, R.W., Belle, A., Dephoure, N., O'Shea, E.K., Weissman, J.S., 2003. Global analysis of protein expression in yeast. Nature 425, 737–741. https://doi.org/10.1038/nature02046

Gilbert, W.V., Zhou, K., Butler, T.K., Doudna, J.A., 2007. Cap-Independent Translation Is Required for Starvation-Induced Differentiation in Yeast. Science 317, 1224–1227. https://doi.org/10.1126/science.1144467

Gismondi, A., Caldarola, S., Lisi, G., Juli, G., Chellini, L., Iadevaia, V., Proud, C.G., Loreni, F., 2014. Ribosomal stress activates eEF2K–eEF2 pathway causing translation elongation inhibition and recruitment of Terminal Oligopyrimidine (TOP) mRNAs on polysomes. Nucleic Acids Research 42, 12668–12680. https://doi.org/10.1093/nar/gku996

Goldman, D.H., Livingston, N.M., Movsik, J., Wu, B., Green, R., 2021. Live-cell imaging reveals kinetic determinants of quality control triggered by ribosome stalling. Molecular Cell 81, 1830-1840.e8. https://doi.org/10.1016/j.molcel.2021.01.029

Han, P., Shichino, Y., Schneider-Poetsch, T., Mito, M., Hashimoto, S., Udagawa, T., Kohno, K., Yoshida, M., Mishima, Y., Inada, T., Iwasaki, S., 2020. Genome-wide Survey of Ribosome Collision. Cell Reports 31, 107610. https://doi.org/10.1016/j.celrep.2020.107610

Hanson, G., Coller, J., 2018. Codon optimality, bias and usage in translation and mRNA decay. Nat Rev Mol Cell Biol 19, 20–30. https://doi.org/10.1038/nrm.2017.91

Harigaya, Y., Parker, R., 2016. Codon optimality and mRNA decay. Cell Res 26, 1269–1270. https://doi.org/10.1038/cr.2016.127

Hartl, F.U., Bracher, A., Hayer-Hartl, M., 2011. Molecular chaperones in protein folding and proteostasis. Nature 475, 324–332. https://doi.org/10.1038/nature10317

Ho, B., Baryshnikova, A., Brown, G.W., 2018. Unification of Protein Abundance Datasets Yields a Quantitative Saccharomyces cerevisiae Proteome. cels 6, 192-205.e3. https://doi.org/10.1016/j.cels.2017.12.004

Holmes, L.E.A., Campbell, S.G., Long, S.K.D., Sachs, A.B., Ashe, M.P., 2004. Loss of Translational Control in Yeast Compromised for the Major mRNA Decay Pathway. Molecular and Cellular Biology.

Hussmann, J.A., Patchett, S., Johnson, A., Sawyer, S., Press, W.H., 2015. Understanding Biases in Ribosome Profiling Experiments Reveals Signatures of Translation Dynamics in Yeast. PLOS Genetics 11, e1005732. https://doi.org/10.1371/journal.pgen.1005732

Ikeuchi, K., Izawa, T., Inada, T., 2019. Recent Progress on the Molecular Mechanism of Quality Controls Induced by Ribosome Stalling. Frontiers in Genetics 9, 743. https://doi.org/10.3389/fgene.2018.00743

Ingolia, N.T., 2014. Ribosome profiling: new views of translation, from single codons to genome scale. Nat Rev Genet 15, 205–213. https://doi.org/10.1038/nrg3645

Ingolia, N.T., Ghaemmaghami, S., Newman, J.R.S., Weissman, J.S., 2009. Genome-Wide Analysis in Vivo of Translation with Nucleotide Resolution Using Ribosome Profiling. Science. https://doi.org/10.1126/science.1168978

Iserman, C., Altamirano, C.D., Jegers, C., Friedrich, U., Zarin, T., Fritsch, A.W., Mittasch, M., Domingues, A., Hersemann, L., Jahnel, M., Richter, D., Guenther, U.-P., Hentze, M.W., Moses,

A.M., Hyman, A.A., Kramer, G., Kreysing, M., Franzmann, T.M., Alberti, S., 2020. Condensation of Ded1p Promotes a Translational Switch from Housekeeping to Stress Protein Production. Cell 181, 818-831.e19. https://doi.org/10.1016/j.cell.2020.04.009

Ito, H., Fukuda, Y., Murata, K., Kimura, A., 1983. Transformation of intact yeast cells treated with alkali cations. Journal of Bacteriology. https://doi.org/10.1128/jb.153.1.163-168.1983

Jackson, R.J., Hellen, C.U.T., Pestova, T.V., 2010. The mechanism of eukaryotic translation initiation and principles of its regulation. Nat Rev Mol Cell Biol 11, 113–127. https://doi.org/10.1038/nrm2838

Janapala, Y., Preiss, T., Shirokikh, N.E., 2019. Control of Translation at the Initiation Phase During Glucose Starvation in Yeast. International Journal of Molecular Sciences 20, 4043. https://doi.org/10.3390/ijms20164043

Joazeiro, C.A.P., 2017. Ribosomal Stalling During Translation: Providing Substrates for Ribosome-Associated Protein Quality Control. Annual Review of Cell and Developmental Biology 33, 343–368. https://doi.org/10.1146/annurev-cellbio-111315-125249

Jochem, M., Ende, L., Isasa, M., Ang, J., Schnell, H., Guerra-Moreno, A., Micoogullari, Y., Bhanu, M., Gygi, S.P., Hanna, J., 2019. Targeted Degradation of Glucose Transporters Protects against Arsenic Toxicity. Molecular and Cellular Biology. https://doi.org/10.1128/MCB.00559-18

Jungfleisch, J., Nedialkova, D.D., Dotu, I., Sloan, K.E., Martinez-Bosch, N., Brüning, L., Raineri, E., Navarro, P., Bohnsack, M.T., Leidel, S.A., Díez, J., 2017. A novel translational control mechanism involving RNA structures within coding sequences. Genome Res. 27, 95–106. https://doi.org/10.1101/gr.209015.116

Juszkiewicz, S., Chandrasekaran, V., Lin, Z., Kraatz, S., Ramakrishnan, V., Hegde, R.S., 2018. ZNF598 Is a Quality Control Sensor of Collided Ribosomes. Molecular Cell 72, 469-481.e7. https://doi.org/10.1016/j.molcel.2018.08.037

Kafri, M., Metzl-Raz, E., Jona, G., Barkai, N., 2016. The Cost of Protein Production. Cell Reports 14, 22–31. https://doi.org/10.1016/j.celrep.2015.12.015

Kang, K.R., Lee, S.-Y., 2001. Effect of serum and hydrogen peroxide on the Ca2+/calmodulin-dependent phosphorylation of eukaryotic elongation factor 2(eEF-2) in Chinese hamster ovary cells. Exp Mol Med 33, 198–204. https://doi.org/10.1038/emm.2001.33

Kapur, M., Ackerman, S.L., 2018. mRNA Translation Gone Awry: Translation Fidelity and Neurological Disease. Trends in Genetics 34, 218–231. https://doi.org/10.1016/j.tig.2017.12.007

Karpinets, T.V., Greenwood, D.J., Sams, C.E., Ammons, J.T., 2006. RNA:protein ratio of the unicellular organism as a characteristic of phosphorous and nitrogen stoichiometry and of the cellular requirement of ribosomes for protein synthesis. BMC Biol 4, 30. https://doi.org/10.1186/1741-7007-4-30

Kenney, J.W., Moore, C.E., Wang, X., Proud, C.G., 2014. Eukaryotic elongation factor 2 kinase, an unusual enzyme with multiple roles. Advances in Biological Regulation 55, 15–27. https://doi.org/10.1016/j.jbior.2014.04.003

Khong, A., Parker, R., 2018. mRNP architecture in translating and stress conditions reveals an ordered pathway of mRNP compaction. Journal of Cell Biology 217, 4124–4140. https://doi.org/10.1083/jcb.201806183

Kim, J.-H., Roy, A., Jouandot, D., Cho, K.H., 2013. The glucose signaling network in yeast. Biochimica et Biophysica Acta (BBA) - General Subjects 1830, 5204–5210. https://doi.org/10.1016/j.bbagen.2013.07.025

Koutmou, K.S., Radhakrishnan, A., Green, R., 2015. Synthesis at the Speed of Codons. Trends in Biochemical Sciences 40, 717–718. https://doi.org/10.1016/j.tibs.2015.10.005

Kozak, M., 1999. Initiation of translation in prokaryotes and eukaryotes. Gene 234, 187–208. https://doi.org/10.1016/S0378-1119(99)00210-3

Kraft, C., Deplazes, A., Sohrmann, M., Peter, M., 2008. Mature ribosomes are selectively degraded upon starvation by an autophagy pathway requiring the Ubp3p/Bre5p ubiquitin protease. Nat Cell Biol 10, 602–610. https://doi.org/10.1038/ncb1723

Lee, C.-Y., Seydoux, G., 2019. Dynamics of mRNA entry into stress granules. Nat Cell Biol 21, 116–117. https://doi.org/10.1038/s41556-019-0278-5

Leprivier, G., Remke, M., Rotblat, B., Dubuc, A., Mateo, A.-R.F., Kool, M., Agnihotri, S., El-Naggar, A., Yu, B., Prakash Somasekharan, S., Faubert, B., Bridon, G., Tognon, C.E., Mathers, J., Thomas, R., Li, A., Barokas, A., Kwok, B., Bowden, M., Smith, S., Wu, X., Korshunov, A., Hielscher, T., Northcott, P.A., Galpin, J.D., Ahern, C.A., Wang, Y., McCabe, M.G., Collins, V.P., Jones, R.G., Pollak, M., Delattre, O., Gleave, M.E., Jan, E., Pfister, S.M., Proud, C.G., Derry, W.B., Taylor, M.D., Sorensen, P.H., 2013. The eEF2 Kinase Confers Resistance to Nutrient Deprivation by Blocking Translation Elongation. Cell 153, 1064–1079. https://doi.org/10.1016/j.cell.2013.04.055

Letzring, D.P., Dean, K.M., Grayhack, E.J., 2010. Control of translation efficiency in yeast by codon–anticodon interactions. RNA 16, 2516–2528. https://doi.org/10.1261/rna.2411710

Li, W., Wang, W., Uren, P.J., Penalva, L.O.F., Smith, A.D., 2017. Riborex: fast and flexible identification of differential translation from Ribo-seq data. Bioinformatics 33, 1735–1737. https://doi.org/10.1093/bioinformatics/btx047

Liu, B., Qian, S.-B., 2014. Translational reprogramming in cellular stress response. WIREs RNA 5, 301–305. https://doi.org/10.1002/wrna.1212

Liu, X., Yao, Z., Jin, M., Namkoong, S., Yin, Z., Lee, J.H., Klionsky, D.J., 2019. Dhh1 promotes autophagy-related protein translation during nitrogen starvation. PLOS Biology 17, e3000219. https://doi.org/10.1371/journal.pbio.3000219

Martinez, M.J., Roy, S., Archuletta, A.B., Wentzell, P.D., Anna-Arriola, S.S., Rodriguez, A.L., Aragon, A.D., Quiñones, G.A., Allen, C., Werner-Washburne, M., 2004. Genomic Analysis of Stationary-Phase and Exit in Saccharomyces cerevisiae: Gene Expression and Identification of Novel Essential Genes. MBoC 15, 5295–5305. https://doi.org/10.1091/mbc.e03-11-0856

Mason, N., Ciufo, L.F., Brown, J.D., 2000. Elongation arrest is a physiologically important function of signal recognition particle. The EMBO Journal 19, 4164–4174. https://doi.org/10.1093/emboj/19.15.4164

Mason, P.B., Struhl, K., 2005. Distinction and Relationship between Elongation Rate and Processivity of RNA Polymerase II In Vivo. Molecular Cell 17, 831–840. https://doi.org/10.1016/j.molcel.2005.02.017

Masser, A.E., Kandasamy, G., Kaimal, J.M., Andréasson, C., 2016. Luciferase NanoLuc as a reporter for gene expression and protein levels in Saccharomyces cerevisiae. Yeast 33, 191–200. https://doi.org/10.1002/yea.3155

Meydan, S., Guydosh, N.R., 2021. A cellular handbook for collided ribosomes: surveillance pathways and collision types. Curr Genet 67, 19–26. https://doi.org/10.1007/s00294-020-01111-w

Moon, S.L., Morisaki, T., Khong, A., Lyon, K., Parker, R., Stasevich, T.J., 2019. Multicolour single-molecule tracking of mRNA interactions with RNP granules. Nat Cell Biol 21, 162–168. https://doi.org/10.1038/s41556-018-0263-4

Mühlhofer, M., Berchtold, E., Stratil, C.G., Csaba, G., Kunold, E., Bach, N.C., Sieber, S.A., Haslbeck, M., Zimmer, R., Buchner, J., 2019. The Heat Shock Response in Yeast Maintains Protein Homeostasis by Chaperoning and Replenishing Proteins. Cell Reports 29, 4593-4607.e8. https://doi.org/10.1016/j.celrep.2019.11.109

Navickas, A., Chamois, S., Saint-Fort, R., Henri, J., Torchet, C., Benard, L., 2020. No-Go Decay mRNA cleavage in the ribosome exit tunnel produces 5′-OH ends phosphorylated by Trl1. Nat Commun 11, 122. https://doi.org/10.1038/s41467-019-13991-9

Nishimura, K., Fukagawa, T., Takisawa, H., Kakimoto, T., Kanemaki, M., 2009. An auxin-based degron system for the rapid depletion of proteins in nonplant cells. Nat Methods 6, 917–922. https://doi.org/10.1038/nmeth.1401

Ogg, S.C., Walter, P., 1995. SRP samples nascent chains for the presenceof signal sequences by interacting with ribosomes at a discrete step during translation elongation. Cell 81, 1075–1084. https://doi.org/10.1016/S0092-8674(05)80012-1

Pakos-Zebrucka, K., Koryga, I., Mnich, K., Ljujic, M., Samali, A., Gorman, A.M., 2016. The integrated stress response. EMBO Rep 17, 1374–1395. https://doi.org/10.15252/embr.201642195

Park, H., Subramaniam, A.R., 2019. Inverted translational control of eukaryotic gene expression by ribosome collisions. PLOS Biology 17, e3000396. https://doi.org/10.1371/journal.pbio.3000396

Pause, A., Sonenberg, N., 1992. Mutational analysis of a DEAD box RNA helicase: the mammalian translation initiation factor eIF-4A. The EMBO Journal 11, 2643–2654. https://doi.org/10.1002/j.1460-2075.1992.tb05330.x

Pechmann, S., Frydman, J., 2013. Evolutionary conservation of codon optimality reveals hidden signatures of cotranslational folding. Nat Struct Mol Biol 20, 237–243. https://doi.org/10.1038/nsmb.2466

Pineau, L., Ferreira, T., 2010. Lipid-induced ER stress in yeast and β cells: parallel trails to a common fate. FEMS Yeast Research 10, 1035–1045. https://doi.org/10.1111/j.1567-1364.2010.00674.x

Pop, C., Rouskin, S., Ingolia, N.T., Han, L., Phizicky, E.M., Weissman, J.S., 2014. Causal signals between codon bias, mRNA structure, and the efficiency of translation and elongation. Molecular Systems Biology 10, 770. https://doi.org/10.15252/msb.20145524

Preissler, S., Reuther, J., Koch, M., Scior, A., Bruderek, M., Frickey, T., Deuerling, E., 2015. Not4-dependent translational repression is important for cellular protein homeostasis in yeast. The EMBO Journal 34, 1905–1924. https://doi.org/10.15252/embj.201490194

Presnyak, V., Alhusaini, N., Chen, Y.-H., Martin, S., Morris, N., Kline, N., Olson, S., Weinberg, D., Baker, K.E., Graveley, B.R., Coller, J., 2015. Codon Optimality Is a Major Determinant of mRNA Stability. Cell 160, 1111–1124. https://doi.org/10.1016/j.cell.2015.02.029

Radhakrishnan, A., Chen, Y.-H., Martin, S., Alhusaini, N., Green, R., Coller, J., 2016. The DEAD-Box Protein Dhh1p Couples mRNA Decay and Translation by Monitoring Codon Optimality. Cell 167, 122-132.e9. https://doi.org/10.1016/j.cell.2016.08.053

Reis, M. dos, Savva, R., Wernisch, L., 2004. Solving the riddle of codon usage preferences: a test for translational selection. Nucleic Acids Research 32, 5036–5044. https://doi.org/10.1093/nar/gkh834

Riba, A., Nanni, N.D., Mittal, N., Arhné, E., Schmidt, A., Zavolan, M., 2019. Protein synthesis rates and ribosome occupancies reveal determinants of translation elongation rates. PNAS 116, 15023–15032. https://doi.org/10.1073/pnas.1817299116

Sabi, R., Tuller, T., 2019. Novel insights into gene expression regulation during meiosis revealed by translation elongation dynamics. npj Syst Biol Appl 5, 1–12. https://doi.org/10.1038/s41540-019-0089-0

Saikia, M., Wang, X., Mao, Y., Wan, J., Pan, T., Qian, S.-B., 2016. Codon optimality controls differential mRNA translation during amino acid starvation. RNA 22, 1719–1727. https://doi.org/10.1261/rna.058180.116

Sanchez, M., Lin, Y., Yang, C.-C., McQuary, P., Campos, A.R., Blanc, P.A., Wolf, D.A., 2019. Cross Talk between eIF2α and eEF2 Phosphorylation Pathways Optimizes Translational Arrest in Response to Oxidative Stress. iScience 20, 466–480. https://doi.org/10.1016/j.isci.2019.09.031

Schleif, R., Hess, W., Finkelstein, S., Ellis, D., 1973. Induction Kinetics of the l-Arabinose Operon of Escherichia coli. Journal of Bacteriology. https://doi.org/10.1128/jb.115.1.9-14.1973

Schneider-Poetsch, T., Ju, J., Eyler, D.E., Dang, Y., Bhat, S., Merrick, W.C., Green, R., Shen, B., Liu, J.O., 2010. Inhibition of eukaryotic translation elongation by cycloheximide and lactimidomycin. Nat Chem Biol 6, 209–217. https://doi.org/10.1038/nchembio.304

Schuller, A.P., Wu, C.C.-C., Dever, T.E., Buskirk, A.R., Green, R., 2017. eIF5A Functions Globally in Translation Elongation and Termination. Molecular Cell 66, 194-205.e5. https://doi.org/10.1016/j.molcel.2017.03.003

Sen, N.D., Zhou, F., Ingolia, N.T., Hinnebusch, A.G., 2015. Genome-wide analysis of translational efficiency reveals distinct but overlapping functions of yeast DEAD-box RNA helicases Ded1 and eIF4A. Genome Res. 25, 1196–1205. https://doi.org/10.1101/gr.191601.115

Shah, P., Ding, Y., Niemczyk, M., Kudla, G., Plotkin, J.B., 2013. Rate-Limiting Steps in Yeast Protein Translation. Cell 153, 1589–1601. https://doi.org/10.1016/j.cell.2013.05.049

Shalgi, R., Hurt, J.A., Krykbaeva, I., Taipale, M., Lindquist, S., Burge, C.B., 2013. Widespread Regulation of Translation by Elongation Pausing in Heat Shock. Molecular Cell 49, 439–452. https://doi.org/10.1016/j.molcel.2012.11.028

Sheff, M.A., Thorn, K.S., 2004. Optimized cassettes for fluorescent protein tagging in Saccharomyces cerevisiae. Yeast 21, 661–670. https://doi.org/10.1002/yea.1130

Sheikh, M.S., Fornace, A.J., 1999. Regulation of translation initiation following stress. Oncogene 18, 6121–6128. https://doi.org/10.1038/sj.onc.1203131

Simms, C.L., Yan, L.L., Zaher, H.S., 2017. Ribosome Collision Is Critical for Quality Control during No-Go Decay. Molecular Cell 68, 361-373.e5. https://doi.org/10.1016/j.molcel.2017.08.019

Sivan, G., Kedersha, N., Elroy-Stein, O., 2007. Ribosomal Slowdown Mediates Translational Arrest during Cellular Division. Molecular and Cellular Biology. https://doi.org/10.1128/MCB.00798-07

Sonenberg, N., Hinnebusch, A.G., 2009. Regulation of Translation Initiation in Eukaryotes: Mechanisms and Biological Targets. Cell 136, 731–745. https://doi.org/10.1016/j.cell.2009.01.042

Souza-Moreira, T.M., Navarrete, C., Chen, X., Zanelli, C.F., Valentini, S.R., Furlan, M., Nielsen, J., Krivoruchko, A., 2018. Screening of 2A peptides for polycistronic gene expression in yeast. FEMS Yeast Research 18, foy036. https://doi.org/10.1093/femsyr/foy036

Spencer, P.S., Siller, E., Anderson, J.F., Barral, J.M., 2012. Silent Substitutions Predictably Alter Translation Elongation Rates and Protein Folding Efficiencies. Journal of Molecular Biology 422, 328–335. https://doi.org/10.1016/j.jmb.2012.06.010

Sweet, T., Kovalak, C., Coller, J., 2012. The DEAD-Box Protein Dhh1 Promotes Decapping by Slowing Ribosome Movement. PLOS Biology 10, e1001342. https://doi.org/10.1371/journal.pbio.1001342

Swisher, K.D., Parker, R., 2010. Localization to, and Effects of Pbp1, Pbp4, Lsm12, Dhh1, and Pab1 on Stress Granules in Saccharomyces cerevisiae. PLOS ONE 5, e10006. https://doi.org/10.1371/journal.pone.0010006

Tahmasebi, S., Khoutorsky, A., Mathews, M.B., Sonenberg, N., 2018. Translation deregulation in human disease. Nat Rev Mol Cell Biol 19, 791–807. https://doi.org/10.1038/s41580-018-0034-x

Tanaka, S., Miyazawa-Onami, M., Iida, T., Araki, H., 2015. iAID: an improved auxin-inducible degron system for the construction of a ‘tight’ conditional mutant in the budding yeast Saccharomyces cerevisiae. Yeast 32, 567–581. https://doi.org/10.1002/yea.3080

Tardu, M., Jones, J.D., Kennedy, R.T., Lin, Q., Koutmou, K.S., 2019. Identification and Quantification of Modified Nucleosides in Saccharomyces cerevisiae mRNAs. ACS Chem. Biol. 14, 1403–1409. https://doi.org/10.1021/acschembio.9b00369

Tavares, C.D.J., Ferguson, S.B., Giles, D.H., Wang, Q., Wellmann, R.M., O'Brien, J.P., Warthaka, M., Brodbelt, J.S., Ren, P., Dalby, K.N., 2014. The Molecular Mechanism of Eukaryotic Elongation Factor 2 Kinase Activation *. Journal of Biological Chemistry 289, 23901–23916. https://doi.org/10.1074/jbc.M114.577148

Teige, M., Scheikl, E., Reiser, V., Ruis, H., Ammerer, G., 2001. Rck2, a member of the calmodulin-protein kinase family, links protein synthesis to high osmolarity MAP kinase signaling in budding yeast. PNAS 98, 5625–5630. https://doi.org/10.1073/pnas.091610798

Tseng-Rogenski, S.S. -I, Chong, J., Thomas, C.B., Enomoto, S., Berman, J., Chang, T., 2003. Functional conservation of Dhh1p, a cytoplasmic DExD/H-box protein present in large complexes. Nucleic Acids Research 31, 4995–5002. https://doi.org/10.1093/nar/gkg712

Tsuboi, T., Viana, M.P., Xu, F., Yu, J., Chanchani, R., Arceo, X.G., Tutucci, E., Choi, J., Chen, Y.S., Singer, R.H., Rafelski, S.M., Zid, B.M., 2020. Mitochondrial volume fraction and translation duration impact mitochondrial mRNA localization and protein synthesis. eLife 9, e57814. https://doi.org/10.7554/eLife.57814

VanInsberghe, M., van den Berg, J., Andersson-Rolf, A., Clevers, H., van Oudenaarden, A., 2021. Single-cell Ribo-seq reveals cell cycle-dependent translational pausing. Nature 597, 561–565. https://doi.org/10.1038/s41586-021-03887-4

Veltri, A.J., D'Orazio, K.N., Lessen, L.N., Loll-Krippleber, R., Brown, G.W., Green, R., 2021. Distinct ribosome states trigger diverse mRNA quality control pathways. https://doi.org/10.1101/2021.12.01.470814

Wang, E.T., Taliaferro, J.M., Lee, J.-A., Sudhakaran, I.P., Rossoll, W., Gross, C., Moss, K.R., Bassell, G.J., 2016. Dysregulation of mRNA Localization and Translation in Genetic Disease. J. Neurosci. 36, 11418–11426. https://doi.org/10.1523/JNEUROSCI.2352-16.2016

Wang, Z., Sun, X., Wee, J., Guo, X., Gu, Z., 2019. Novel insights into global translational regulation through Pumilio family RNA-binding protein Puf3p revealed by ribosomal profiling. Curr Genet 65, 201–212. https://doi.org/10.1007/s00294-018-0862-4

Weinberg, D.E., Shah, P., Eichhorn, S.W., Hussmann, J.A., Plotkin, J.B., Bartel, D.P., 2016. Improved Ribosome-Footprint and mRNA Measurements Provide Insights into Dynamics and Regulation of Yeast Translation. Cell Reports 14, 1787–1799. https://doi.org/10.1016/j.celrep.2016.01.043

Wu, C.C.-C., Zinshteyn, B., Wehner, K.A., Green, R., 2019. High-Resolution Ribosome Profiling Defines Discrete Ribosome Elongation States and Translational Regulation during Cellular Stress. Molecular Cell 73, 959-970.e5. https://doi.org/10.1016/j.molcel.2018.12.009

Yip, M.C.J., Shao, S., 2021. Detecting and Rescuing Stalled Ribosomes. Trends in Biochemical Sciences 46, 731–743. https://doi.org/10.1016/j.tibs.2021.03.008

Yu, C.-H., Dang, Y., Zhou, Z., Wu, C., Zhao, F., Sachs, M.S., Liu, Y., 2015. Codon Usage Influences the Local Rate of Translation Elongation to Regulate Co-translational Protein Folding. Molecular Cell 59, 744–754. https://doi.org/10.1016/j.molcel.2015.07.018

Zhao, T., Chen, Y.-M., Li, Y., Wang, J., Chen, S., Gao, N., Qian, W., 2021. Disome-seq reveals widespread ribosome collisions that promote cotranslational protein folding. Genome Biology 22, 16. https://doi.org/10.1186/s13059-020-02256-0

Zid, B.M., O'Shea, E.K., 2014. Promoter sequences direct cytoplasmic localization and translation of mRNAs during starvation in yeast. Nature 514, 117–121. https://doi.org/10.1038/nature13578